

Deriving laws of statistical, analytical and fluid mechanics

An International Baccalaureate MYP Personal Project

Andrea Kouta Dagnino

Supervisor: Enrica Minetti

Deledda International School

September 2019



Deriving laws of statistical, analytical and fluid mechanics

A. K. Dagnino

5th September 2019

We present a study of selected physical phenomena in statistical, analytical and fluid mechanics. In Chapter 1, calculations and derivations of Planck's law and Rydberg's formula are given, following the historical development of Black-Body radiation theory and early quantum mechanics. We apply our theoretical knowledge of radiation and flame spectroscopy to understand how fire behaves in micro gravity in absence of convective currents.

In the second chapter, we immediately introduce the concept of surface energy and define surface tension accordingly. A derivation of the Young-Laplace equation is presented, and is applied to solve problems in fluid mechanics. More precisely, we address capillary action, the formation of menisci, and the shape of puddles. Finally, we close the chapter showing the applicability of surface tension in the study of minimal surfaces.

The third and fourth chapters both study the motion of Frisbees. Various studies were conducted mostly examining either the aerodynamics or the mechanics behind flying disks. We attempt to treat both topics collectively. We first introduce the use of summation convention and tensor notation. Next, we provide a conceptual explanation of the stress tensor, and apply this knowledge to derive the Navier-Stokes equation and provide a justification for the Bernoulli Principle. We derive the equation of translational motion for the Frisbee by taking drag and lift forces into consideration. A python simulation is then constructed to solve these equations of motion. In the final chapter, we initially examine the kinematics of rigid bodies, and digress to quantitatively describe the effect of fictitious forces such as the Coriolis force in the formation of cyclones. Starting from Newtonian Mechanics we derive the Inertia tensor and the principle of conservation of angular momentum. Finally, the equations of motion for uniform and torque free precession are presented and implemented to derive the equation of rotational motion for a Frisbee.

This project was carried out as part of the International Baccalaureate Middle Years Program Personal Project, during the Summer of 2019.

Contents

1 Fire and its physical properties	5
1.1 Introduction	5
1.2 Overview on Black-Body radiation	6
1.3 A catastrophe for Light: UV Catastrophe	6
1.4 The resolution: a derivation of Planck's Law and Energy Quantisation	12
1.4.1 Standard Derivation	12
1.4.2 Bose-Einstein Statistics and a new derivation	13
1.5 Wien's Approximation, Raleigh-Jeans Law and the Stephan Boltzmann Law	16
1.6 Flame Spectroscopy: deriving Rydberg's formula	18
1.7 Spectral Lines of Hydrogenic Atoms	21
1.8 Flames in microgravity, and other phenomena of fire	23
1.9 Conclusion	26
2 Surface Tension	28
2.1 Defining Surface Tension	28
2.2 Deriving the Young-Laplace Equation	31
2.2.1 Floating Bodies	33
2.3 Capillary Action	36
2.3.1 Jurin's Law	36
2.3.2 The Concave Meniscus ($\theta < \frac{\pi}{2}$)	37
2.3.3 Capillary Length λ and the shape of puddles	40
2.4 Minimal Surfaces	43
2.5 Conclusion	43
3 Frisbees and Disks	45
3.1 Introduction	45
3.2 A mathematical prelude on Summation Convention	46
3.3 The Stress Tensor	49
3.4 Deriving the Cauchy Momentum equation for Incompressible Flow	52
3.5 The Bernoulli Principle and how Lift is generated	55
3.6 Equation of Motion for a Frisbee in Flight	57

3.7	Simulating Frisbee Flight	59
4	Rotation and the Motion of Spin Stabilised Disks	61
4.1	Introduction	61
4.2	Kinematics of Rotation	63
4.2.1	The Coriolis Effect	65
4.2.2	Euler Angles	68
4.3	Dynamics of Rigid Bodies	69
4.3.1	What are Rigid Bodies?	69
4.3.2	The Inertia Tensor	70
4.3.3	Angular Momentum	71
4.3.4	Euler's Equations	73
4.4	Gyroscopic Precession	74
4.4.1	Uniform Precession	74
4.4.2	Torque-Free Precession	76
4.5	Spin Stabilised Disk and Precession	78
4.6	Conclusion	79
A	Appendix A Python Codes	80
A.1	Code 1: Minimal Surface Plots	80
A.2	Code 2: Streamlines for Vector Field	81
A.3	Code 3: Frisbee Flight Simulations	82

List of Figures

1.1	To the left, a box containing standing waves, with nodes at its ends. This allows the waves to bounce off and not lose energy until thermal equilibrium is reached. To the right, a box containing waves, with non-zero amplitudes at its walls. Hence, incident radiation upon the walls causes energy loss.	7
1.2	View of the Box radiator, and decomposition of wavelength into components	8
1.3	Coordinate Plane with n_x, n_y, n_z as axes.	9
1.4	Plot comparing the curve given by the Rayleigh Jeans law and the actual curve for blackbody radiation. We let $h = c = k = 1$	12
1.5	Explanation of Bose Einstein Distribution, showing the analogous of our model for particles.	14
1.6	Apparatus for Flame Spectroscopy	19
1.7	Phase transitions in Lyman series, and the corresponding spectral lines.	22
1.8	Photograph of a Flame and explanation of how combustion works	25
1.9	Fuel reaction rate contours for a symmetrical laminar flame, at varying gravitational fields. Taken from A. Alsairafi, J.S. T'ien, S.T. Lee, D.L. Dietrich and H.D. Ross. "Modelling Candle Flame Behaviour in Variable Gravity", presented at the "Seventh International Workshop on Microgravity Combustion and Chemically Reacting Systems", 2003. p. 263	26
2.1	Diagram showing dynamics behind surface tension in a droplet	29
2.2	Analogy between surface energy and potential energy minimization.	30
2.3	Pressure inside and outside of a spherical droplet or convex meniscus	31
2.4	Infinitesimal patch over which surface tension acts along the edges	32
2.5	Body placed on a fluid depresses its surface, but doesn't necessarily sink due to surface tension and buoyancy.	34
2.6	Capillary rise for a concave meniscus	36
2.7	Profile of a concave meniscus	38
2.8	Menisci for contact angles $40^\circ, 50^\circ, 70^\circ$, setting $\lambda = 1$	39
2.9	Comparison between puddles with $h > \lambda$ and $h < \lambda$	41
2.10	a) Plot of a Catenoid b) Plot of Henneberg Surface c) Plot of Helicoid	44

3.1	Fluid running between a fixed and moving plate	49
3.2	Diagram dividing fluid into infinitesimally thin layers, explaining how viscosity acts as a shear stress on a fluid	50
3.3	Shear and Normal stress acting on an infinitesimal volume element	51
3.4	Streamline for the Vector Field $\mathbf{F}(x, y) = \sin x \sin y \hat{\mathbf{x}} + \cos x \cos y \hat{\mathbf{y}}$	56
3.5	Lift generated at various angles of attack	57
3.6	Increment in Lift when using Flaps, as opposed to increasing the angle of attack .	57
3.7	Air flow over and under a frisbee in flight	58
3.8	Trajectories of Frisbees thrown at $v_0 = 15$, with varying angles of attack	59
4.1	Explaining why Frisbees veer to the right/left due to Gyroscopic Precession . . .	62
4.2	Kinematics of a Body in a Rotating Frame vs. Inertial Frame	63
4.3	Angular Frequency of a rotating rigid body	64
4.4	Coriolis Effect on a Rotating Disk	66
4.5	The formation of cyclones in the Northern Hemisphere	68
4.6	Specifying a body's orientation using Euler Angles	69
4.7	Geometrical Interpretation of Gyroscopic Precession	77

Chapter 1

Fire and its physical properties

Contents

1.1	Introduction	5
1.2	Overview on Black-Body radiation	6
1.3	A catastrophe for Light: UV Catastrophe	6
1.4	The resolution: a derivation of Planck's Law and Energy Quantisation	12
1.4.1	Standard Derivation	12
1.4.2	Bose-Einstein Statistics and a new derivation	13
1.5	Wien's Approximation, Raleigh-Jeans Law and the Stephan Boltzmann Law	16
1.6	Flame Spectroscopy: deriving Rydberg's formula	18
1.7	Spectral Lines of Hydrogenic Atoms	21
1.8	Flames in microgravity, and other phenomena of fire	23
1.9	Conclusion	26

1.1 Introduction

Since its "discovery" about 2 million years ago by the Homo Erectus,¹ fire has been a fascinating phenomenon. Despite its presence in our daily lives for millennia, fire and its properties have been studied in depth by scientists for only a few centuries.² Indeed, many of its most notable and alluring characteristics, such as its "glow", have only been explained in the last century or so with the rise of quantum mechanics. Hence, it is easy for one to wonder why fire has a certain shape, colour and glow. Indeed, without the notions of *quantisation* and *energy levels*, the two main processes behind the glow of fire, black body radiation and gas atomic excitation, wouldn't be explainable. Hence, we shall dedicate this first chapter to the study of these two phenomena in order to answer some of the aforementioned questions.

1.2 Overview on Black-Body radiation

We shall now begin with our study, by first defining "fire", and Black-Body radiation. According to Cambridge Dictionary,³ a flame is

"a stream of hot, burning gas from something on fire".

— Cambridge Dictionary

This reaction therefore emits thermal electromagnetic radiation. Indeed, any body with a non-zero absolute temperature will emit some form of electromagnetic radiation.⁴ The intensity of the electromagnetic radiation as a function of its frequency is referred to as the spectral radiance. This emission of radiation is due to the acceleration of the electrons within the atoms of the ignited body. The acceleration of these charges will produce an electromagnetic field, converting thermal kinetic energy to thermal electromagnetic energy.⁴

A black body radiator is an optimal body for the study of such phenomena, since they are in thermodynamic equilibrium. More precisely, a black body is any object capable of absorbing all radiation incident upon it. Thus, since there is no net flow of energy due to its state of equilibrium, it emits all the absorbed heat, and radiates the thermal energy in the form of electromagnetic energy, in a form called thermal electromagnetic radiation. It is both a perfect emitter and absorber.⁴ The relationship between the intensity of the electromagnetic radiation and the frequency of the radiation are given in Planck's law of radiation, which gives the distribution of the energy of thermal radiation (in the case of a black body, black body radiation) over the electromagnetic frequency spectrum at a given temperature.⁵ It is worthy to note that black bodies have an optimum frequency for which the intensity of emitted radiation is optimized, and this frequency is dependent only on the temperature of the body.⁶

This is the exact process through which a metal rod, when heated to a sufficiently high temperature, will start glowing. In reality, the thermal energy from the combustion reaction is transferred to the rod by increasing the kinetic energy of the atoms within the rod. The acceleration of such particles creates an electromagnetic field, electromagnetic radiation is emitted. The "glow" that a blacksmith may see is in truth the radiation with frequency lying in the visible spectrum of light. If we were to look at the rod through a UV camera, we'd see different radiation with different intensity. To determine the intensity of radiation in a certain range of frequencies, we repeat that Planck's law is essential. Hence it shall be the focus of the following two sections to derive this fundamental law from first principles.

1.3 A catastrophe for Light: UV Catastrophe

We will closely follow the derivation given in *Tenn* (2013).⁷ Consider a cubical box of side length L , with perfectly conductive walls, and a small perforation applied to one face. Under ideal

conditions, this would be a black body, as any radiation within it would bounce off the walls until it is completely absorbed.

Let us now consider an electromagnetic wave travelling inside this cube. It is essential to that until thermal equilibrium is actually reached, the radiation waves must persist. Hence, the electromagnetic wave must have nodes at two opposite faces of the cube. Otherwise, any incident radiation may lose energy due to its non-zero tangential component.⁹

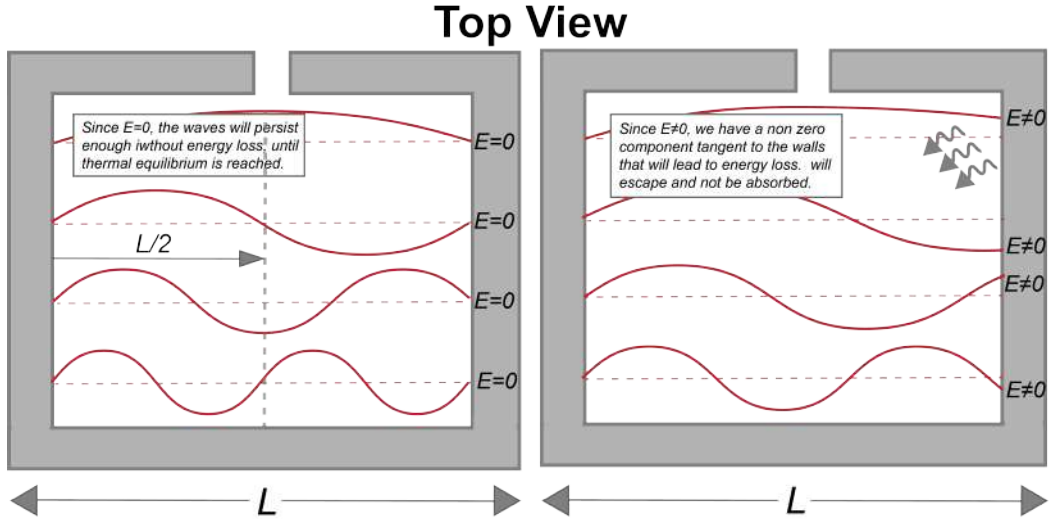


Figure 1.1: To the left, a box containing standing waves, with nodes at its ends. This allows the waves to bounce off and not lose energy until thermal equilibrium is reached. To the right, a box containing waves, with non-zero amplitudes at its walls. Hence, incident radiation upon the walls causes energy loss.

This means that the half-wavelength of the electromagnetic wave must be a divisor of L:

$$\frac{n_x \lambda_x}{2} = \frac{n_y \lambda_y}{2} = \frac{n_z \lambda_z}{2} = L \quad (1.1)$$

It follows that the allowed values for the wave vector components are:

$$k_x = \frac{\pi n_x}{L}, k_y = \frac{\pi n_y}{L}, k_z = \frac{\pi n_z}{L}. \quad (1.2)$$

Looking at the cube in three dimensions, it is easy to see that the wavelengths can be expressed as their directional cosines:

$$\lambda_x = \frac{\lambda}{\cos \alpha}, \lambda_y = \frac{\lambda}{\cos \beta}, \lambda_z = \frac{\lambda}{\cos \gamma}, \quad (1.3)$$

so that:

$$n_x = \frac{2L \cos \alpha}{\lambda}, n_y = \frac{2L \cos \beta}{\lambda}, n_z = \frac{2L \cos \gamma}{\lambda}. \quad (1.4)$$

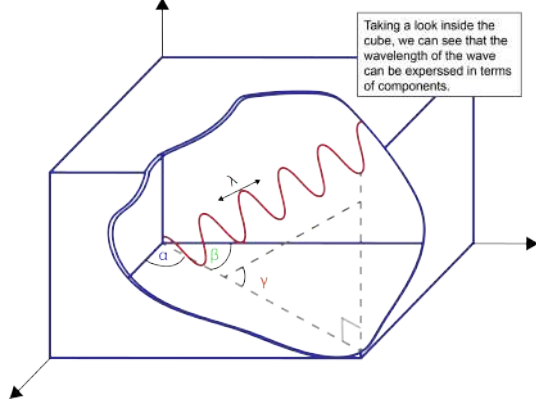


Figure 1.2: View of the Box radiator, and decomposition of wavelength into components

Squaring both sides of (1.4), adding the squared components give:

$$n_x^2 + n_y^2 + n_z^2 = \frac{4L^2}{\lambda^2} = R^2 \quad (1.5)$$

where we used the fact that the sum of the squared directional cosines of an orthogonal basis system is one.

$$\cos^2 \alpha + \cos^2 \beta + \cos^2 \gamma = 1 \quad (1.6)$$

The same result could be derived by exploiting the classical wave equation.⁸

The Wave Equation

$$\nabla^2 \mathbf{A} = \frac{1}{c^2} \frac{\partial^2 \mathbf{A}}{\partial t^2} \quad (1.7)$$

The solution to this PDE can be solved, and setting boundary conditions for a stationary wave so that it has zero amplitudes at the wall,⁹ we have that:

$$A(x, y, z) = A_0 \sin \frac{n_x \pi x}{L} \sin \frac{n_y \pi y}{L} \sin \frac{n_z \pi z}{L} \quad (1.8)$$

substituting into the equation gives (1.5):

$$n_x^2 + n_y^2 + n_z^2 = \frac{4L^2}{\lambda^2} = R^2$$

as required.

We have that the sum of the squared ratios of $2L$ and the wavelength must be constant. In other words, plotting this in a graph using $n_x - n_y - n_z$ as basis vectors/coordinates (see Figure 1.3), we'd get a sphere centered at the origin of radius $R = \frac{2L}{\lambda}$. However, note that n_x, n_y and n_z

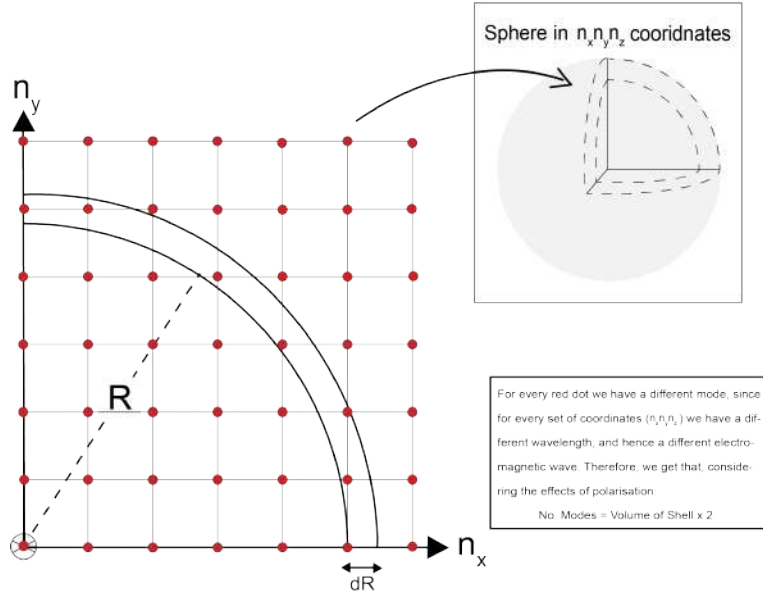


Figure 1.3: Coordinate Plane with n_x, n_y, n_z as axes.

can only be positive, since wavelengths are proportional to the L with positive proportionality looking at (1.1).

The allowed frequencies are:

$$v = \frac{c}{\lambda} = \frac{c}{2L} \sqrt{n_x^2 + n_y^2 + n_z^2} = \frac{cR}{2L} \quad (1.9)$$

so that, differentiating

$$dv = \frac{c}{2L} dR \quad (1.10)$$

, where c is the speed of light ($c \approx 3.0 \times 10^6$) Let us now denote the number of modes at a certain frequency v with $N(v)$, so that $N(v)dv$ is the number of modes with a frequency between v and $v + dv$. This value is equal to the volume of the shell of the octant with the n_i values corresponding to the frequency range. By having a variation in the frequency we have, in our 3-D diagram, a change in R (such that $R(v) \in [R, R + dR]$) using (1.10). Finally, recall that any electromagnetic wave has two distinct modes of vibration, two polarisations. Thus, for each point in our 3-D system we have two independent modes, leading to a factor of two in our expression accounting for this effect. Taking these reflections into consideration:

$$\underbrace{N(v)dv}_{\text{no. modes}} = \overbrace{\frac{4\pi R^2 dR}{8}}^{\text{volume of shell}} 2 = \pi R^2 dR = \frac{8\pi v^2 L^3}{c^3} dv \quad (1.11)$$

This will be fundamental, the number of modes with a range of frequencies between v and $v + dv$ is equal to:

$$N(v)dv = \frac{8\pi v^2 L^3}{c^3} dv \quad (1.12)$$

Hence, we can multiply this result to the average energy per mode $\langle H \rangle$ to calculate the total energy in a frequency range: $H_{tot}dv$, the spectral energy. Dividing the spectral energy by the volume of the box gives the spectral energy density, the expression we're looking for:

$$\overbrace{\int_0^\infty u_v(T)dv}^{\text{Energy density}} = \frac{H_{tot}}{L^3} \quad (1.13)$$

In other words, the spectral energy density in the frequency range is equal to the energy in the frequency range (spectral energy) over the volume of the box:

$$u_v dv = \frac{\overbrace{\langle H \rangle N_v dv}^{\text{Spectral energy}}}{L^3} \quad (1.14)$$

Moreover, notice that integrating over infinity for v yield the total number of modes in the box, which is clearly infinite since we have standing waves phased with the length of the cube. This is indeed true, since integrating $\int_0^\infty N(v)dv \rightarrow \infty$

Let us now assume that the waves have persisted enough so that the system has reached thermal equilibrium. Therefore, they each have a temperature T , with energy H . Using Boltzmann's Probability Distribution in classical statistical mechanics:

$$P(H) = Ce^{-\frac{H}{kT}} \quad (1.15)$$

the average energy of a mode with temperature T in thermodynamic equilibrium is:

$$\langle H \rangle = \frac{\int_0^\infty HP(H)dH}{\int_0^\infty P(H)dH} = \frac{\int_0^\infty He^{-\frac{H}{kT}}dH}{\int_0^\infty e^{-\frac{H}{kT}}dH} = -\frac{d}{d\beta} \ln \left(\int_0^\infty e^{-\beta H} dH \right) = kT$$

where $\beta = \frac{1}{kT}$. We also used the fact that the average energy of a mode is given by:

$$\langle H \rangle = -\frac{dZ}{d\beta}, \quad Z = \sum_{n=0}^{\infty} e^{\beta H_n} \quad (1.16)$$

for energy levels $H_{n=0,1,\dots}$. We have therefore reached the *equipartition theorem*.¹⁰

Theorem 1 (Equipartition Theorem). *The energy of a system is shared equally amongst all energetically accessible degrees of freedom of such system. Hence system will generally try to maximise its entropy by distributing its energy amongst all modes. For example, the vibrational energy of a single molecule oscillator heated to a temperature T will be:*

$$\langle H_{vib} \rangle = kT \quad (1.17)$$

Using this result, we have that the energy of all modes of the cavity in the frequency range

v and $v + dv$ is given by the product of the number of modes and the energy per mode:

$$N(v)dv \cdot \langle H \rangle = \frac{8\pi v^2 L^3}{c^3} dv \cdot kT \quad (1.18)$$

The spectral energy density function $u_v(T)$ is the total energy per unit frequency interval over the volume of the cube (per unit volume would be more correct). Using (1.14):

$$u_v(T)dv = \frac{8\pi v^2 kT}{c^3} dv \quad (1.19)$$

$$u_v(T) = \frac{8\pi v^2 kT}{c^3} \quad (1.20)$$

Hence, we have that the spectral energy density function is actually a function defining the spectral energy (electromagnetic radiation energy) per unit volume in terms of the frequency of radiation. The fact that this is a function in terms of frequency and not only temperature makes it "spectral" as we are dealing with a spectrum. The same argument would apply using wavelengths or angular frequencies instead of normal frequency.

By equating the spectral energy density per unit frequency with the total energy per unit frequency per unit volume we got the desired result. Note that the spectral energy density is defined as the flow of spectral radiance (which is actually the spectral power over surface area) over the speed of light:

$$u_v(T) = \frac{1}{c} \iint_S B_v dS \quad (1.21)$$

Since black body radiation is isotropic (it is invariant with respect to direction), $u_v(T)$ may be taken out of the integral and multiplied by unit area 4π :

$$\frac{8\pi v^2 kT}{c^3} = \frac{4\pi B_v}{c} \quad (1.22)$$

which finally gives

Rayleigh-Jeans Law

$$B_v = \frac{2v^2 kT}{c^2} \quad (1.23)$$

This is the famous Rayleigh-Jeans equation which threw the entire 20th century scientific community into turmoil upon its publishing in 1905. Indeed, note that as we take $v \rightarrow \infty$, our result for spectral radiance approaches infinity when taking its integral over all frequencies (taking this integral gives the overall radiance due to ALL frequencies):

$$\int_0^\infty B_v(T) dv = \infty \quad (1.24)$$

This is known as the ultraviolet catastrophe. In short, the Rayleigh Jeans equation works well according to experimental data for lower frequencies, but diverges from data for higher frequencies (such as Ultraviolet radiation), as can be seen in Figure 1.4. On the other hand, we have Wien's Approximation (which will be derived later) which coincides with experimental data for higher frequencies, but greatly diverges for lower frequencies.¹¹

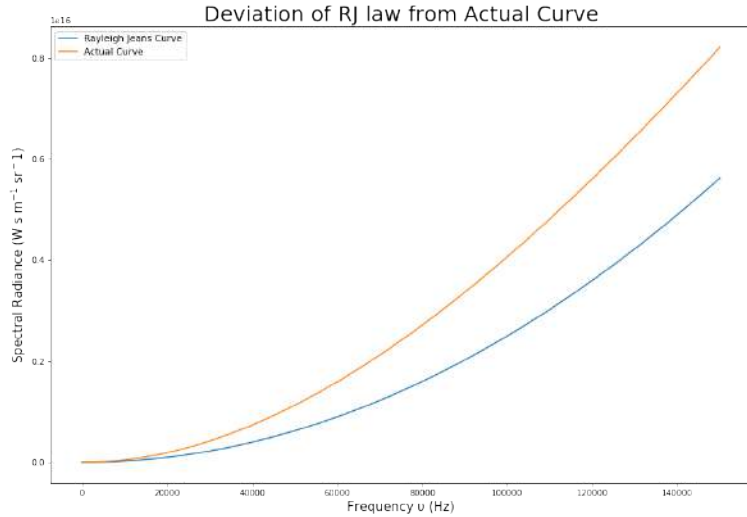


Figure 1.4: Plot comparing the curve given by the Rayleigh Jeans law and the actual curve for blackbody radiation. We let $h = c = k = 1$

1.4 The resolution: a derivation of Planck's Law and Energy Quantisation

1.4.1 Standard Derivation

The only flaw in the argument adopted during the derivation of the Rayleigh-Jeans law is we assumed that each mode had a continuous spectrum of energy. To resolve the UV catastrophe, Max Planck's postulated like others (such as Albert Einstein, who in 1905 postulated quantisation of the energy of photons to explain the photoelectric effect¹²) that the energy of these modes was "quantised", satisfying:

$$E = n \underbrace{hv}_{\text{photon energy}} , \quad n \in \mathbb{N} \quad (1.25)$$

where h is Planck's constant. Therefore, Planck postulated that all energies were integer multiples of the energy of a single photon hv . The new probability distribution is not continuous anymore, it is discrete. Hence we shall not use integration to evaluate the average energy of one mode, but we shall use infinite sums. We have:

$$H = Ce^{\frac{-nhv}{kT}} \quad (1.26)$$

so that

$$\langle H \rangle = \frac{\sum_{n=0}^{\infty} nhv \cdot P(H)}{\sum_{n=0}^{\infty} P(H)} = -\frac{d}{d\beta} \ln \left(\sum_{n=0}^{\infty} (e^{-\beta h v})^n \right) = -\frac{d}{d\beta} \ln (1 - e^{-\beta h v}) = \frac{h v}{e^{\frac{h v}{k T}} - 1} \quad (1.27)$$

Thus, replacing kT with $\frac{h v}{e^{\frac{h v}{k T}} - 1}$ we get:

$$u_v(T) = \frac{8\pi v^2}{c^3} \left(\frac{h v}{e^{\frac{h v}{k T}} - 1} \right) \quad (1.28)$$

and finally we reach the famous result:

Planck's Law of Radiation (1905)

$$B_v(T) = \frac{2v^2}{c^2} \left(\frac{h v}{e^{\frac{h v}{k T}} - 1} \right) \quad (1.29)$$

Note that Planck's law can be rewritten as:

$$B_v(T) = \underbrace{\frac{2v^2 k T}{c^2}}_{\text{Rayleigh-Jeans}} \underbrace{\left(\frac{h v}{e^{\frac{h v}{k T}} - 1} \right)}_{\text{quantum correction factor}} \quad (1.30)$$

where we have written on the left the Rayleigh Jeans equation, and next to it the quantum correction factor derived by Planck. Note that for low frequencies, the quantum corrector factor is negligible, whereas for higher frequencies it is considerably large. This hints to the fact that the Rayleigh-Jeans equation could indeed be derived from Planck's law using Taylor Series approximations for $\beta h v \ll 1$.

1.4.2 Bose-Einstein Statistics and a new derivation

We could have also derived this result using Bose-Einstein distribution, following the video by Dermot O'Reilly.¹³

Bose-Einstein Distribution

$$N(H) = g(H) \underbrace{\left(\frac{1}{e^{\beta H} - 1} \right)}_{\text{Bose-Einstein factor}} , \quad \beta = \frac{1}{k T} \quad (1.31)$$

Let us now discuss the physical interpretation of this equation, with the help of Figure 1.5. The Bose-Einstein distribution tells us that the expected number of particles (in our case modes) in energy state H is given in (1.36), where $\beta = \frac{1}{k T}$ is the "coldness factor", and where k is the Boltzmann constant. Firstly, note that the term $g(H)$ is known as the "degeneracy" of the energy level. This degeneracy is defined to be the number of energy states per unit volume

corresponding to the same energy level. Hence, it is equal to:

$$g(H) = \frac{dN_H}{dH} \quad (1.32)$$

since we are trying to find the number of energy states (N_H) corresponding to one energy level H . It may be viewed as a density of energy states per energy level (in our case energy level H). To the

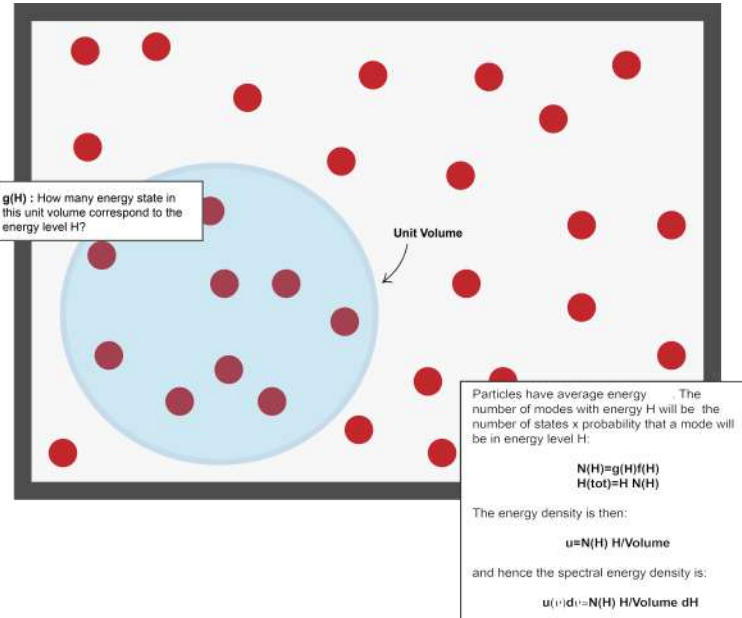


Figure 1.5: Explanation of Bose Einstein Distribution, showing the analogous of our model for particles.

right of $g(H)$ we have a "Bose-Einstein factor". This is the probability of finding a particle with energy level H . This distribution now makes sense. We are multiplying the **number of energy states** per unit volume with energy level H , and multiplying it by the probability of a **particle** having that **energy level**, to get the **number of particles in the energy level H** , $N(H)$. Please note the difference between energy state and energy level. One particle is in one energy state, but different energy states may correspond to the same energy level. Hence we might have various particles with the same energy level, which is why we're calculating the density of energy states corresponding to the energy level H and not state. Consider the derivation of equation (1.11). Integrating over the whole octant of the sphere, we get the number of allowed energy states:

$$N_H = 2\left(\frac{1}{8}\right)\left(\frac{4}{3}\pi R^3\right) = \frac{\pi R^3}{3} \quad (1.33)$$

Using de Broglie relations:

$$E = hv = \frac{hcR}{2L} \quad (1.34)$$

and plugging into (1.25) we get:

$$N_H = \frac{8\pi L^3}{3h^3 c^3} E^3 \quad (1.35)$$

We can now calculate the density of energy states/degeneracy of energy states by taking the derivative of N_H with respect to H as explained earlier:

$$g(H) = \frac{dN_H}{dH} = \frac{8\pi L^3}{h^3 c^3} H^2 \quad (1.36)$$

We now have all the information needed for the Bose-Einstein distribution. Substituting into (1.31):

$$N(H) = \frac{8\pi L^3}{h^3 c^3} H^2 \left(\frac{1}{e^{\frac{H}{kT}} - 1} \right) \quad (1.37)$$

This gives the expected number of modes with energy H . The expected number of modes with energy between H and $H + dH$ is then:

$$N(H)d(H) = \frac{8\pi L^3}{h^3 c^3} H^3 \left(\frac{1}{e^{\frac{H}{kT}} - 1} \right) dH \quad (1.38)$$

The total energy is then the integral from 0 to ∞ of $\overbrace{N(H)dH}^{\text{no. modes in range}} H$. This is because we're making the energy of the modes in the energy range dH vary from null to infinity. Note that this assumption for the energy of a mode doesn't allow for negative absolute temperatures. Indeed, for there to be a negative temperature, modes must have an upper bound to their energy level,¹⁴ a condition that isn't satisfied in this derivation. We then get that the total energy of all modes in the box is given by:

$$H_{tot} = \int_0^\infty \frac{8\pi L^3}{h^3 c^3} H^3 \left(\frac{1}{e^{\frac{H}{kT}} - 1} \right) dH \quad (1.39)$$

Let us use the fact that the total energy of the system per unit volume is equal to the energy density of the modes. The energy density is then equal to the spectral energy density integrated over all frequencies. Therefore, we get:

$$\int_0^\infty u_v(T)dv = \frac{H_{tot}}{L^3} = \int_0^\infty \frac{8\pi H^3}{h^3 c^3} \left(\frac{1}{e^{\frac{H}{kT}} - 1} \right) dH \quad (1.40)$$

and finally, using the fact that $dH = h dv$ we get that:

$$u_v(T)dv = \frac{8\pi H^3}{h^3 c^3} \left(\frac{1}{e^{\frac{H}{kT}} - 1} \right) h dv \quad (1.41)$$

which gives:

$$u_v(T) = \frac{8\pi h v^3}{c^3} \left(\frac{1}{e^{\frac{H}{kT}} - 1} \right)$$

as found earlier. Thus, we have derived Planck's law using two methods. First, we tried to analytically derive the spectral energy density $u_v(T)$, and then use its relationship with spectral

radiance to derive a final expression. The second method resorted to the Bose-Einstein distribution, and then used the relationship between total energy and spectral energy density to work back to the required expression.

Integrating over infinity to cover all frequencies emitted by a perfect black body at temperature T , we get:

$$B(T) = \int_0^\infty B_v(T)dv = \sigma T^4 \quad (1.42)$$

where $\sigma = \frac{2\pi^5 k^4}{15c^2 h^3}$ is a constant which will be derived in the next section. If we had integrated the Rayleigh Jeans equation, we would have gotten a divergent result:

$$B(T) = \int_0^\infty B_v(T)dv \longrightarrow \infty \quad (1.43)$$

1.5 Wien's Approximation, Raleigh-Jeans Law and the Stephan Boltzmann Law

Now that we have derived Planck's law, one may wonder whether or not it is possible to derive more "primitive" forms of this formula, namely the By adopting simple Taylor Expansions about 0 (for the Rayleigh-Jeans law), or assuming $v \gg$, we can easily go back to the two previous identities, following once again Dermot O'Reilly lecture¹³ and notes from the NRAO.⁹

Let us start with the Rayleigh-Jeans Law. Starting from Planck's law

$$B_v(T) = \frac{2v^2}{c^2} \left(\frac{hv}{e^{\frac{nhv}{kT}} - 1} \right) \quad (1.44)$$

let us now assume that $\beta hv \ll 1$, as in the case for low frequency radiation. Then, we can use Taylor expansions for the Bose Einstein factor to simplify out the expression:

$$B_v(T) \approx \frac{2v^2}{c^2} \left(\frac{hv}{1 + \beta hv + \frac{1}{2}(\beta hv)^2 - 1} \right) = \frac{2v^2 kT}{c^2} \quad (1.45)$$

which is the Rayleigh Jeans Law we had derived earlier. Through this derivation, however, it is easy to see why this approximation works well for low frequencies and long wavelengths.

Let us now consider once again Planck's law:

$$B_v(T) = \frac{2v^2 hv}{c^2} \left(\frac{1}{e^{\frac{nhv}{kT}} - 1} \right) = \frac{2v^2 hv}{c^2} \left(\frac{e^{-\beta hv}}{1 - e^{-\beta hv}} \right) \quad (1.46)$$

Let us now assume that $\beta hv \gg 0$, as in the case for high frequency radiation. We find:

$$B_v(T) = \frac{2v^2 hv}{c^2} \left(\frac{e^{-\beta hv}}{1 - e^{-\beta hv}} \right)^0 = \frac{2v^2 hv e^{-\beta hv}}{c^2} \quad (1.47)$$

We have now reached the Wien Approximation:

Wien's Approximation

$$B_v(T) = \frac{2v^2hv}{c^2} e^{-\beta hv} \quad (1.48)$$

Note that Wien's approximation works perfectly for higher frequencies and lower wavelengths, but starts to break down at lower frequencies. Hence it is "complementary" to the Rayleigh-Jeans equation. There was another important result derived by Willhelm Wien, *Wien's Displacement Law*.⁶ Note that the radiation curve for each temperature has a wavelength/frequency which yields the highest radiance. The displacement law gives a formula for this wavelength λ_{max} . Recall once more Wien's approximation:

$$B_v(T) = \frac{2v^2hv}{c^2} e^{-\beta hv} \quad (1.49)$$

At the "peak" of the curve, we have that $\frac{\partial B_v}{\partial \lambda}|_{\lambda_{max}} = 0$, thus:

$$\frac{\partial B_v}{\partial \lambda} = 2hc^3 \left(\frac{-5}{\lambda^6} e^{-\beta hv} + \frac{2hc^3}{\lambda^5} e^{-\beta hv} \frac{\beta hc}{\lambda^2} \right) = \left(-\frac{5}{\lambda^6} + \frac{\beta hc}{\lambda^7} \right) 2hc^3 e^{-\beta hv} \quad (1.50)$$

Setting this equal to zero yields:

$$\frac{\beta hc}{\lambda^7} = \frac{5}{\lambda^6} \implies \lambda = \frac{\beta hc}{5} \quad (1.51)$$

Finally, we get:

$$\lambda_{max} = \frac{hc}{5kT} \quad (1.52)$$

Note that if we had used Planck's law, we would have gotten a different result for the factor in the denominator, although this deviation is almost negligible. Indeed, using Planck's law, Wien's displacement law becomes

$$\lambda_{max} = \frac{hc}{xkT} \quad (1.53)$$

where $x \approx 4.965$. Moreover, if we had used Rayleigh-Jeans law, we clearly would not have gotten a value for λ_{max} , demonstrating another fallacy in the result.

Now, imagine drawing infinite radiation curves for every temperature on the Kelvin scale, and then connecting the peaks, the λ_{max} points. Then, what function would we expect to achieve? Looking at Wien's displacement law it is easy to see that this function would be a hyperbola with asymptotes as the y-x axes. Taking once again its derivative we get $\frac{d\lambda}{dT} = -\frac{hc}{5kT^2}$. As the temperature increases, the peak of the radiation curve moves to the left (as expected from the shape of the hyperbola obtained from (1.53)).

Finally, we shall now derive an expression for the power (per unit area) radiated from thermal radiation, the *Stephan-Boltzmann law*. Indeed, note that the radiated power per unit area is equal

to the integral of Planck's law for spectral radiance, over all wavelengths/frequencies:

$$\frac{P}{A} = \int_0^\infty I_v(T)dv = \frac{2\pi k^4 T^4}{h^3 c^2} \frac{\pi^4}{15} \quad (1.54)$$

where we have used the result that $\int_0^\infty \frac{x^3}{e^x - 1} = \frac{\pi^4}{14}$.

Rewriting, we get the famous result for *radiant emittance*, or intensity of radiation:

Stephan Boltzmann Law

$$\frac{P}{A} = \sigma T^4, \quad \sigma = \frac{2\pi^5 k^4}{15c^2 h^3} \quad (1.55)$$

The Stephan Boltzmann law gives us the "radiant emittance" of a body at a temperature T. The reasoning behind the fourth power is clear using dimensional analysis. The energy of a particle is simply kT (following classical mechanics), time can be expressed as $\frac{h}{E} = \frac{h}{kT}$, so that power is $\frac{(kT)^2}{h}$. Length can be expressed as "speed times time", hence $c \frac{h}{kT}$, so that area is length squared, $(c \frac{h}{kT})^2$. Dividing power by area we get the desired result (with the negligence of the constant σ).

We have now concluded our study of black-body radiation. To summarize, any body with non-zero absolute temperature will emit thermal radiation. Some special bodies, "black bodies", will absorb all incident electromagnetic radiation, and emit it in the form of black body radiation. This gives an explanation for the glow of metals when heated by a blacksmith, or the glow of fire as well (as we shall see at the end of the chapter). There were mainly two laws trying to describe this type of radiation, the Rayleigh Jeans law and Wien's approximation. Both however failed considerably at one end of the spectrum. This problem would be solved with the introduction of *energy quantisation* by Max Planck, who derived a new Law of radiation in 1905. This was a mathematical model which fit perfectly with all the experimental data that had been collected.⁵

1.6 Flame Spectroscopy: deriving Rydberg's formula

We will now continue our study by investigation emission spectroscopy, and its relation with flames. Emission spectroscopy, as the name suggests, is the study of the electromagnetic radiation emitted when an atom is transitioning from a high energy level to a low energy level. By analysing the spectrum of wavelengths from the emitted radiation, one can determine the elemental composition of a substance. This is because each element has a specific individual emission spectrum, analogous to human fingerprints, which can be used to identify an unknown compound.¹⁵

There are many ways to perform emission spectroscopy, flame tests being among the oldest (first used by Robert Bunsen in 1859¹⁶). During flame spectroscopy, the substance is placed on a wire (usually nichrome wire), and then placed on a non-luminous flame. It is important to note

this distinction regarding luminous and non-luminous flames. The former is visible by the naked eye, and most of the radiation emitted has wavelength in the visible spectrum. Non-luminous flames, instead, are not visible by the naked eye. Hence, the reason a non-luminous flame is used is simply to avoid the flame's colour due to the excitation of the compound being confused with the flame's natural colour.¹⁶

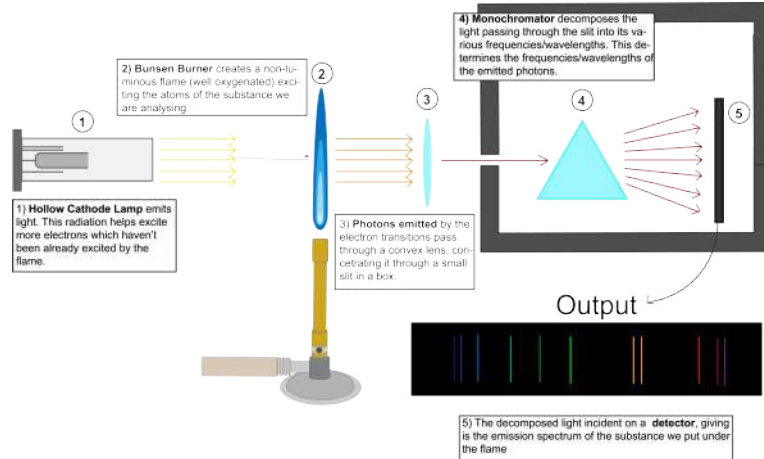


Figure 1.6: Apparatus for Flame Spectroscopy

Let us now consider what is actually happening during a flame spectroscopy. When the substance is put on the flame, we are adding thermal energy to the system. Hence, the electrons in the substance go through a process of excitation, moving from their ground state to excited levels. The electron however is in a very unstable state, and thus jumps back to its ground state, this is "de-excitation". Due to the principle conservation of energy, this energy level transition must release energy in the form of electromagnetic radiation. It follows that the energy of the radiation emitted by the electron during its de-excitation must be equal to the difference in the electron's energy between the two energy levels.

According to this "jump" from one energy level to another, the emitted radiation will have different wavelengths, giving the flame its distinct colour when analyzing substance. When we then concentrate the light emitted by the flame into a prism (in its classical set up, a flame test would do so using a telescope), we have "emission spectrum lines". Each line represents the wavelength of the emitted radiation. Since there are various possible transitions for the electron, we will have various spectral lines.¹⁵

Let us now try to derive a relation between the wavelength of this radiation, and the transition in the energy levels, closely following a derivation given by the NRAO (National Radio Astronomy Observatory).⁹

Consider an electron of charge $-e$ and mass m , revolving at a velocity v_N at a radius r_N from the nucleus with mass M and charge $+e$. Then, let us hypothesize that the angular momentum

of the electron is quantized, given by the relation:

$$L_N = \frac{Nh}{2\pi} \quad (1.56)$$

Equating the forces acting radially on the electron:

$$m \frac{v_N^2}{r_N} = \frac{e^2}{4\pi\epsilon_0 r_N^2} \quad (1.57)$$

These two latter equations yield the speed and radius of the electron:

$$v_N = \frac{e^2}{2\epsilon_0 nh}, \quad r_N = \frac{\epsilon_0 n^2 h^2}{\pi m e^2} \quad (1.58)$$

The energy of an electron in the n th energy level is then:

$$E_N = -\frac{me^4}{8\epsilon_0^2 n^2 h^2} \quad (1.59)$$

Then, for an electron moving from the n th energy level to the q th energy level:

$$\Delta E = \frac{me^4}{8\epsilon_0 h^2} \left(\frac{1}{q^2} - \frac{1}{n^2} \right) = hv \quad (1.60)$$

where we equated the change in energy to the energy of the emitted photon. Using the fact that $c = v\lambda$, we get the Rydberg-Balmer formula:

Rydberg-Balmer Formula

$$\frac{1}{\lambda} = \frac{me^4}{8c\epsilon_0^2 h^3} \left(\frac{1}{q^2} - \frac{1}{n^2} \right) \quad (1.61)$$

where $\frac{me^4}{8c\epsilon_0^2 h^3}$ is the Rydberg constant ($R \approx 1.097 \times 10^7 \text{ m}^{-1}$). Note that this equation works perfectly well with Hydrogen atoms and hydrogen-like atoms with only one electron. Instead, when we add multiple electrons, the Rydberg-Balmer formula soon starts to break down, due to omission of quantum interactions.

We can also derive an expression for the spontaneous emission rate of electrons. Let $n = q + \delta q$, so that when $\delta q \ll q$ (hence for small transitions), the Rydberg equation can be approximated to:

$$v = R \left(\frac{1}{q^2} - \frac{1}{(q + \delta q)^2} \right) \approx R \left(\frac{q^2 + 2q\delta q + (\delta q)^2 - q^2}{q^2(q^2 + 2q\delta q + (\delta q)^2)} \right) \approx \frac{2R\delta q}{q^3} \quad (1.62)$$

Then, the radiated power by an electron is given by Larmor's formula:

$$P = \frac{q^2 a^2}{6\pi\epsilon_0 c^3} \quad (1.63)$$

In our case, we have an oscillating dipole, hence it has dipole moment $er_N \sin(wt)$, so that the time averaged power is:

$$\langle P \rangle = \overbrace{\frac{e^2}{6\pi\epsilon_0 c^2} (w^2 r_N)^2}^{\text{acceleration}} \langle \cos^2(wt) \rangle = \frac{e^2}{12\pi\epsilon_0 c^3} \left(\frac{\epsilon_0 q^2 h^2}{\pi m e^2} \right)^2 (2\pi\nu)^4 \quad (1.64)$$

Then, we have that the spontaneous emission rate from q to $q-1$, which we shall denote as $T_{q,q-1}$ is equal to the power emitted by one electron over by the energy emitted during the transition (the energy of one photon). Hence:

$$T_{q,q-1} = \frac{\frac{e^2}{12\pi\epsilon_0 c^3} \left(\frac{\epsilon_0 q^2 h^2}{\pi m e^2} \right)^2 (2\pi\nu)^4}{h\nu} = \frac{4e^2 \left(\frac{\epsilon_0 q^2 h^2}{\pi m e^2} \right)^2 \pi^4 \nu^3}{3h\pi\epsilon_0 c^2} \quad (1.65)$$

This finally reduces down to:

$$A_{t,t-1} = \frac{\pi m^3 e^{10}}{48c^5 n^5 \epsilon_0^4 h^6} \quad (1.66)$$

1.7 Spectral Lines of Hydrogenic Atoms

Now that we have derived the Rydberg Balmer formula, it is quite simple to explain what exactly is going on in the emission spectrum of hydrogen. Indeed, observing typical spectral lines, each coloured line represents a jump from one energy level to another. One might wonder how a hydrogen atom with one electron may produce various spectral lines. In truth, the number of electrons in an atom doesn't effect the number of spectral lines, the number of allowed energy levels does.

As can be seen from the Figure 1.7, we can let the electron jump from an arbitrary energy level n to its ground state. It turns out that for a hydrogen atom, as we increase the principal quantum number (higher energy level), we get that to return back to its ground state the electron emits a convergent wavelength of radiation. It is important to note that this is the shortest wavelength in the series. The wavelengths of transitions back to the ground state is known as the Lyman series, and this convergent wavelength when $n \rightarrow \infty$ (which we shall denote as $Ly_\infty \approx 91.13$ nm). Indeed, using the Rydberg-Balmer formula, it is easy to see that:

$$\frac{1}{\lambda} = \lim_{n \rightarrow \infty} \frac{me^4}{8ce_0^2 h^3} \left(\frac{1}{n^2} - 1 \right) \implies \lambda = \frac{8ce_0^2 h^3}{me^4} \quad (1.67)$$

giving the desired result. The same process can be used to evaluate the wavelength emitted when an electron transitions back to its second energy level, giving the *Balmer Series*. As we increase the principal quantum number, we get a convergent wavelength equal to 364.51 nm (denoted H_∞). Notice that this is in the visible spectrum. This means that some spectral lines in the Balmer series must be visible to the naked eye, and that is indeed true. There are four lines in this series that are in the visible spectrum, as can be seen in figure .

It is also important to note that each spectral line in the hydrogen emission spectrum has a particular name, depending on what series it belongs to. Any transition from an excited state to the ground state belongs to the *Lyman series*. The transition from $2 \rightarrow 1$ will have wavelength 121.57 nm, and is called the Ly α line (Lyman alpha line). The transition from $3 \rightarrow 1$ is the Ly β line and so on. This means that all transitions in the Lyman series will lie in the ultraviolet band, since the wavelength must lie in the interval $[Ly_{\infty}, Ly\alpha]$, which ranges from the shortest wavelength in the series Ly ∞ , to the longest Ly α .

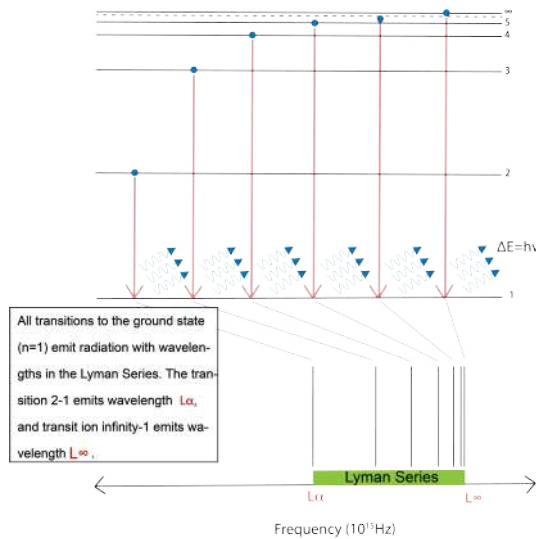


Figure 1.7: Phase transitions in Lyman series, and the corresponding spectral lines.

The same applies to the Balmer series. Any transition to the second energy level will fall into the Balmer series. The transition from $3 \rightarrow 2$ is the Ba α , it is the red line seen in the visible spectral lines for Hydrogen. Notice that for the Balmer series, the wavelengths lie in the range $[H_{\infty}, H\alpha]$, which spans across both the visible band and the UV band. The spectral lines in the visible spectrum are the transitions $n \rightarrow 2$ where $n = 3, 4, 5, 6$. This whole process can be applied to all series, which are in fact infinite. (We also have another method of naming spectral lines, mostly adopted by astronomers. Let α denote the transition $n + 1 \rightarrow n$, β denote the transition $n + 2 \rightarrow n$ and so forth. Then, the spectral line is named H(greek letter) n . For a transition $34 \rightarrow 31$, we have H31 γ)⁹

One might wonder why we have, out of virtually infinite lines in the Balmer series, only four in the visible spectrum. This is because as the energy level from which the electron transitions increases (as the principal number increases), the energy difference grows smaller. Consider once again the Rydberg formula. We can re-write (1.59) as:

$$E_N = -\frac{R_E}{n^2} \quad (1.68)$$

where R_E is known as the Rydberg Energy ($R_E \approx 13.6\text{eV}$). This is the energy of an electron in a hydrogenic atom in its ground state (this is easy to see by setting $n = 1$). Then, as we

increase the principal quantum number n , we have a smaller and smaller difference in the energy. In other words, the energy levels grow closer and closer together. This must also mean that the wavelengths from transitions must grow closer and closer as n increases, explaining why we have a convergent result when approaching infinity. Thus, we have that the wavelength grow closer and closer in the same series, so that the initial spectral lines (for the Balmer series, $H\alpha$, $H\beta$, $H\gamma$ etc...) must be farther apart than other spectral lines. Due to this uneven distribution, there are less lines in the visible spectrum than in the UV spectrum.

To summarize, when adding energy to an atom, the electrons jump to a higher energy level, and then jump back down to their original state. Throughout this process of atomic de-excitation, the electron must release energy in form of electromagnetic radiation. By equating the difference in energy between two levels to the energy of a photon, we are able to derive the wavelength of such radiation, the Rydberg-Balmer formula. This works quite well for hydrogenic atoms (which have only one electron). The group of all these wavelengths forms an emission spectrum, made up of individual spectral lines corresponding to a single transition. These spectral lines can then be grouped into series, depending on which level the electron fall back to (Lyman series if it falls back to its ground state, Balmer series if it falls to 2nd energy level and so forth). The wavelengths in a series "X" must lie in the range

$$[X_\infty, X_\alpha] \quad (1.69)$$

where X_∞ is the shortest wavelength obtained in the series by setting $n = \infty$, and X_α is the longest wavelength obtained by setting $n = i+1$ (where i is the energy level to which all electrons fall back to in the series).

1.8 Flames in microgravity, and other phenomena of fire

Let us now investigate the last phenomenon regarding fire. Consider a standard flame on Earth. When we ignite the candle, some wax surrounding the wick is melted, and this now liquid wax rises up the wick through capillary motion, approximately following Jurin's law which gives the height of a liquid in a column. If we model the fibers in the wick to be approximate columns, then the height to which the wax absorbed by the wick rises is:

$$h = \frac{2\gamma \cos \theta}{\rho g r} \quad (1.70)$$

When the fuel (wax in our case) reaches the flame, it vaporizes and turns into gas. Notice that in microgravity as $g \approx 0$, we have that the liquid would fill the capillary tube. Throughout this process, the heat of the flame breaks down the molecular bonds in the fuel, breaking it down into hydrogen and carbon atoms, and then react with the oxygen surrounding the flame. In a sense, the hydrogen and carbon atoms snap away, by adding heat to these molecules, the individual atoms can overcome the intramolecular forces and "break". We should stop here to investigate

more deeply how this combustion process is occurring. Indeed, one often finds heat included in the equation for combustion, which is completely correct. When oxygen atoms hit the carbon atoms and the hydrogen atoms that have snapped away, one doesn't expect an actual combustion to happen. This is because the oxygen must hit the hydrogen atoms with sufficient energy. This is clear if we consider the principle of conservation of energy. By hitting the hydrogen atoms with energy, it can then be converted into thermal energy during the chemical reaction. By hitting the hydrogen atoms with enough energy, they are able to react together, and form water molecules. This heat increases the kinetic energy of the system, and hence more and more oxygen atoms can hit these hydrogen atoms, snap together, and form water molecules. The same reasoning applies for carbon atoms and oxygen atoms. Therefore, it follows that this is an exothermic reaction, and thus in addition to carbon dioxide and water (in a gaseous state), heat is also radiated outwards. If there is a poor oxygen/fuel supply, then we have an incomplete combustion. Not all of the fuel or oxygen is combusted, and hence there are some other products to the reaction, mainly carbon particles called soot which haven't reacted completely, and hence escape. This process repeats cyclically, as the heat from the combustion reaction melts more wax, which in turn is drawn up by the wick and so forth. Consider the air surrounding the flame. As it gets warmed up, it moves up, displacing the colder air down.¹⁷ Let us consider an "air packet". By the Ideal Gas Law, the pressure of a gas at a temperature T and density ρ :

$$PV = nRT \implies P = \rho RT \quad (1.71)$$

Let us now consider the net force acting on an object of mass m , density ρ_m immersed in a liquid of density ρ_l :

$$F = -mg + \rho_l Vg \quad (1.72)$$

Thus, we find that, by equating this expression to Newton's Second Law, we get for the acceleration of the object (taking upward direction as positive):

$$a = g \left(\frac{\rho_l}{\rho_m} - 1 \right) \quad (1.73)$$

Then, $a > 0$ whenever $\rho_l > \rho_m$. Hot air particles have more kinetic energy, and the gas expands if we don't have considerable restraints on volume. Consequently, since hot air is less dense than the colder air, it will rise. This problem can also be approached from a statistical mechanics point of view. Particles in hot air have a higher temperature, and therefore a higher kinetic energy. These particles then have more energy to convert into potential gravitational energy and rise compared to cold air. Hence, they have a higher probability to "occupy" more potential energy. The air at the base of the flame gets heated, and hence by the process described earlier, must rise up, and the colder oxygen must fall back to the base of the flame (feeding it), creating a convection current. These currents cause the "tear drop" shape of a flame on Earth. Moreover, the soot (carbon particles) are dragged by the currents upwards, and burn at the tip of the flame, giving it a yellowish tone. Indeed, it is mostly thanks to black-body radiation and atomic

excitation/de-excitation that flames have distinct colours. The soot particles get heated up by the flame, and start to glow! In both cases, we know that temperature plays a role in determining this colour, as well as the fuel used.

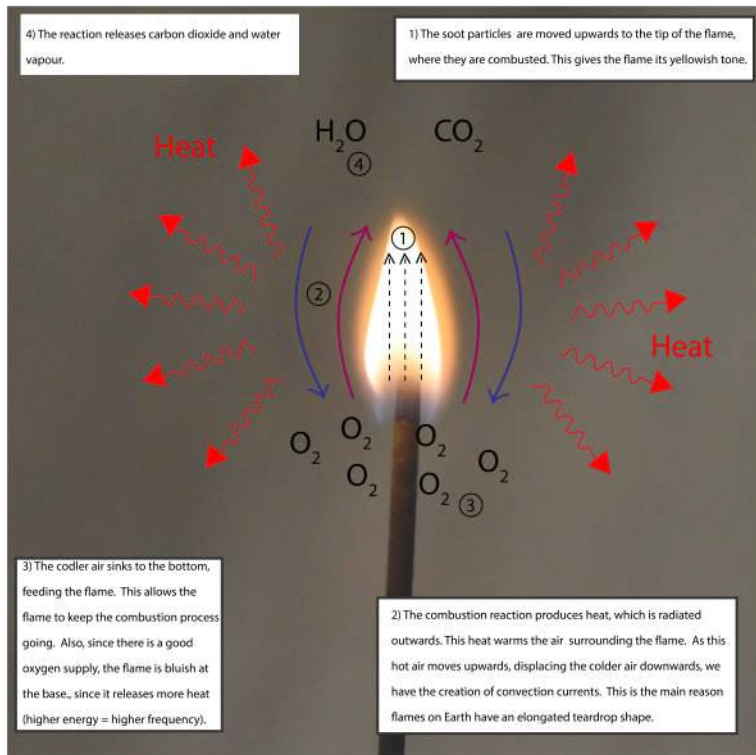


Figure 1.8: Photograph of a Flame and explanation of how combustion works

It is therefore interesting to ask ourselves what would happen if we lit a candle in outer space, where gravity doesn't act on the flame. Indeed, this has been the inquiry question of various experiments conducted by NASA on the International Space Station, the FLEX experiments. These experiments have shown that fire in spaces behaves very differently compared to Earth. In a research¹⁸ conducted by A. Alsairafi, J.S. T'ien, S.T. Lee, D.L. Dietrich and H.D. Ross, a model for a laminar symmetric flame with wick of diameter 1mm, length 5mm, it was shown that the flame would get elongated as gravitational acceleration increased from $0g$ to $3g$, and then decreased from $3g$ and $60g$, and then blows off (observe Figure 1.6, taken from their paper¹⁸). This was done by employing the Navier Stokes equations.

Since there is no gravity acting on the flame, these convection currents don't form. The hot gases and the cold gases don't move, but pile up around the flame. Hence, the flame, radiating heat spherically, will have a spherical shape, there is no set of axis pointing "up" for currents. The flame takes its natural spherical shape. The reason the flame blows off or weakens at enhanced gravity is because capillary action isn't strong enough to draw off the liquid wax to the top of

the wick (which is easy to see observing Jurin's law, where $h \propto \frac{1}{g}$). It is also interesting to notice that the flame is not yellow/orange, but it is blue, with rare sudden "bursts". This is because the combustion is complete, and indeed the short yellow bursts are actually soot particles which are then combusted completely. You might remember that the flame in a typical stove is indeed blue, with some small yellowish bursts at the tip. This is the same process, but under the influence of gravity. The combustion is complete, all the fuel is combusted, and hence we have an exothermic reaction releasing high quantities of heat. One might be wondering why complete combustions have bluish flames. Hotter flames excite their electrons to higher energy levels. Hence, when they transition back to their original states, a lot of energy in form of electromagnetic radiation is released. Hence, the radiation must have a high frequency, which lies in the bluish range of the spectrum, giving the flame this colour. Note that this emission also happens when soot is combusted, but it is contrasted by the Black body radiation, and hence is often neglected.

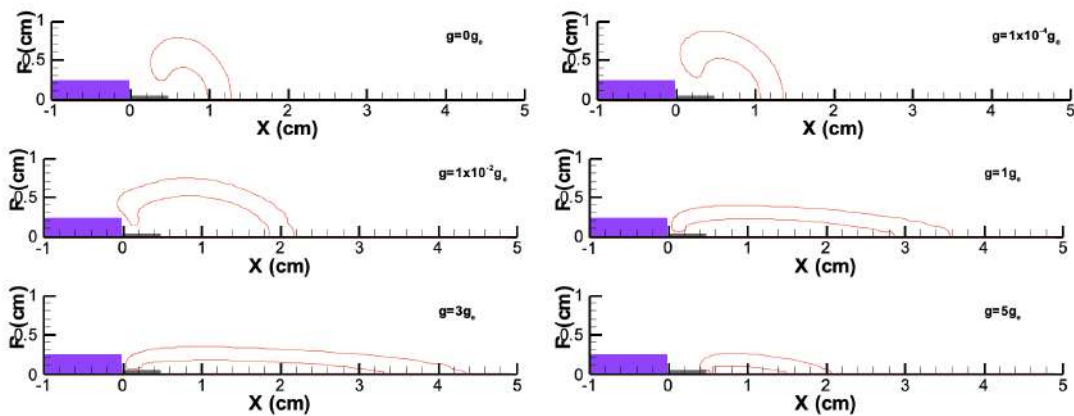


Figure 1.9: Fuel reaction rate contours for a symmetrical laminar flame, at varying gravitational fields. Taken from A. Alsairafi, J.S. T'ien, S.T. Lee, D.L. Dietrich and H.D. Ross. "Modelling Candle Flame Behaviour in Variable Gravity", presented at the "Seventh International Workshop on Microgravity Combustion and Chemically Reacting Systems", 2003. p. 263

1.9 Conclusion

We can now answer some of the questions posed at the beginning of the chapter after having discussed the main phenomena that govern how fire works. We have already answered what gives fire its shape in its previous question. Convection currents are formed when air surrounding the flame is heated, giving it a tear drop shape, and "stretching" it upwards. we shall now attempt to answer what gives a flame its colour. This happens mostly, as mentioned previously, through two processes, Black-body radiation (for lower temperature regions) and Atomic excitation (for higher temperature regions).

Consider a flame subdivided into regions according to its temperature.¹⁹ The base of the flame, the *non-luminous* zone has a temperature of around 600°C, it is the coolest part. The

radiation doesn't have a long enough wavelength to be detected by the naked eye, and hence is non-luminous. This zone is surrounded by the *blue zone*, which (as explained earlier) has a very good supply of oxygen, and has an approximate temperature of 800 ° C. The heat from this zone breaks down the hydrocarbons in the wax. The hydrogen atoms snap away first, and combines with oxygen atoms to form water vapour. Carbon instead may then form carbon dioxide, or, if uncombusted, form soot particles. The creation of these soot particles, however, occurs mostly in the *dark orange* region, with temperature of around 1000 °C. Evidently, black body radiation occurs mostly as the soot particles move from the dark region to the luminous zone, heating up and consequently glowing until they reach the tip of the flame. This gives it its orange-yellowish colour. We then have the *luminous zone*, which is yellowish/white at the center. This is where impartial combustion occurs, explaining its colour. The atoms aren't excited enough, and hence the frequency of the resulting electromagnetic radiation is low. Temperatures range around 1200 °C in this zone. Finally, we reach the hottest zone of the flame, the *veil*. This layer surrounds the luminous zone, and reaches temperatures of approximately 1400 ° C . Complete combustion occurs here, and hence the wavelength of the electromagnetic radiation is high enough that it may not be visible, which is why it is "non-luminous".

Chapter 2

Surface Tension

Contents

2.1	Defining Surface Tension	28
2.2	Deriving the Young-Laplace Equation	31
2.2.1	Floating Bodies	33
2.3	Capillary Action	36
2.3.1	Jurin's Law	36
2.3.2	The Concave Meniscus ($\theta < \frac{\pi}{2}$)	37
2.3.3	Capillary Length λ and the shape of puddles	40
2.4	Minimal Surfaces	43
2.5	Conclusion	43

2.1 Defining Surface Tension

It would be impossible for a person not to encounter the entralling phenomenon that is *surface tension*. From taking a shower to washing hands with soap, and even the movement of foam when making tea, surface tension plays a central role, governing the dynamics and statics of interactions between fluids. It is defined as:

The tension of the surface film of a liquid caused by the attraction of the particles in the surface layer by the bulk of the liquid, which tends to minimize surface area.²⁰

— Lexico Dictionary

To understand how surface tension occurs, imagine looking at a water droplet under an immensely strong electron microscope, capable of clearly displaying individual water molecules. Firstly, consider the water molecules at the center of the droplet. These will feel cohesive forces from neighbouring water molecules. Hence, they will be "pulled" in all directions and will experience no net force. Let us now consider water molecules at the edge of the droplet, adjacent to the so-called "interface" surface (an imaginary surface delimiting two phases, such as water

and air). Clearly, these molecules will experience both a cohesive force from neighbouring water molecules, but also adhesive forces from the nearby air molecules. Due to the imbalance between cohesive and adhesive forces, a net inward force will act on the outer layer of the droplet, giving it a spherical shape (see Figure 2.1)

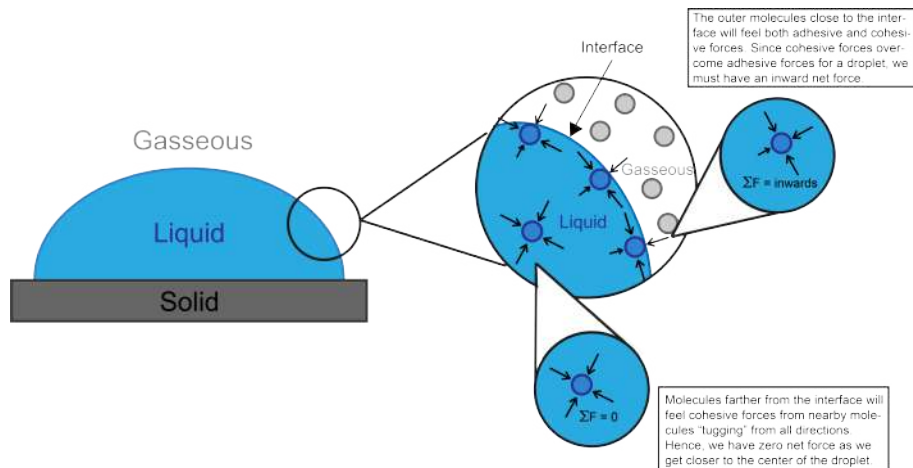


Figure 2.1: Diagram showing dynamics behind surface tension in a droplet

One might wonder why a droplet doesn't take a rectangular shape, or a pyramidal shape. The answer lies in surface optimization and the tendency of nature to minimize potential energy. Indeed, surface tension γ has units $\frac{J}{m^2}$, energy per unit area. It is the energy needed to increase the droplet's surface area. If insufficient force acts on the droplet trying to increase its surface, then it will try to minimize it, "pushing" or "resisting" against any such force.

To better illustrate this idea, consider an arbitrary volume of water. We are asked to create a surface from that volume of water requiring the least effort. To do so, it is essential to note that the molecules forming this surface will oppose resistance to any increase in surface area due to cohesive forces, especially near the interface. In other words, the greater the surface area of this surface, the more work will be done to construct it. To use the least energy, the droplet will therefore have largest possible Volume-Surface ratio, trying to fit in the volume of water in the smallest possible surface area (the problem of defining a shape with the largest volume-surface ratio is known as the *Isoperimetric Inequality*). It can be proven²¹ that the sphere has the largest $V - S$ ratio. Any liquid will naturally rearrange itself into a sphere, as it requires the least energy (more formally, it has the least *surface energy*).

By taking a spherical shape, the least work is required to increase surface area, the droplet essentially minimizes its surface energy (the energy needed to create the surface). This is quite similar to a ball rolling up a hill. When we increase the surface area of a droplet, this requires energy input, just like trying to roll a ball up a slope. If we release the ball on this slope, it will try to minimize its potential energy, and fall back down. Analogously, the droplet will try minimizing its surface energy, resisting against any attempt at increasing surface area.

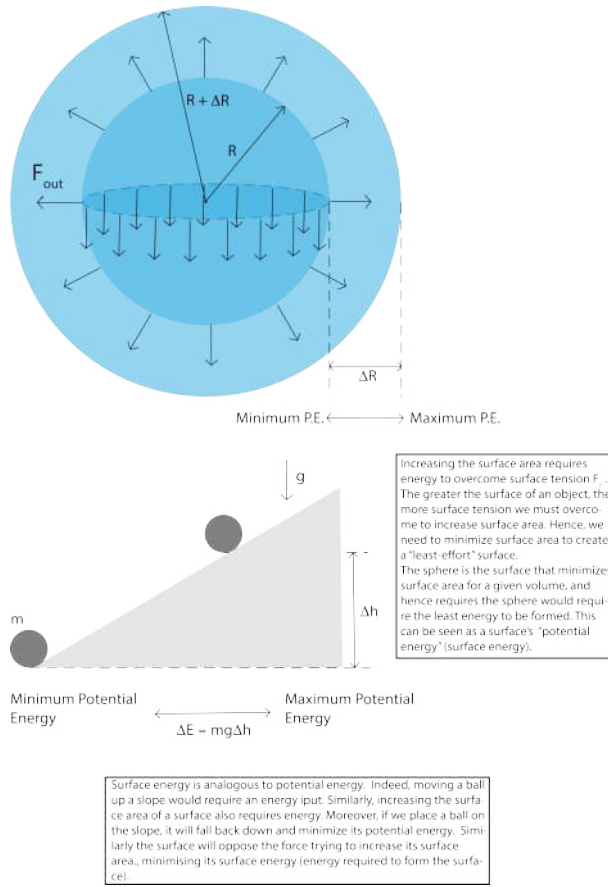


Figure 2.2: Analogy between surface energy and potential energy minimization.

We can therefore define surface tension as the energy needed to increase the surface area of a liquid by unit area. It may also be considered as the force acting against deforming the surface per unit length. The higher the surface tension of a surface is, the less it is prone to increasing its surface area.

As hinted earlier, surface tension governs several phenomena we observe daily. As soon as we wake up, we usually go to the bathroom, and wash our face/hands. The reason we use soap is not only because of its antibacterial qualities, but also because it reduces surface tension of water. Thus, when coming into contact with our hands, water will be more easily deformed, entering into the crevices and wrinkles on our palms, and removing dirt. Another common way to observe surface tension is when making tea or coffee. Indeed, the reader has probably noticed the formation of foam and bubbles on the surface of the liquid. Usually, this foam collects either at the center of the surface, or at its circumference, for reasons we will allude to later on. The goal of this chapter will be to develop the physical laws describing surface tension, and related phenomena.

2.2 Deriving the Young-Laplace Equation

We shall now derive the Young-Laplace equation, without which most of the results in the rest of the chapter wouldn't be known. We will closely follow the derivation given in *Siqvel and Skjæveland, (2015)*.²³ Surface tension can be defined as the force per unit length exerted on any fluid against increasing its surface area. Consider a curved surface, as shown below, representing the boundary between a liquid region and a gaseous region (known as the interface). Recall that when crossing this surface, there will be a change in pressure, called the Laplace Pressure (see Fig 1.3). As we can see, the internal pressure must counteract the outer atmospheric pressure, as well as the surface tension acting tangentially on its surface. This means that the pressure inside the droplet will obviously be larger than the outer pressure. Furthermore, this discontinuity in pressure when crossing the interface may also be seen as an explanation of why droplets try minimizing surface area. The internal pressure will keep increasing until it counteracts both the outward pressure and surface tension, which can be done by reducing the surface area of the droplet.

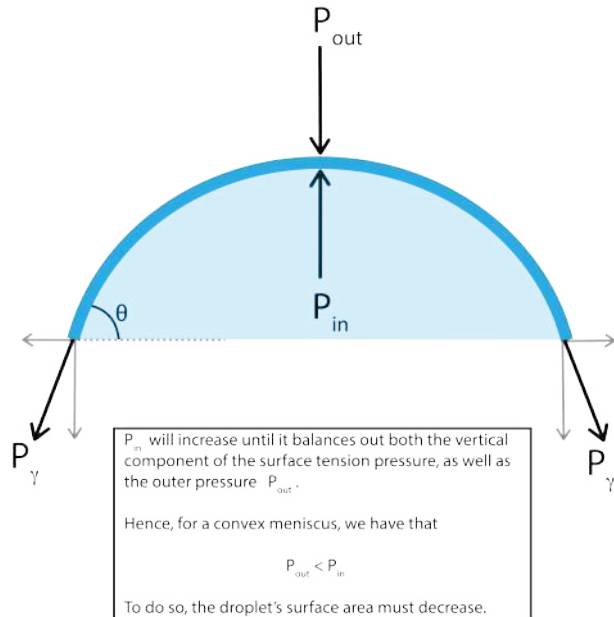


Figure 2.3: Pressure inside and outside of a spherical droplet or convex meniscus

For an infinitesimal patch of this surface, the net force F_P caused by the pressure difference ΔP will be:

$$dF_P = \Delta P dS = \Delta P dL_1 dL_2 \quad (2.1)$$

We can then use the fact that $dL_1 = 2R_1 d\theta_1$ and $dL_2 = 2R_2 d\theta_2$:

$$dF_P = \Delta P dS = \Delta P (2R_1 d\theta_1)(2R_2 d\theta_2) \quad (2.2)$$

Consider the surface tension force acting on the patch. Since we defined surface tension γ to be

the force per unit length acting on the patch, then the total surface tensile force acting on it will be $\gamma \times$ infinitesimal length:

$$dF_\gamma^{(1)} = \gamma dL_2, \quad dF_\gamma^{(2)} = \gamma dL_1 \quad (2.3)$$

We can now take the total components acting vertically against F_P . Since there will be two forces of magnitude $dF_\gamma^{(1)}$ and two forces of magnitude $dF_\gamma^{(2)}$, we get that this component is:

$$2dF_\gamma^{(1)} \sin \theta_2 + 2dF_\gamma^{(2)} \sin \theta_1 \quad (2.4)$$

Recall that surface tension acts tangentially to the surface. Hence, $dF_\gamma^{(1)}$ acts on the principal line 2, and $dF_\gamma^{(2)}$ acts on the principal line 1.

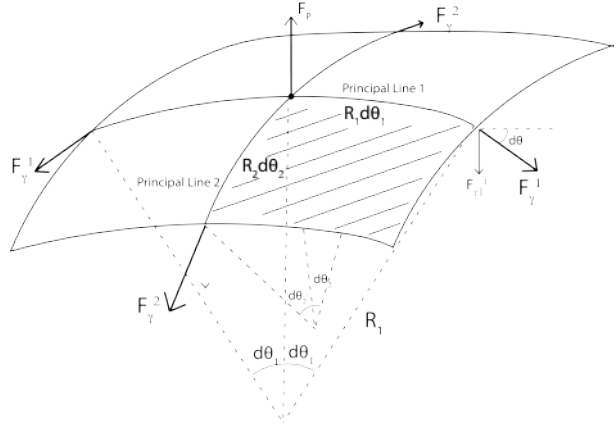


Figure 2.4: Infinitesimal patch over which surface tension acts along the edges

We then use the small angle approximation $\sin x \approx x$ for simplification, and substituting our expressions for $dL_1, 2$:

$$dF_\gamma = \gamma(2(2R_1d\theta_1)d\theta_2 + 2(2R_2d\theta_2)d\theta_1). \quad (2.5)$$

For a static droplet, we must have that: $dF_P = dF_\lambda$. Hence:

$$\overbrace{\Delta P}^{Nm^{-2}} = \underbrace{\gamma}_{Fm^{-1}} \underbrace{\frac{R_1 + R_2}{R_1 R_2}}_{m^{-1}} \quad (2.6)$$

and finally we reach the Young-Laplace equation:

Young-Laplace Equation

$$\Delta P = \gamma \left(\frac{1}{R_1} + \frac{1}{R_2} \right) \quad (2.7)$$

Let's stop a moment to analyze what this equation represents. The term on the right, ΔP , is the change in pressure when moving through the interface. On the right hand side, we have an expression with units $N \cdot m^{-2}$. This tells us that the more curved a surface is (the smaller $R_{1,2}$ are), the greater the Laplace pressure. This is expected, as we have a greater component due to

surface tension against which internal pressure must act against. This widens the gap between pressure inside and outside.

Furthermore, as $R_{1,2} \rightarrow \infty$ (we get a flat surface, a plane), we have that the Laplace pressure decreases very quickly $\Delta P \rightarrow 0$. This makes sense, and agrees with the well known result that the pressure difference acting on a flat surface must be zero for equilibrium to be satisfied, a property that isn't necessarily true for curved surfaces as demonstrated.

We extend our formula further, using some notions of differential geometry.²⁴ Note that the mean curvature of a surface at a point, H can be defined as the arithmetic mean of the minimum and maximum curvature (principal curvatures):

$$H = \frac{1}{2}(\kappa_1 + \kappa_2) \quad (2.8)$$

where κ_1, κ_2 , the principal curvatures of the surface. This then clearly yields for our patch:

$$H = \frac{1}{2}\left(\frac{1}{R_1} + \frac{1}{R_2}\right) \quad (2.9)$$

where, as discussed earlier, R_1 and R_2 are the radii of principal curvatures at point P.

$$\Delta P = \gamma(2H) \quad (2.10)$$

Using Frenet-Serret equations, we know that the mean curvature is:

$$H = -\frac{1}{2}\nabla \cdot \hat{\mathbf{n}} = -\frac{1}{2}|\nabla \cdot \left(\frac{\nabla f}{|\nabla f|}\right)| \quad (2.11)$$

which allows us to write more generally:

$$\Delta P = -\gamma(\nabla \cdot \hat{\mathbf{n}}) \quad (2.12)$$

This is a non linear partial differential equation, which relates the pressure difference through an interface and the shape of the interface surface. For positive curvature (e.g. concave meniscus), the Laplace pressure will be negative, whereas for negative curvature (e.g. convex meniscus), the Laplace pressure will be positive. Oddly, for a convex meniscus, the pressure outside is actually greater than the pressure just under the meniscus. As we will see later, the Young-Laplace equation is extremely powerful when solving problems for curved liquid surfaces. Three such problems are the floating body, the shape of the meniscus and the profile of a water droplet. These can all be solved by utilizing the Young-Laplace PDE.

2.2.1 Floating Bodies

We shall now address the first problem introduced earlier, the statics of floating bodies, using the approach in *D. J. Vella*, (2007)²⁵

Consider an object (such as a metal pin, which is denser than water) of sufficiently small mass m "suspended" on a liquid. This object is not submerged, assuming the surface tension forces F_γ between the molecules of the liquid are strong enough not to let the interface surface rip. However, the object displaces water to its sides, and will therefore feel a buoyant force F_B .

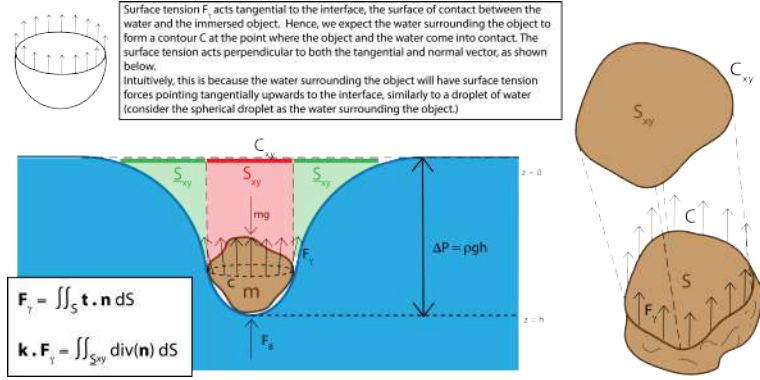


Figure 2.5: Body placed on a fluid depresses its surface, but doesn't necessarily sink due to surface tension and buoyancy.

Hence, for equilibrium we must have that $F_B + F_{\gamma\parallel} = mg$, where $F_{\gamma\parallel}$ is the component of F_γ acting vertically. Moreover, since pressure is defined as the force applied per unit surface area, $F = - \iint_S P dA$. Using the Laplace-Young equation:

$$\mathbf{k} \cdot \mathbf{F}_\gamma = F_{\gamma\parallel} = -\gamma \int_{S_{xy}} \nabla \cdot \hat{\mathbf{n}} \, dA \quad (2.13)$$

where S is the surface of contact between the floating body and the liquid, the interface surface. Furthermore, S_{xy} is the projection of S on the $x - y$ plane, and \bar{S}_{xy} is $\mathbb{R}^2 \setminus S_{xy}$. We could also derive this result using the definition of surface tension as the force per length applied on the interface surface. Indeed, defining C as the contact line between the object and water expressed as an arc parametrized vector function $\mathbf{r} = \mathbf{r}(l)$, we get that:

$$\mathbf{F}_\gamma = \gamma \int_C \dot{\mathbf{r}} \times \hat{\mathbf{n}} \, dl \quad (2.14)$$

We took the cross product $\dot{\mathbf{r}} \times \hat{\mathbf{n}}$ because the surface tension force is orthogonal to both the vector tangent to \mathbf{r} and the normal to the liquid surface \mathbf{n} . Integrating over C then gives the length and direction over which surface tension acts. We can now evaluate the component of the tensile force acting vertically:

$$F_{\gamma\parallel} = \gamma \int_C \mathbf{k} \cdot (\dot{\mathbf{r}} \times \hat{\mathbf{n}}) \, dl \quad (2.15)$$

This is equivalent to projecting the contact line on the $x - y$ plane, forming C_{xy} , and then evaluating the component of the surface tension force acting vertically along $\hat{\mathbf{n}}$. This new path will have arc length l' and normal vector \mathbf{n}' (this can be seen as transforming the integral using

$l \rightarrow l'$ and $\mathbf{r} \times \mathbf{n} \rightarrow \mathbf{n}'$) so that we get:

$$F_{\gamma\parallel} = \gamma \int_{C_{xy}} \hat{\mathbf{n}} \cdot \hat{\mathbf{n}}' dl' = \gamma \int_{C_{xy}} \hat{\mathbf{n}} \cdot dl' \quad (2.16)$$

We can now use the two dimensional Divergence Theorem²⁶ to simplify this integral.

Theorem 2 (2D Divergence Theorem). *Let S be a region enclosed by a smooth curve ∂S , with normal vector $\hat{\mathbf{n}}$). Then, the following holds for any vector field \mathbf{F} such that $\nabla \cdot \mathbf{F} \neq 0$:*

$$\iint_S \nabla \cdot \mathbf{F} dA = \int_{\partial S} \mathbf{F} \cdot d\hat{\mathbf{n}} \quad (2.17)$$

Since C_{xy} is simply the boundary of S_{xy} , we can define \bar{S}_{xy} as $\mathbb{R}^2 \setminus S_{xy}$, with boundary \bar{C}_{xy} . We then have that:

$$\int_{C_{xy}} \hat{\mathbf{n}} \cdot dl' = - \int_{C_{xy}} -\hat{\mathbf{n}} \cdot dl' = - \int_{\bar{S}_{xy}} \nabla \cdot \hat{\mathbf{n}} dA \quad (2.18)$$

so that we finally reach:

$$F_{\gamma\parallel} = -\gamma \iint_{\bar{S}_{xy}} \nabla \cdot \hat{\mathbf{n}} dA \quad (2.19)$$

as required. By taking into account buoyant forces, we can then write by balancing forces:

$$-\iint_{\bar{S}_{xy}} \nabla \cdot \hat{\mathbf{n}} dA + \frac{F_B}{\gamma} = \frac{mg}{\gamma} \quad (2.20)$$

Consider now the two fluids separated by an interface. Denoting the liquid density ρ , the variation in vertical pressure between the two phases (liquid and gas) will be $\Delta P = \rho gh$, where h is the depression in the liquid. We can then write:

$$\iint_{\bar{S}_{xy}} \rho gh dA = mg - F_B \quad (2.21)$$

where we have used the Young-Laplace equation. Let us now evaluate F_B , the buoyant force acting on this object. We get using the Archimedean principle:

$$F_B = \rho gh S_{x,y} \quad (2.22)$$

Taking the ratio between the two yields:

$$\frac{F_B}{F_{\gamma\parallel}} = \frac{S_{xy}}{\bar{S}_{xy}} \quad (2.23)$$

This demonstrates that as the size of the object decreases, S_{xy} will also decrease, and hence this ratio will decrease. For smaller objects, such as needle pins, contrary to common belief, buoyancy is not the main reason they float, it is surface tension. Thus, we can conclude that objects with greater density than water can still float as long as they are small enough.

2.3 Capillary Action

Capillary action is another mechanism caused by surface tension, and leads to various interesting phenomena, such as the formation of menisci and the shape puddles and droplets.

When a liquid is placed in a narrow tube or cylinder of sufficiently small radius, this liquid may "rise" upwards. The adhesive forces overcome the cohesive forces, then the liquid molecules will be pulled by the walls of the container, rising.

2.3.1 Jurin's Law

Before we address the meniscus problem introduced earlier, it is important to allude to the phenomenon of capillary action to truly understand the mechanism behind which menisci actually form, using two standard arguments to derive Jurin's Law²⁷²⁸

Let us consider a cylinder filled with water, of radius R . Assuming that the meniscus has a spherical shape (we'll see later on how to more accurately define the profile of a meniscus) with contact angle θ with the cylinder's walls. It can be shown that the radius of curvature of the interface is $R \sec \theta$, so that the Laplace pressure is:

$$\Delta P = -\frac{2\gamma}{R \sec \theta} \quad (2.24)$$

Furthermore, the Laplace pressure can also be defined as:

$$\Delta P = P_{atm} - P_{men} = -\frac{2\gamma}{R \sec \theta} \quad (2.25)$$

Let us now consider two communicating vases as shown below.

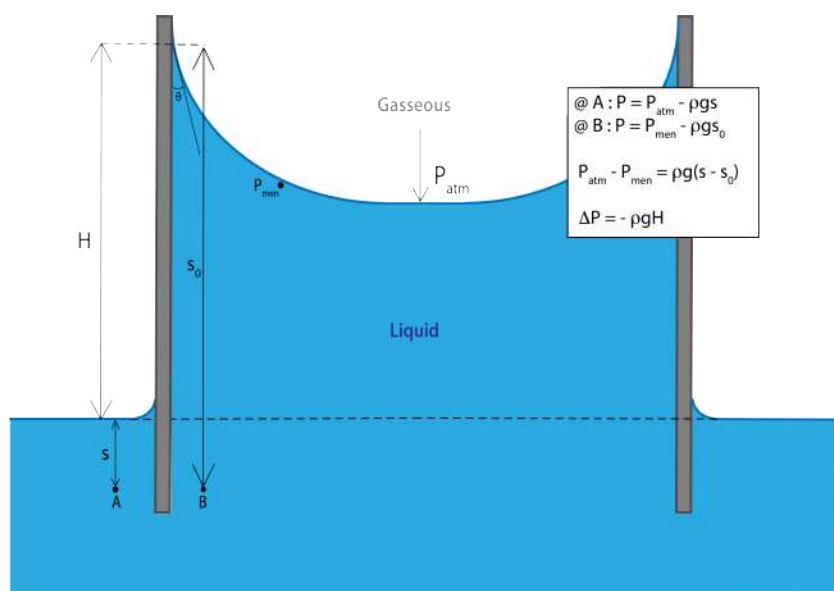


Figure 2.6: Capillary rise for a concave meniscus

Since pressure at equal heights in communicating vases must be equal, it follows that the pressure at an arbitrary height s under the water level is:

$$P_s = P_{atm} - \rho g s \quad (2.26)$$

for the "outer" vase. For the inner vase, the tube, we have that:

$$P_s = P_{men} - \rho g s_0 \quad (2.27)$$

where s_0 is defined as shown in Figure, P_{men} is the pressure at the meniscus. Equating these two expressions finally gives:

$$P_{atm} - P_{men} = \rho g(s - s_0) = -\rho g H \quad (2.28)$$

Using the Young-Laplace equation, we arrive at:

$$\rho_l g H = \frac{2\gamma}{R \sec \theta} \quad (2.29)$$

Rearranging we get Jurin's famous law for capillary rise

Jurin's Law

$$H = \frac{2\gamma \cos \theta}{R \rho g} \quad (2.30)$$

We could have also derived this result by equating forces as shown in *J. Pellicer et al.* (1995).²⁷ The weight due to the column of water must be equal to the surface tension forces acting along the meniscus perimeter, causing the liquid to rise:

$$F_\gamma = 2\pi R \gamma \cos \theta = F_g = \pi \rho R^2 g H \quad (2.31)$$

Again, we should check boundary conditions to see if our answer makes physically sense. Jurin's law tells us that $H \propto \frac{1}{R\rho}$. The denser the liquid, the higher it will rise (there are some exceptions such as mercury). Moreover, the narrower the tube, the greater the rise. Both sound physically intuitive and are correct.

2.3.2 The Concave Meniscus ($\theta < \frac{\pi}{2}$)

Notice that the size of the meniscus plays a huge role in the derivation of Jurin's law. As seen earlier, the balance between cohesive and adhesive forces determines the shape of a meniscus (more specifically the contact angle formed with a wall, which defines the shape of a meniscus).

Consider once again a liquid placed in a tube. If liquid molecules are more attracted to the walls than to other liquid molecules (when adhesive forces overcome cohesive forces), one

intuitively expects the meniscus to be concave. The molecules at the edges will be "dragged" upwards by adhesive forces, similar to a water column in a capillary tube would rise. Nearby molecules will move alongside as a result of cohesive forces. This may be easier to imagine if we interpret the cohesive forces as "chains": if the molecules at the edges move upwards, nearby molecules will move too. As we get farther from the tubes, these effects become more and more negligible, until they are null at the center of the container.

Instead, if the cohesive forces overcome the adhesive forces, then the meniscus will have a convex profile (similar to a droplet or puddle), since liquid molecules will try to "clump" all together, amassing near the center of the meniscus. Another major consequence is that we will have the "opposite" of capillary action, capillary fall. Instead of rising, the liquid molecules will try to "stick together", and actually fall (often observed in mercury). It follows that the equations governing puddles, droplets and menisci will be the same, as the conditions leading to their formation are identical.

Observe the right side of a meniscus in a cylinder containing a liquid column. We will set $z = 0$ as the height at which the meniscus "converges" towards, and denote the contact angle with the wall of the cylinder as θ , as shown below.

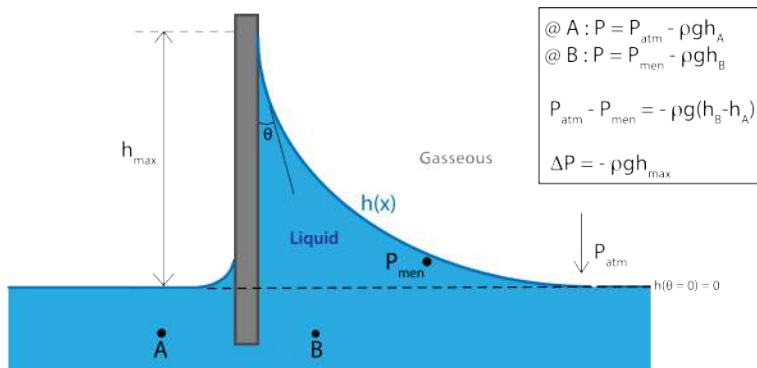


Figure 2.7: Profile of a concave meniscus

Using (2.28), and following *Berg*, 2009, we can write that:

$$\gamma \nabla \cdot \hat{\mathbf{n}} = -\rho g z \quad (2.32)$$

which can be used to define the shape of the meniscus. Indeed, if we define the surface of the meniscus as $f(x, z) = z - h(x)$, then:

$$\hat{\mathbf{n}} = \frac{\nabla f}{|\nabla f|} = \frac{\hat{\mathbf{z}} - h_x(x)\hat{\mathbf{x}}}{\sqrt{1 + h_x(x)^2}} \quad (2.33)$$

and we finally reach:

$$\nabla \cdot \hat{\mathbf{n}} = \frac{-h_{xx}(x)}{(1 + h_x(x)^2)^{\frac{3}{2}}} \approx -h_{xx}(x) \quad (2.34)$$

for $h_x(x) < 1$. Substituting into (2.32) we get the second order partial differential equation:

$$-\gamma \frac{\partial^2 h}{\partial x^2} = \rho g h, \quad h_x(0) = -\cot \theta, \quad (2.35)$$

whose solution is:

$$h(x) = \lambda \cot \theta e^{-\frac{x}{\lambda}} \quad (2.36)$$

where $\lambda = \sqrt{\frac{\gamma}{\rho g}}$ is the so called "Capillary length". This is another fundamental variable in the study of capillarity.¹ This expression gives the profile of a meniscus at a distance x from the wall of the container. As the capillary length increases, we expect that meniscus to be more curved (see next section), which agrees with our expression. A similar argument holds for the contact angle θ .

Some profiles for concave menisci at different contact angles are given.

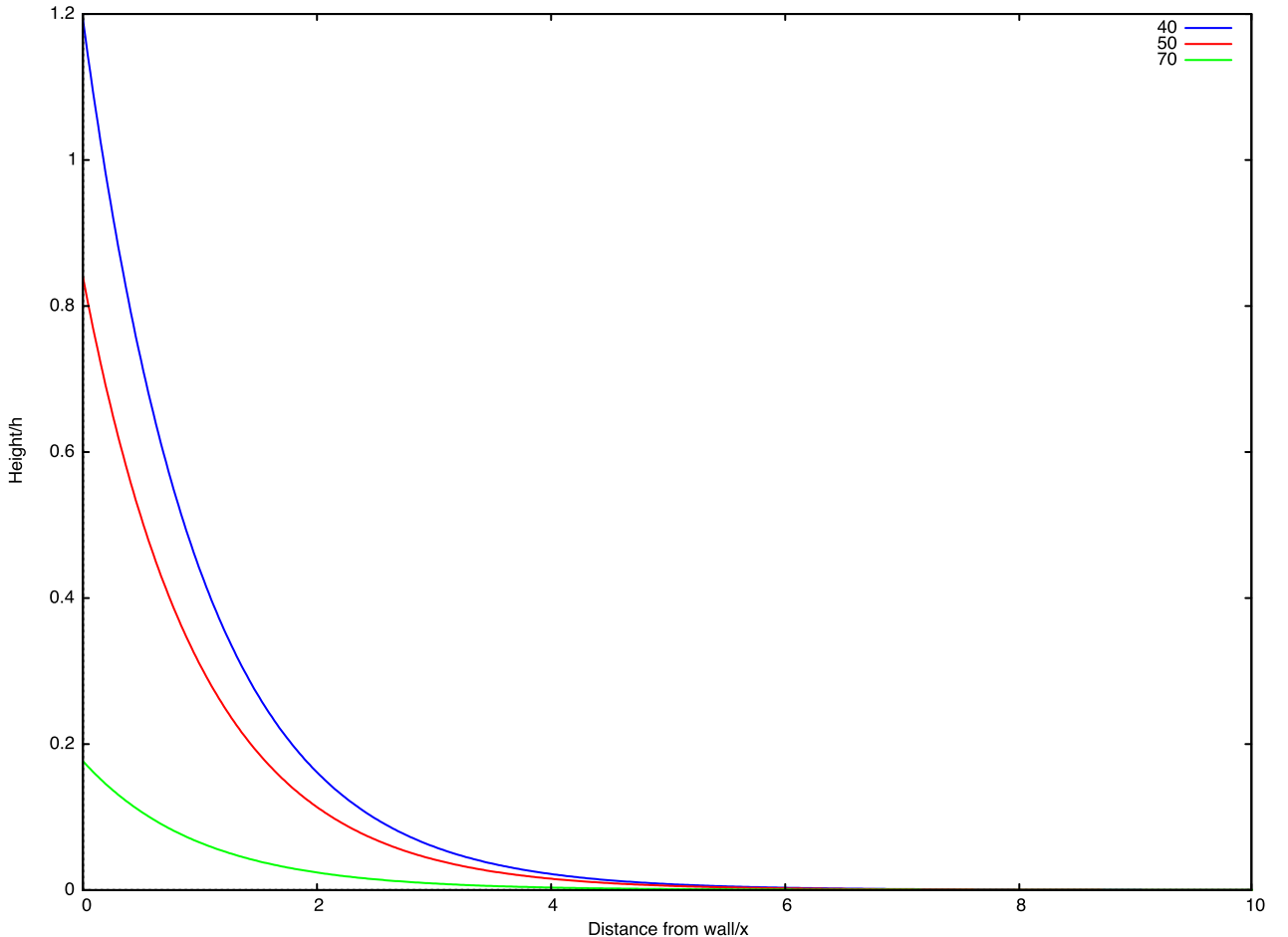


Figure 2.8: Menisci for contact angles $40^\circ, 50^\circ, 70^\circ$, setting $\lambda = 1$

¹We could have derived a similar result for a convex meniscus ($\theta > \frac{\pi}{2}$), by applying the initial condition $h_x(0) = \tan \theta$, giving as a solution:

$$h(x) = -\lambda \tan \theta e^{-\frac{x}{\lambda}} \quad (2.37)$$

2.3.3 Capillary Length λ and the shape of puddles

Consider a water droplet or puddle on a solid surface. We then know that the Laplace pressure at two points A, B inside this droplet, of radius of curvature R_A, R_B respectively is then:

$$\Delta P_A = \frac{2\gamma}{R_A}, \quad \Delta P_B = \frac{2\gamma}{R_B} \quad (2.38)$$

We then have that the pressure difference between these two points is:

$$\Delta P_A - \Delta P_B = 2\gamma \left(\frac{1}{R_A} - \frac{1}{R_B} \right) \quad (2.39)$$

This is equal to the vertical hydrostatic pressure difference ρgh , where h is the height difference between the A and B. Equating the two yields:

$$\left(\frac{1}{R_A} - \frac{1}{R_B} \right) = \frac{h}{2\frac{\gamma}{\rho g}} \quad (2.40)$$

Using dimensional analysis, we can conclude that the term $\frac{\gamma}{\rho g}$ must have units of $[\mathbf{L}]^2$, so that we may define the capillary length as:

$$\lambda = \sqrt{\frac{\gamma}{\rho g}} \quad (2.41)$$

The physical interpretation for this value is the distance over which a liquid-gas interface is curved. Thus, it follows that capillary length plays a vital role in determining the shape of a droplet or puddle. This is evident when analyzing cases where $h \gtrless \lambda$.³¹

Case 1: $h > \lambda$

For droplets where $h > \lambda$, we then have using (2.40) that

$$\frac{1}{R_A} - \frac{1}{R_B} >> 0 \quad (2.42)$$

It follows that the radius of curvature at point B will be greater than at point A. This means that the curvature decreases as we move upwards, and hence we expect the top part of the droplet to be flat, and become more curved as we move downwards.

Case 2: $h < \lambda$

Using our physical intuition, for $h < \lambda$ we expect the droplet to have a spherical shape. Indeed, using the same procedure, we get that:

$$\frac{1}{R_A} - \frac{1}{R_B} \approx 0 \quad (2.43)$$

This means that the radius of curvature between any two arbitrary points A, B inside the droplet is the same. Hence, we must have a spherical droplet.

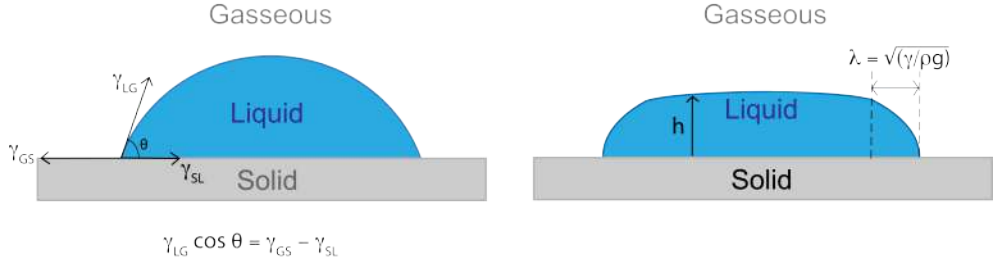


Figure 2.9: Comparison between puddles with $h > \lambda$ and $h < \lambda$.

One might now wonder how to calculate the maximum height of a droplet on an ideal smooth hydrophobic surface. We have that the net energy density or net force per unit length acting on the contour of the three phases(solid, liquid, gas), the interface, must be null. If we denote the surface tension of the solid-liquid, liquid-gas and gas-solid interface as $\gamma_{SL}\gamma_{LG}\gamma_{GS}$, and the contact angle as θ , then balancing force per unit length between these three phases:³⁰

$$\gamma_{SL} + \gamma_{LG} \cos \theta = \gamma_{GS} \quad (2.44)$$

which can be rearranged into the Young equation (not to be mistaken with the Young-Laplace equation):

Young Equation

$$\cos \theta = \frac{\gamma_{GS} - \gamma_{SL}}{\gamma_{LG}} \quad (2.45)$$

As the surface tension between the liquid and gas phases increases, the angle of contact must decrease. This agrees with Young's equation. Since surface tension is essentially how much a surface pushes against increasing its surface area, if surface tension is greater, we expect its surface area to get smaller and smaller, causing a decrease in contact angle.

Going back to the derivation in subsection 2.3.2, we can write:

$$-\rho g x = \frac{\gamma g_{xx}(x)}{(1 + g_x(x)^2)^{\frac{3}{2}}} \quad (2.46)$$

Substituting $q = g_x(x)$, we can solve this ODE:

$$-\frac{1}{2} \rho g h^2 = \frac{\gamma q}{\sqrt{1 + q^2}} + C \quad (2.47)$$

$$= \gamma \cos \theta + C \quad (2.48)$$

We can now set initial conditions $h(\theta = 0) = 0$, so that $C = -\gamma$. Finally, we have the result:³²

$$h = \sqrt{\frac{2\gamma}{\rho g} (1 - \cos \theta)} \quad (2.49)$$

which can be rewritten using Young's equation:

$$h = \sqrt{\frac{2}{\rho g}(\gamma - \gamma_{GS} + \gamma_{SL})} \quad (2.50)$$

The same result can be rewritten as

$$h = 2\lambda \sin\left(\frac{\theta}{2}\right) \quad (2.51)$$

Observing figure 2.9, notice that we can define a *spread factor* S as the difference between the surface energies trying to "spread" the droplet (pointing outwards), and the surface energies pointing inwards:

$$S = \gamma + \gamma_{SL} - \gamma_{GS} \quad (2.52)$$

so that we finally reach:

$$h = \sqrt{\frac{2S}{\rho g}} \quad (2.53)$$

This makes sense from a physical standpoint. Indeed, one would expect that for a puddle of droplet to have a greater maximum height, it would be "pushing inwards" more than it would be "pushing outwards". In other words, the greater the spreading parameter S is, the more spherical we'd expect the droplet to be. This agrees with (2.53). To conclude, we provide a table to summarize our results on menisci.

Concave Meniscus	Convex Meniscus
$h(x) \approx \lambda \cot \theta e^{-\frac{x}{\lambda}}$	$h(x) \approx -\lambda \tan \theta e^{-\frac{x}{\lambda}}$
$h_{max} = \sqrt{\frac{2\gamma}{\rho g}(1 - \sin \theta)}$	$h_{max} = \sqrt{\frac{2\gamma}{\rho g}(1 - \cos \theta)}$
$h_{max} \approx \lambda \cot \theta$	$h_{max} \approx \lambda \tan \theta$

Table 2.1: Table Summarizing Shape of Menisci

2

²We could have also derived the formula for a concave meniscus. Consider:

$$-\frac{1}{2}\rho gh^2 = \frac{\gamma q}{\sqrt{1+q^2}} + C = \gamma \frac{\tan \theta}{\sqrt{1+\tan^2 \theta}} + C = \gamma \sin \theta$$

Using the initial condition that $h(q = \infty) = 0$:

$$h = \sqrt{\frac{2\gamma}{\rho g}(1 - \sin \theta)}$$

2.4 Minimal Surfaces

Consider a soap film produced when immersing a frame into a water-soap solution. Since we have no change in pressure when moving through the interface layer, it follows from Laplace's equation that the mean curvature of this soap film must be zero. Such types of surfaces that minimize surface area by having zero mean curvature at all points are called minimal surfaces.³³ Indeed, *A. Presley (2012)* gives the definition of a minimal surface as:

A minimal surface is a surface whose mean curvature is zero everywhere.

They are given by the solutions to the *minimal surface equation*:³⁴

Minimal Surface Equation

$$\nabla \cdot \left(\frac{\nabla f}{(1 + |\nabla f|^2)^{\frac{1}{2}}} \right) = 0 \quad (2.54)$$

Quite obviously, a simple plane would satisfy this equation. Another solution is the Helicoid, the second non-trivial solution to be discovered after the Catenoid (see Fig. 2.10).

Note that, except for the plane, all other solutions of the minimal surface equation will have non-zero curvature at some points. However, they average out at every point to be zero. Moreover, all these surfaces have a "soap film frame", the frame that contains the set of all points the surface must contain, while still minimizing its surface area. For the Catenoid and the Helicoid, these frames are quite easy to imagine. The former is generated when immersing two elliptical rings parallel to each other in soap, whereas the latter is formed when using a helix. These surfaces were plotted on python, and the code is given below for availability to the reader (in case the reproduction of these results is necessary):

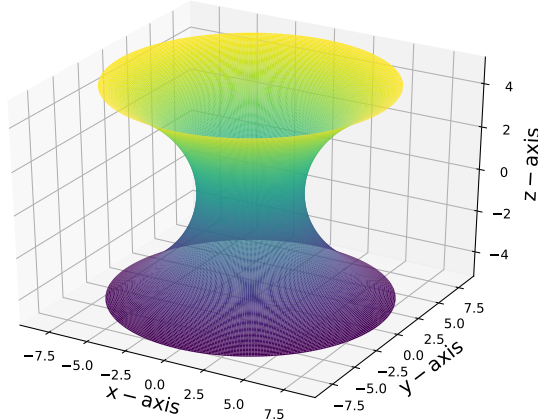
2.5 Conclusion

A definition for surface tension was given, and this definition was used to conceptually understand some phenomena related to surface tension, such as the formation of droplets, the clumping of bubbles on the surface of certain liquids such as water, and the reason we use soap when washing our hands. A mathematical model was developed to fit these insights, firstly by deriving the Young-Laplace Law. We then saw how this equation can be used to model interactions between fluids, especially between liquids and gases, by examining floating bodies, menisci and capillary action. Lastly, we saw how a challenging problem in the field of pure mathematics, minimal surfaces, can be simplified using soap films and surface tension.

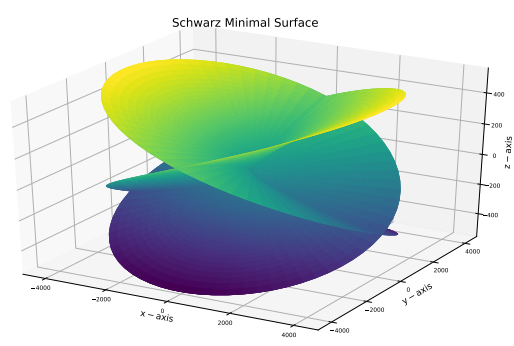
One could have also used trigonometric identities and have shown that:

$$h = \sqrt{\frac{2}{\rho g}(1 - \cos \psi)} = \sqrt{\frac{2}{\rho g}(1 - \cos(90 - \pi))} = \sqrt{\frac{2}{\rho g}(1 - \sin \theta)}$$

Catenoid for $c = 3$

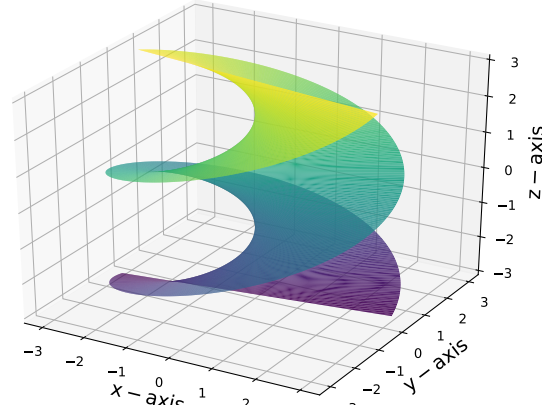


(a)



(b)

Helicoid for $k = 1$



(c)

Figure 2.10: a) Plot of a Catenoid b) Plot of Henneberg Surface c) Plot of Helicoid

Chapter 3

Frisbees and Disks

Contents

3.1	Introduction	45
3.2	A mathematical prelude on Summation Convention	46
3.3	The Stress Tensor	49
3.4	Deriving the Cauchy Momentum equation for Incompressible Flow	52
3.5	The Bernoulli Principle and how Lift is generated	55
3.6	Equation of Motion for a Frisbee in Flight	57
3.7	Simulating Frisbee Flight	59

3.1 Introduction

The modern Frisbee was initially invented in 1958 by Walter Frederick Morrison, who named his invention *The Flyin-Saucer* after various Unidentified Flying Objects were sighted. All rights were then sold to Wham-O, who renamed the disk *Frisbee*, supposedly after hearing Yale students refer to the disk by *frisbie*. Sales escalated tremendously after Wham-O redesigned the toy, making it more accurate.

To address the problem of determining the motion of a Frisbee (or more generally a disk), we must point out two fundamental ideas: the *Bernoulli Principle*, and the *Conservation of Angular Momentum*. We shall mostly treat the first concept in this chapter, and treat rigid body dynamics in the next chapter. Hence, only at the end of the next two chapters will we have the answer to the burning question: how does a Frisbee fly?

Light and flexible, the Frisbee is still a source of entertainment, and despite its simplistic design, the physics behind their trajectories has been rarely investigated. Indeed, little research has been conducted examining the Frisbee's motion computationally, experimentally or theoretically.

Firstly, *Schuurmans* (1990)⁴⁴ explained conceptually the *turnover effect*, describing how gyroscopic stability allows Frisbees not to turn over and fall during their flight. methods which

shall be introduced more rigorously here were applied, such as the Bernoulli principle. The paper addresses the irregularity in the distribution of lift force throughout a normal disk, causing it to flip over, and then attempts to explain how imparting enough rotational momentum to the disk avoids any notable change in the disk's orientation. The paper clearly points out the importance of gyroscopic precession in subsequent sections.

Hubbard Hummel (2000)⁴⁵ also investigated the dynamics of Frisbee flight, and formalized the ideas in *Schuurmans* (1990), providing equations of motion for the discus. Methods to determine aerodynamic coefficients were also introduced, and simulations were run for disk flights with different initial conditions. Iterative approximations were then used to predict aerodynamic coefficients for other flights. Similar efforts were made by *Morrison* (2005)⁴⁶ which also provided a numerical model for the motion of a Frisbee in flight using Euler's method. *Motoyama* (2002)⁴⁸ provided refreshing alternatives to the antiquate explanation on the generation of lift by Bernoulli's principle. Furthermore, unlike previously mentioned research, turbulence effects were also taken into account.

3.2 A mathematical prelude on Summation Convention

Before delving into the tedious and heavy derivation that will follow, it may be useful to introduce summation convention to simplify calculations later on, following Chapter 26 from *Mathematical Methods for Physics and Engineering*.⁴⁹ There is only one "rule" in this notation: if a subscript appears precisely twice in a term of an expression (called dummy subscript), it is summed over the values this subscript can take. *e.g.* for $j = 1, 2, 3$, we can write $a_{ij}b_{jk} = a_{i1}b_{1k} + a_{i2}b_{2k} + a_{i3}b_{3k}$. Therefore, one can also write that:

$$\partial_i f_i = \frac{\partial f_1}{\partial x_1} + \frac{\partial f_2}{\partial x_2} + \frac{\partial f_3}{\partial x_3} = \nabla \cdot \mathbf{f} \quad (3.1)$$

$$\mathbf{e}_i \partial_i \psi = \frac{\partial \psi}{\partial x_1} \mathbf{e}_1 + \frac{\partial \psi}{\partial x_2} \mathbf{e}_2 + \frac{\partial \psi}{\partial x_3} \mathbf{e}_3 = \nabla \psi \quad (3.2)$$

which shows the just how powerful this convention is in shortening expressions. If we let $\mathbf{f} = f_i \mathbf{e}_i$, then the Del operator must be defined as:

$$\nabla = \mathbf{e}_i \partial_i \quad (3.3)$$

Moreover, note that a subscript may never appear more than twice in a term. We must therefore take great care when changing subscripts. For example, consider $a_{ik}b_{jk}\delta_{kj}$, where δ_{kj} is defined as the *Kronecker-Delta*:

$$\delta_{kj} = \begin{cases} 1 & \text{if } k = j \\ 0 & \text{otherwise.} \end{cases} \quad (3.4)$$

Then, we mustn't write $a_{ij}b_{jj}$ but should instead use $a_{ik}b_{jk}$. Clearly, the Kronecker-Delta symbol plays an important role in writing scalar products between vectors. Consider two vectors $\mathbf{a} = a_i \mathbf{e}_i$ and $\mathbf{b} = b_j \mathbf{e}_j$. We can write their scalar product as:

$$\mathbf{a} \cdot \mathbf{b} = a_i \mathbf{e}_i b_j \mathbf{e}_j \quad (3.5)$$

$$= a_i b_j \mathbf{e}_i \mathbf{e}_j \quad (3.6)$$

$$= a_i b_j \delta_{ij} \quad (3.7)$$

since $\mathbf{e}_i \cdot \mathbf{e}_i = 0$ and $\mathbf{e}_i \cdot \mathbf{e}_j = 1$ (for $i \neq j$). We can also define the analogous of the Kronecker delta for cross products, the *Levi-Civita* symbol:

$$\epsilon_{ijk} = \begin{cases} +1 & \text{if } (i, j, k) \text{ is an even permutation of 1,2,3} \\ -1 & \text{if } (i, j, k) \text{ is an odd permutation of 1,2,3} \\ 0 & \text{otherwise.} \end{cases} \quad (3.8)$$

Recall that an even permutation is an arrangement that requires an even number of individual permutations of $(1, 2, 3)$ (e.g. $(1, 2, 3) \rightarrow (2, 1, 3) \rightarrow (2, 3, 1)$), whereas an odd permutation requires an odd number of transitions (e.g. $(1, 2, 3) \rightarrow (2, 1, 3)$). We have that:

$$\epsilon_{123} = \epsilon_{231} = \epsilon_{312} = +1, \quad \epsilon_{321} = \epsilon_{132} = \epsilon_{213} = -1, \quad \text{others} = 0 \quad (3.9)$$

One might wonder how the Levi-Civita symbol may be useful in simplifying cross product calculations. In a Right Handed Cartesian Basis: $\mathbf{e}_1 \times \mathbf{e}_2 = \mathbf{e}_3$, whereas $\mathbf{e}_2 \times \mathbf{e}_1 = -\mathbf{e}_3$. The same holds for $\mathbf{e}_2 \times \mathbf{e}_3$ and $\mathbf{e}_3 \times \mathbf{e}_1$. We may then generalize these results and say that $\mathbf{e}_i \times \mathbf{e}_j = \epsilon_{ijk} \mathbf{e}_k$. Once again let us consider two vectors $\mathbf{a} = a_i \mathbf{e}_i$ and $\mathbf{b} = b_j \mathbf{e}_j$. Their cross product is:

$$\mathbf{a} \times \mathbf{b} = (a_i \mathbf{e}_i) \times (b_j \mathbf{e}_j) \quad (3.10)$$

$$= a_i b_j (\mathbf{e}_i \times \mathbf{e}_j) \quad (3.11)$$

$$= \epsilon_{ijk} a_i b_j \mathbf{e}_k \quad (3.12)$$

The analogy between the Levi-Cevita and the Kronecker-Delta symbols is now clear: $\mathbf{e}_i \cdot \mathbf{e}_j = \delta_{ij}$, whereas $\mathbf{e}_i \times \mathbf{e}_j = \epsilon_{ijk} \mathbf{e}_k$. One can use the cyclic properties of the Levi-Cevita symbol and write $\epsilon_{ijk} = \epsilon_{kij} = \epsilon_{jki}$. We then find:

$$\mathbf{a} \times \mathbf{b} = \epsilon_{kij} a_i b_j \mathbf{e}_k \quad (3.13)$$

$$= \epsilon_{ijk} a_j b_k \mathbf{e}_i \quad (3.14)$$

$$\mathbf{a} \times \mathbf{b} = \epsilon_{jki} a_i b_j \mathbf{e}_k \quad (3.15)$$

$$= \epsilon_{ijk} a_k b_i \mathbf{e}_j \quad (3.16)$$

where we relabelled the indices.¹ We can now express all of vector calculus more succinctly using this new summation convention we have developed. Consider the curl of a vector field \mathbf{F} :

$$\nabla \times \mathbf{F} = \epsilon_{ijk} \partial_j F_k \mathbf{e}_i \quad (3.17)$$

We can also derive identities for the scalar and cross triple product:

$$\mathbf{a} \cdot (\mathbf{b} \times \mathbf{c}) = \epsilon_{ijk} a_i b_j c_k \mathbf{e}_i \cdot \mathbf{e}_i \quad (3.18)$$

$$= \epsilon_{ijk} a_i b_j c_k \quad (3.19)$$

$$\mathbf{a} \times (\mathbf{b} \times \mathbf{c}) = a_j \mathbf{e}_j \times (\epsilon_{klm} b_l c_m \mathbf{e}_k) \quad (3.20)$$

$$= (\mathbf{e}_j \times \mathbf{e}_k) a_j (\epsilon_{klm} b_l c_m) \quad (3.21)$$

$$= \epsilon_{ijk} \epsilon_{klm} a_j b_l c_m \mathbf{e}_i \quad (3.22)$$

Recall the so-called *bac-cab* identity: $\mathbf{a} \times (\mathbf{b} \times \mathbf{c}) = \mathbf{b}(\mathbf{a} \cdot \mathbf{c}) - \mathbf{c}(\mathbf{a} \cdot \mathbf{b})$. Using summation convention:

$$\mathbf{b}(\mathbf{a} \cdot \mathbf{c}) - \mathbf{c}(\mathbf{a} \cdot \mathbf{b}) = b_l \mathbf{e}_l (a_j \cdot c_m) - \delta_{im} c_m (a_j \cdot b_l) \mathbf{e}_m \quad (3.23)$$

$$= \delta_{il} b_i (a_j \cdot c_m) \mathbf{e}_i - c_m (a_j \cdot b_l) \mathbf{e}_i \quad (3.24)$$

$$= [\delta_{il} b_l (\delta_{jm} a_j c_m) - \delta_{im} c_m (\delta_{jl} a_j b_l)] \mathbf{e}_i \quad (3.25)$$

$$= [(\delta_{il} \delta_{jm} - \delta_{im} \delta_{jl}) a_j b_l c_m] \mathbf{e}_i \quad (3.26)$$

Comparing (3.25) and (3.22), we get an essential result in Linear Algebra:

$$\boxed{\epsilon_{ijk} \epsilon_{klm} = (\delta_{il} \delta_{jm} - \delta_{im} \delta_{jl})} \quad (3.27)$$

Going back to (3.18), we know that the scalar product between three vectors is:

$$\mathbf{a} \cdot (\mathbf{b} \times \mathbf{c}) = \det \begin{pmatrix} a_1 & a_2 & a_3 \\ b_1 & b_2 & b_3 \\ c_1 & c_2 & c_3 \end{pmatrix} = \epsilon_{ijk} a_i b_j c_k \quad (3.28)$$

We have therefore derived a definition for the determinant of a matrix. More generally, for a

¹In (3.15) $i \rightarrow k, j \rightarrow i, k \rightarrow j$ and in (3.13) $i \rightarrow j, j \rightarrow k, k \rightarrow i$

matrix A:

$$A = \begin{pmatrix} a_{11} & a_{12} & a_{13} \\ a_{21} & a_{22} & a_{23} \\ a_{31} & a_{32} & a_{33} \end{pmatrix} \quad (3.29)$$

the determinant is specified as:

$$\det A = \epsilon_{ijk} a_{1i} a_{2j} a_{3k} \quad (3.30)$$

3.3 The Stress Tensor

Let us now try to apply our knowledge of subscript notation to the study of the stress tensor, following Lecture series at Texas AM University.³⁵ Imagine a fluid running between two plates separated by a distance h . The bottom one is fixed, whereas the top one is free to move. Moreover, assume that the fluid doesn't slip on either plate, giving us the boundary condition:

$$v_{\text{plate}} = v(y) \quad \text{for } y = 0, h \quad (3.31)$$

One can experimentally verify that the shear stress (stress acting parallel to the surface it is acting upon) acting on the fluid is equal to the force exerted on the top plate as the fluid moves with velocity \mathbf{v} at $y = h$.

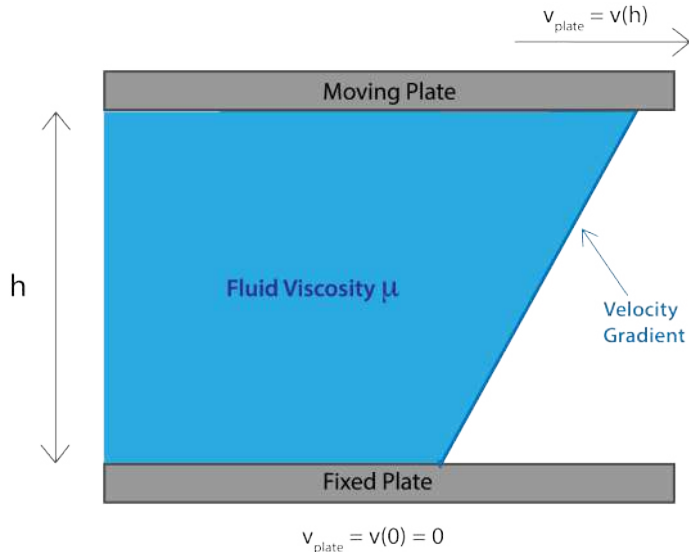


Figure 3.1: Fluid running between a fixed and moving plate

As a result of empirical observations, Newton's law of Viscosity states that:

$$\frac{F}{A} = \mu \frac{v}{H} \quad (3.32)$$

The term $\frac{v}{H}$ could be seen as the average velocity gradient, it is the average rate at which velocity changes moving up the liquid. Assuming that the liquid is Newtonian (the viscosity doesn't vary with velocity), then we can write more generally that:

$$\frac{dF_x}{dA_y} = \mu \frac{\partial v_x}{\partial y} \quad (3.33)$$

Physically, this means that the shear stress acting in the direction \hat{x} on an infinitesimal area of a fluid perpendicular to the vector \hat{y} is directly proportional to the rate of change of velocity in the \hat{x} direction with respect to position.

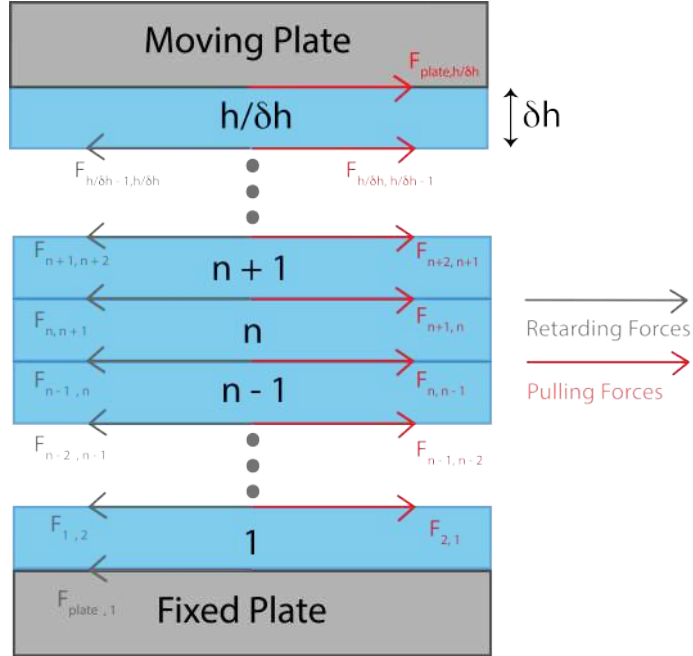


Figure 3.2: Diagram dividing fluid into infinitesimally thin layers, explaining how viscosity acts as a shear stress on a fluid

Consider dividing the fluid into various layers of infinitesimal height δH , and consider layers $n - i, n, n + 1$. Since each layer is infinitesimally thin, they will each have a distinct velocity. Viscosity will always try to reduce any difference in velocity, trying to "straighten" the velocity gradient into a vertical line. We then expect the $(n - 1)^{\text{th}}$ layer to apply some retarding viscous force on the n^{th} layer, trying to reduce the velocity difference. Consequently, by Newton's Third Law, the n^{th} layer must apply a viscous force "pulling" the lower layer to increase its velocity and reduce the velocity difference. Similar mechanics apply for the $n^{\text{th}} - (n + 1)^{\text{th}}$ layer couple. Thus, layer n will feel shearing stress from the top and bottom layers. The shearing stress experienced by a liquid is simply a result of internal drag in the fluid trying to minimize the velocity gradient. Intuitively, we expect that as the difference in velocity increases from one "layer" to another (which is interpreted as $\frac{\partial v_x}{\partial y}$), there should be more shear stress acting on the fluid. Not only, as the viscosity of the fluid increases, so should the shear stress. These everyday observations coincide with our equation.

Consider an infinitesimal volume element of a Newtonian fluid as shown below, and suppose we wanted to find an expression for the stress forces (shearing forces and normal forces combined) acting on this volume element⁴⁷ (ignoring pressure which shall be dealt with later on). Let us

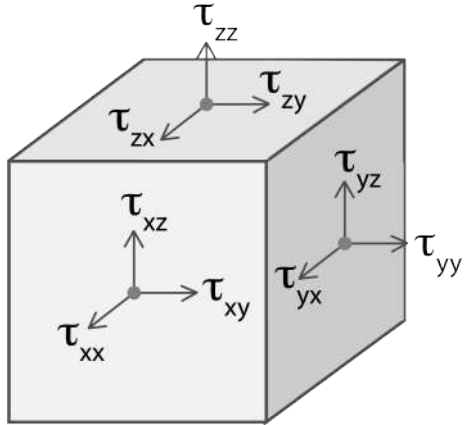


Figure 3.3: Shear and Normal stress acting on an infinitesimal volume element

define τ_{ij} as the stress acting on a plane perpendicular to \mathbf{e}_i in the direction \mathbf{e}_j e.g. τ_{12} is the stress acting on the yz plane in the \mathbf{e}_2 direction. Note that when $i \neq j$, we have shearing stress, parallel to the plane it is acting on. Instead, when $i = j$ we have a normal force, perpendicular to the plane it is acting on. This distinction is the main reason we can't just add stress acting in the x direction, y direction and z direction. τ_{xy} is a shearing stress, whereas τ_{yy} is normal stress, and although they act in the same direction, they must not be added due to this difference in the manner they act on a surface (parallel or perpendicular). It follows that each plane on a Cartesian coordinate system will have three stresses acting on it, two shearing stresses and one normal stress, with a total of 9 stress components for all three planes. We must therefore try to find a mathematical object capable of representing 9 components, and the answer as we shall see later, is a *tensor*. Let us first specify the stress forces acting on the yz -plane:

$$\tau_{xy} = \frac{dF_x}{dA_x} + \frac{dF_y}{dA_y} = \mu \left(\frac{\partial v_x}{\partial y} + \frac{\partial v_y}{\partial x} \right) \quad (3.34)$$

$$\tau_{xz} = \frac{dF_x}{dA_z} + \frac{dF_z}{dA_x} = \mu \left(\frac{\partial v_x}{\partial z} + \frac{\partial v_z}{\partial x} \right) \quad (3.35)$$

$$\tau_{xx} = \frac{dF_x}{dA_x} + \frac{dF_x}{dA_x} = 2\mu \frac{\partial v_x}{\partial x} \quad (3.36)$$

Using subscript notation, we can write that in general:

$$\tau_{ij} = \mu \left(\frac{\partial v_j}{\partial i} + \frac{\partial v_i}{\partial j} \right) = \begin{pmatrix} \tau_{xx} & \tau_{xy} & \tau_{xz} \\ \tau_{yx} & \tau_{yy} & \tau_{yz} \\ \tau_{zx} & \tau_{zy} & \tau_{zz} \end{pmatrix} \quad (3.37)$$

which is known as the *viscous stress tensor/deviatoric stress tensor*. Note that i, j can each have 3 values. Hence, this short equation actually represents 9 separate equations, this is the mathematical object we were looking for! Quantities of these kind are referred to as *Tensors*. A tensor may be defined as:

An algebraic object invariant under Cartesian transformations that contains d^n com-

ponents, where d is the dimension of space and n is the tensor rank (number of subscripts needed to specify this tensor).³⁸

It should be obvious that all physical laws are invariant to changes in coordinate system (Cartesian transformations), and can therefore be expressed in the form of tensors. For example, vectors can be specified with one index, $\mathbf{v} = v_i \mathbf{e}_i$, this is a first rank tensor. Similarly, a scalar has no subscripts, it is a fixed quantity with one component and is therefore a zero rank tensor. It follows that the viscous stress tensor is a second rank tensor, with 3^2 components, 3 components for the direction they act in, and 6 components for the plane they act on

3.4 Deriving the Cauchy Momentum equation for Incompressible Flow

We shall now begin our derivation of the Navier Stokes equation, following arguments from *Batchelor* (1967)³⁶ and *Coleman* (2010).³⁷ Consider Newton's Second Law for an arbitrary surface:

$$\mathbf{F} = m\mathbf{a} \quad (3.38)$$

Let the velocity of this fluid be defined as $\mathbf{v}(t, x, y, z) = u_1 \mathbf{e}_1 + u_2 \mathbf{e}_2 + u_3 \mathbf{e}_3$. We can define the body force \mathbf{B} as the force exerted on this surface per unit volume:

$$\mathbf{B} = \rho \frac{d}{dt} \mathbf{v}(t, x, y, z) \quad (3.39)$$

$$= \rho \left(\frac{\partial \mathbf{v}}{\partial t} + \frac{\partial \mathbf{v}}{\partial x_1} \frac{\partial x_1}{\partial t} + \frac{\partial \mathbf{v}}{\partial x_2} \frac{\partial x_2}{\partial t} + \frac{\partial \mathbf{v}}{\partial x_3} \frac{\partial x_3}{\partial t} \right) \quad (3.40)$$

$$= \rho \underbrace{\left(\frac{\partial \mathbf{v}}{\partial t} + \partial_i \mathbf{v} \frac{\partial x_i}{\partial t} \right)}_{\frac{D\mathbf{v}}{Dt}} \quad (\text{sum convention}) \quad (3.41)$$

Denoting $\frac{D\mathbf{v}}{Dt} = \partial_t + \mathbf{v}(\nabla \cdot \mathbf{v})$ as the material derivative, we find:

$$\rho \frac{D\mathbf{v}}{Dt} = \mathbf{B} \quad (3.42)$$

which is the Cauchy Momentum expression in its most general (and probably most useless) form. We can now define the body force by examining which forces act on an infinitesimal volume element. Following our previous analysis, we expect both external forces \mathbf{f} as well as forces due to internal stress (deviatoric stress tensor and pressure) to act on the fluid. We denote the general

stress tensor as:

$$\sigma = \begin{pmatrix} \sigma_{11} & \tau_{12} & \tau_{13} \\ \tau_{21} & \sigma_{22} & \tau_{23} \\ \tau_{31} & \tau_{32} & \sigma_{33} \end{pmatrix} \quad (3.43)$$

$$= - \begin{pmatrix} p & 0 & 0 \\ 0 & p & 0 \\ 0 & 0 & p \end{pmatrix} + \begin{pmatrix} \sigma_{11} + p & \tau_{12} & \tau_{13} \\ \tau_{21} & \sigma_{22} + p & \tau_{23} \\ \tau_{31} & \tau_{32} & \sigma_{33} + p \end{pmatrix} \quad (3.44)$$

$$= -pI + T \quad (3.45)$$

where T is the viscous stress tensor we saw earlier. Note that the diagonal entries ($i = j$) of the general stress tensor must have both a component due to normal stress and a component due to pressure. Hence, comparing terms in diagonal entries of the viscous stress tensor T with (3.37):

$$\tau_{ii} = \sigma_{ii} + p \implies \sigma_{ij} = -p\delta_{ij} + \tau_{ij} \quad (3.46)$$

We rewrite our definition for the viscous stress tensor in summation convention:

$$\tau_{ij} = \mu(\partial_j u_i + \partial_i u_j) \quad (3.47)$$

from which it follows that:

$$\sigma_{ij} = \mu(\partial_j u_i + \partial_i u_j) - p\delta_{ij} \quad (3.48)$$

Let us take the divergence of the stress tensor, which will give us the body force contribution from fluid stress (pressure and viscous stress). One might wonder why the divergence of the general stress tensor will give us the stress force per unit volume acting on this fluid. Taking a more physical approach, the divergence will tell us how much the tensor acting on this fluid may be a "sink" or a "source" of stress. In other words, the divergence will tell us whether the tensor is a source or sink of momentum which is equivalent to the stress force by the principle of conservation of momentum. Mathematically, consider the variation in viscous stress forces throughout our infinitesimal volume element. The viscous stress must increase by $\partial_j \tau_{ij}$. Then:

$$F_i = (\partial_j \tau_{ij} \Delta V) \quad (3.49)$$

$$= (\nabla \cdot T)_i \Delta V \implies (\nabla \cdot T)_i = \frac{F_i}{\Delta V} = \mathbf{b} + \nabla p \quad (3.50)$$

where T is the viscous stress tensor in matrix form.² We then get the i^{th} component of the

²Please do note that there is a difference between a tensor of second rank and a matrix. The former is invariant to Cartesian transformations, whereas the latter, being just a grid of numbers, does not fulfill this requirement.

divergence of the stress tensor is:

$$(\nabla \cdot \sigma)_i = (\nabla \cdot T)_i - \nabla p \quad (3.51)$$

$$= \mathbf{b} + \nabla p - \nabla p \quad (3.52)$$

$$= \mathbf{b} \quad (3.53)$$

As we can see, taking the divergence of the general stress tensor will give us the body force exerted on the fluid. Below are the calculations for this divergence:

Summation Notation

$$(\nabla \cdot \sigma)_i = \partial_j \sigma_{ij} \quad (3.54)$$

$$= \mu \partial_j (\partial_i u_j + \partial_j u_i) - \partial_i p \delta_{ij} \quad (3.55)$$

$$= \mu (\partial_i \partial_j u_j + \partial_j \partial_j u_i) - \partial_i p \delta_{ij} \quad (3.56)$$

$$= \mu (\nabla^2 u_i + \partial_i \partial_j u_j) - \partial_i p \delta_{ij} \quad (3.57)$$

$$= \mu \nabla^2 u_i + \mu \partial_i (\nabla \cdot \mathbf{v})^0 - \nabla p \quad (3.58)$$

$$= \mu \nabla^2 u_i - \nabla p \quad (3.59)$$

Normal Notation

$$(\nabla \cdot \sigma)_i = \frac{\partial \sigma_{i1}}{\partial x_1} + \frac{\partial \sigma_{i2}}{\partial x_2} + \frac{\partial \sigma_{i3}}{\partial x_3} \quad (3.60)$$

$$= \mu \left[\frac{\partial}{\partial x_1} \left(\frac{\partial u_1}{\partial x_i} + \frac{\partial u_i}{\partial x_1} \right) + \frac{\partial}{\partial x_2} \left(\frac{\partial u_2}{\partial x_i} + \frac{\partial u_i}{\partial x_2} \right) + \frac{\partial}{\partial x_3} \left(\frac{\partial u_3}{\partial x_i} + \frac{\partial u_i}{\partial x_3} \right) \right] - \nabla p \quad (3.61)$$

$$= \mu \left[\left(\frac{\partial^2 u_i}{\partial x_1^2} + \frac{\partial^2 u_i}{\partial x_2^2} + \frac{\partial^2 u_i}{\partial x_3^2} \right) + \left(\frac{\partial^2 u_1}{\partial x_1 \partial x_i} + \frac{\partial^2 u_2}{\partial x_2 \partial x_i} + \frac{\partial^2 u_3}{\partial x_3 \partial x_i} \right) \right] - \nabla p \quad (3.62)$$

$$= \mu \left[\nabla^2 u_i + \frac{\partial}{\partial x_i} \left(\frac{\partial u_1}{\partial x_1} + \frac{\partial u_2}{\partial x_2} + \frac{\partial u_3}{\partial x_3} \right) \right] - \nabla p \quad (3.63)$$

$$= \mu \left[\nabla^2 u_i + \frac{\partial}{\partial x_i} (\nabla \cdot \mathbf{v})^0 \right] - \nabla p \quad (3.64)$$

$$= \mu \nabla^2 u_i - \nabla p \quad (3.65)$$

We have given derivations using both normal and summation convention for the reader to be able to clearly compare what certain terms in the former derivation may correspond to. It follows that:

$$\nabla \cdot \sigma = \mu \nabla^2 \mathbf{v} - \nabla p \quad (3.66)$$

$$\mathbf{B} = \mathbf{f} + \mu \nabla^2 \mathbf{v} - \nabla p \quad (3.67)$$

Plugging this into (3.42) yields the famous Cauchy Momentum equation:

Cauchy Momentum Equation

$$\rho \frac{D\mathbf{v}}{Dt} = \mathbf{f} + \mu \nabla^2 \mathbf{v} - \nabla p \quad (3.68)$$

As we can see, this is a reformulation of Newton's second law for an incompressible fluid, taking viscosity into account (negligible viscosity yields Euler's equation for conservation of momentum).

3.5 The Bernoulli Principle and how Lift is generated

We shall now derive the Bernoulli principle from the Cauchy momentum equation⁴⁶⁴⁸ for an incompressible fluid of negligible viscosity, such as air. Denoting the gravitational potential as ψ , we can rewrite the Cauchy momentum equation as:

$$\rho \mathbf{v} \cdot \nabla \mathbf{v} = \mathbf{f} - \nabla p \quad (3.69)$$

$$= \nabla \psi - \nabla p \quad (3.70)$$

Using the property:

$$\rho \mathbf{v} \cdot \nabla \mathbf{v} = \rho \left[\nabla \left(\frac{1}{2} v^2 \right) - \mathbf{v} \times (\nabla \times \mathbf{v}) \right]^3 \quad (3.74)$$

we can then write:

$$\nabla \left(\frac{\rho}{2} v^2 + p - \psi \right) = \mathbf{v} \times (\nabla \times \mathbf{v}) \quad (3.75)$$

$$\therefore \mathbf{v} \cdot \nabla \left(\frac{1}{2} \rho v^2 + p - \psi \right) = \mathbf{v} \cdot \mathbf{v} \times (\nabla \times \mathbf{v}) \quad (3.76)$$

$$\mathbf{v} \cdot \nabla \left(\frac{1}{2} \rho v^2 + p - \psi \right) = 0 \quad (3.77)$$

$$\therefore \frac{1}{2} \rho v^2 + p - \psi = C \quad (3.78)$$

along streamlines for some constant C .

³This property can be easily proven using summation notation:

$$\mathbf{v} \times (\nabla \times \mathbf{v}) = \epsilon_{ijl} \epsilon_{lmk} v_j \partial_m v_k \quad (3.72)$$

$$= (\delta_{im} \delta_{jk} - \delta_{ik} \delta_{jm}) v_j \partial_m v_k = \delta_{im} \delta_{jk} (v_j \partial_m v_k) - \delta_{ik} \delta_{jm} (v_j \partial_m v_k) \quad (3.73)$$

$$= v_k \partial_i v_k - v_m \partial_m v_k = \frac{1}{2} \nabla (v^2) - \mathbf{v} \cdot \nabla \mathbf{v} \quad (3.74)$$

where we used the property: $\mathbf{v} \nabla \mathbf{v}$

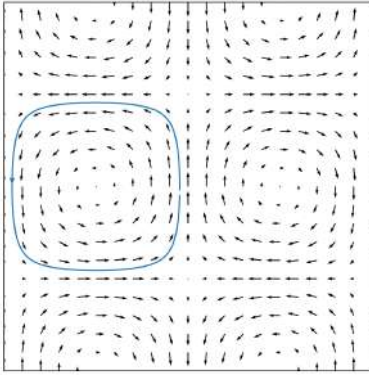


Figure 3.4: Streamline for the Vector Field $\mathbf{F}(x, y) = \sin x \sin y \hat{\mathbf{x}} + \cos x \cos y \hat{\mathbf{y}}$

Streamlines are curves tangent to the vector field \mathbf{v} . Hence, the angle between \mathbf{A} and \mathbf{v} must be 0. It follows that the solution to $\mathbf{v} \cdot \mathbf{A} = 0$ along streamlines is $\mathbf{A} = 0$ assuming the fluid is non-stationary ($|\mathbf{v}| \neq 0$). We have now reached a fundamental result in classical fluid dynamics, the Bernoulli principle:

Bernoulli Principle

$$\frac{1}{2}\rho v^2 + p - \psi = C \text{ along streamlines} \quad (3.79)$$

The Bernoulli Principle tells us that in high pressure regions, a fluid has low velocity and in low pressure regions, a fluid has high velocity. This is the driving force behind the mainstream explanation for lift. Indeed, schools often teach that an aircraft wing produces lift thanks to a difference in velocity between the air over and the air under. Since the air has to move a greater distance over the wing (due to its curvature), it must travel faster to meet up with the air under the wing in time. Therefore, there is greater pressure under the wing, generating lift.

Although partially correct, this explanation does raise various questions. How does an airplane fly upside down? How do planes with flat wings fly? Furthermore, studies, such as [a short video by Holger Babinski at the University of Cambridge](#), have shown that the air over the wing doesn't travel faster in order to "meet up" with the air under the wing. Obviously, this explanation alone can't explain how lift is generated in full detail.

In truth, pressure difference isn't solely responsible for lift as explained in Motoyama (2002).⁴⁸ When air moves over a wing, it follows its curvature due to the Coandă effect (the tendency of fluids to follow a surface, such as a jet of water following a cup's outer surface when wet). When the air leaves the wing, it is directed downwards, causing the air under the wing to be deflected down as well. By Newton's Third Law, there must be a reaction force pushing the wing upwards, this is lift. To generate more lift, it suffices to increase the angle of attack, directing even more air downwards.

Flaps work following this principle. They help direct more air downwards without necessarily increasing the angle of attack. Note that when the angle of attack is increased exceedingly, then

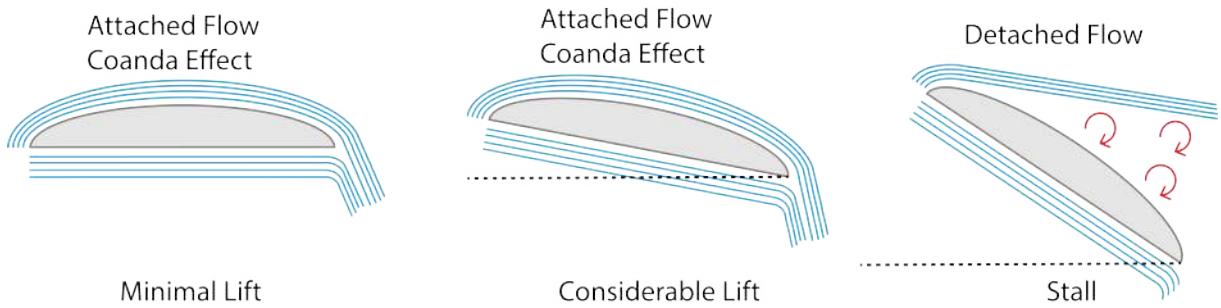


Figure 3.5: Lift generated at various angles of attack

the air streams will have a harder time following the wing's surface, leading to the formation of turbulent vortices. Therefore, little to no lift is generated and we reach stall

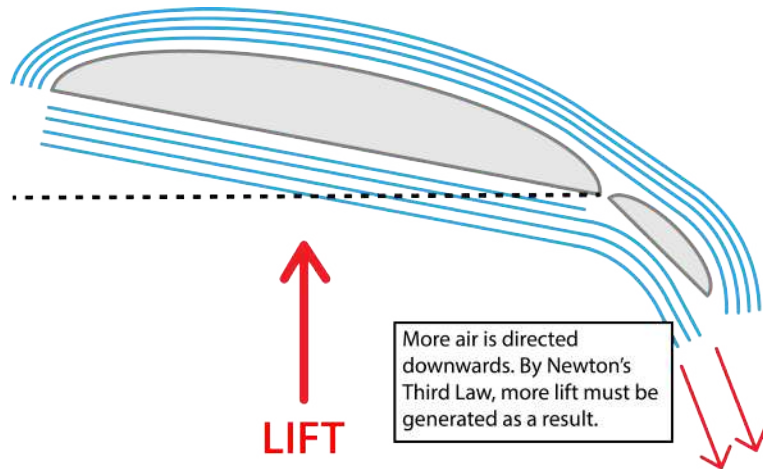


Figure 3.6: Increment in Lift when using Flaps, as opposed to increasing the angle of attack

Finally, it must also be noted that pressure difference does play a role in generating lift. Indeed, the air above a wing is more "compressed" due to their geometry. By the principle of conservation of mass, the air flowing through this "compressed" region must be equal to the air flowing under the wing. In other words, the air must move faster over the wing to conserve flow rate. Invoking the Bernoulli principle, lift must be generated.

3.6 Equation of Motion for a Frisbee in Flight

After having conceptually explained the dynamics behind flight, we will now try to formalize our discussion and derive the equations of motion for a Frisbee.

Let us denote the velocity and pressure below the Frisbee to be v_1, p_1 respectively, and the velocity and pressure above the Frisbee to be v_2, p_2 . Then, neglecting the change in height, the

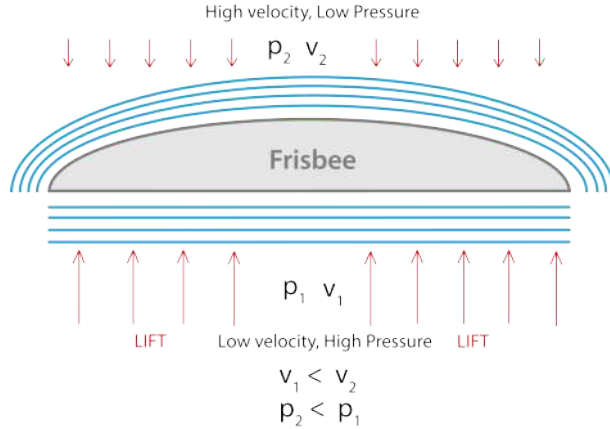


Figure 3.7: Air flow over and under a frisbee in flight

Bernoulli principle tells us that:

$$\frac{\rho v_1^2}{2} + p_1 = \frac{\rho v_2^2}{2} + p_2 \quad (3.80)$$

$$\frac{\rho(v_2^2 - v_1^2)}{2} = p_1 - p_2 \quad (3.81)$$

$$\frac{\rho}{2}(v_2^2 - v_1^2) = \Delta P \quad (3.82)$$

$$\frac{C_L \rho}{2} v_2^2 = \frac{F_L}{A} \quad (3.83)$$

$$F_L = \frac{1}{2} \rho A C_L v_2^2 \quad (3.84)$$

where C_L is the coefficient of lift defined as linearly related to the angle of attack *alpha*:

$$C_L = \underbrace{(C_{L0} + C_{L\alpha})}_{\text{depend on shape}} \alpha \quad (3.85)$$

Similarly:

$$F_D = \frac{1}{2} \rho A C_D v_2^2 \quad (3.86)$$

where:

$$C_D = C_{D0} + C_{D\alpha}(\alpha - \alpha_0)^2 \quad (3.87)$$

and we denoted the angle which generates the least lift with α_0 . We now get the system of differential equations:

$$\begin{cases} m \frac{dv_x}{dt} = -\frac{1}{2} \rho A C_D v_x^2 \sec \theta^2 \\ m \frac{dv_y}{dt} = \frac{1}{2} \rho A C_D v_x^2 \sec \theta^2 - mg \end{cases} \quad (3.88)$$

3.7 Simulating Frisbee Flight

Due to the complexities that arised when analytically solving this system of differential equations, numerical methods were employed. Runge-Kutta methods were used to produce height vs distance trajectories for a Frisbee thrown at varying angles of attack with initial velocity 15m/s . The following parameters were adopted: $m = 0.175\text{kg}$, $\rho = 1.23\text{kg/m}^3$, the Frisbee radius was 0.14cm , $C_{D0} = 0.08$, $C_{D\alpha} = 2.72$, $\alpha_0 = -4^\circ$, $C_{L0} = 0.15$, $C_{L\alpha} = 1.4$. The code used for this simulation can be found in Appendix A. The simulation's results are shown below:

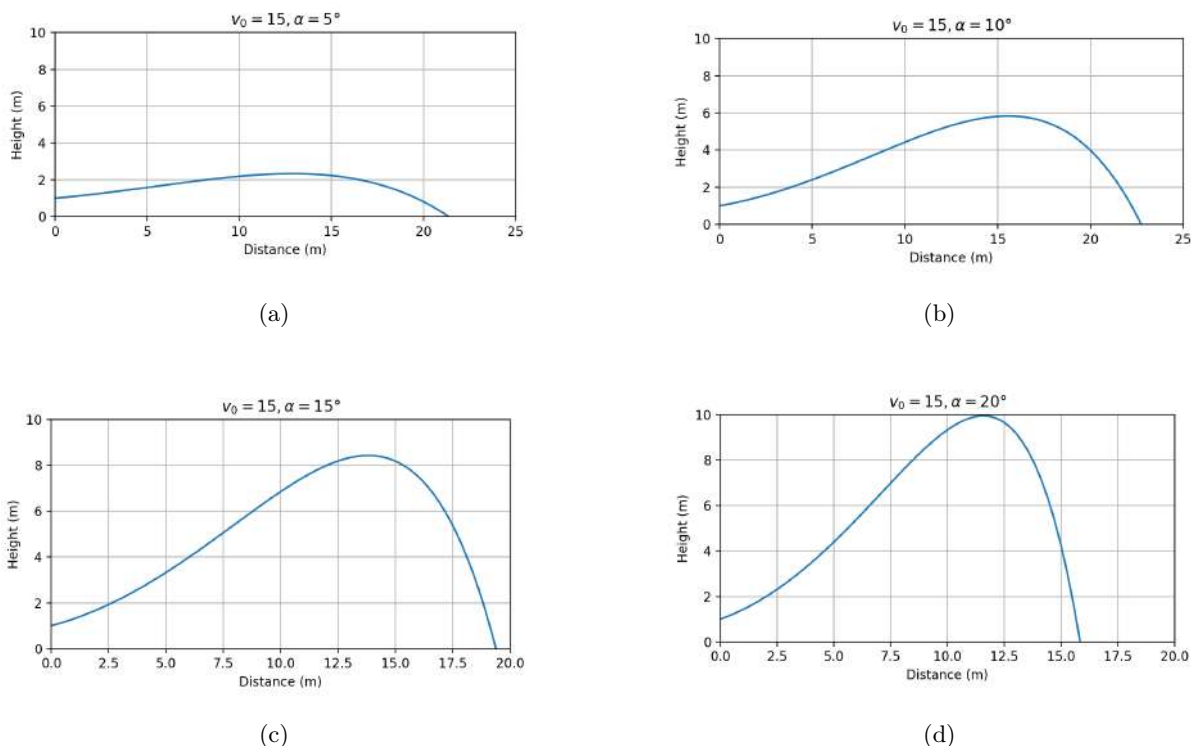


Figure 3.8: Trajectories of Frisbees thrown at $v_0 = 15$, with varying angles of attack

Two major features of these plots must be addressed. Firstly, an inflection point must always occur between the instant the Frisbee is thrown and the instant it reaches its maximum height H . As the angle of attack increases, this inflection point gets closer and closer to H . Furthermore, the second half of the trajectory is "compressed" compared to the first half. As the angle of attack increases, this asymmetry becomes more and more noticeable. This is clearly due to drag, since our coefficient of drag is quadratically related to the angle of attack. In the initial half of the flight, the drag forces aren't as noticeable and are contrasted by lift forces, pushing the frisbee upward. Once the disk reaches its maximum height, it starts accelerating downwards. The drag forces are now substantial, greatly reducing the Frisbee's horizontal acceleration. By the time the Frisbee falls to the ground, it will have travelled only a small distance horizontally.

Consider 3.8a. For a small angle of attack, more horizontal velocity is imparted to the Frisbee than vertical velocity. Thus, as expected, the Frisbee's maximum height was the lowest, around

2.36m, and travelled 21.44m horizontally. Hence, the lift force was very minimal, and the Frisbee fell to the ground quickly. With greater angles of attack, the Frisbee had a greater maximum height. One might intuitively expect that the greatest height would be achieved when throwing the disk vertically upwards. However, this is not the case, since the optimum height (13.43 m) was achieved when $\alpha = 65^\circ$. One plausible explanation could be that when throwing a Frisbee directly (or almost) upwards, then very little lift can be generated, reducing the maximum height that can be achieved. After a critical angle, as explained earlier, the Coanda effect won't take place, and the upper air streams won't follow the Frisbee's surface. However, our simulations don't take the Coanda effect into account. Another plausible explanation could be that imparting very little if not no horizontal velocity will not generate any lift, and hence the frisbee will act like a projectile.

Consider 3.8b. As we can see, more vertical velocity is imparted on the Frisbee, which travels a greater horizontal distance, 22.67m. It turns out that the Frisbee travels the farthest (23.29m) when $\alpha = 8^\circ$. For greater angles of attack, as shown in 3.8c and 3.8d, the Frisbee went significantly higher, but had a shorter range due to the significance of drag forces. All these results coincide with the conclusions made in *Morrison (2005)*.⁴⁶

Chapter 4

Rotation and the Motion of Spin Stabilised Disks

Contents

4.1	Introduction	61
4.2	Kinematics of Rotation	63
4.2.1	The Coriolis Effect	65
4.2.2	Euler Angles	68
4.3	Dynamics of Rigid Bodies	69
4.3.1	What are Rigid Bodies?	69
4.3.2	The Inertia Tensor	70
4.3.3	Angular Momentum	71
4.3.4	Euler's Equations	73
4.4	Gyroscopic Precession	74
4.4.1	Uniform Precession	74
4.4.2	Torque-Free Precession	76
4.5	Spin Stabilised Disk and Precession	78
4.6	Conclusion	79

4.1 Introduction

Having ended our study of the aerodynamical properties of a flying discus, we must now consider the mechanical properties of this body. "How does a Frisbee not flip over?", "Why does a Frisbee wobble?" and other questions cannot be answered purely using fluid mechanics. We must therefore refer to the dynamics of rigid bodies, and study seemingly unrelated phenomena such as gyroscopic precession.

In the previous chapter, we made a comparison between a wing and a Frisbee to describe how lift is generated. However, it must be noted that unlike wings, where one can distribute lift

over a region on the aerofoil, Frisbees have an irregular distribution of lift. Indeed, as explained in *M. Schuurmans*, (1990),⁴⁴ the flying disk usually has more lift exerted on the back half due to the curved rim. If we consider the air flow under the Frisbee, it is easy to see how the rims will produce turbulence on the back end, causing air to move more slowly on the back. This will in turn cause greater lift. Clearly however, the Frisbee still doesn't flip over despite the net torque acting upon it, why? Not only, the Frisbee also displays some sort of "wobbly" motion, which increases when spin is reduced, and is almost negligible for high rotational frequency.

Furthermore, a Frisbee can be noticed to veer to the left or to the right (depending on the direction of rotation) despite not being thrown at a banked angle. Note that all these phenomena, which are formally known as spin stabilisation and precession, also arise in gyroscopic motion.

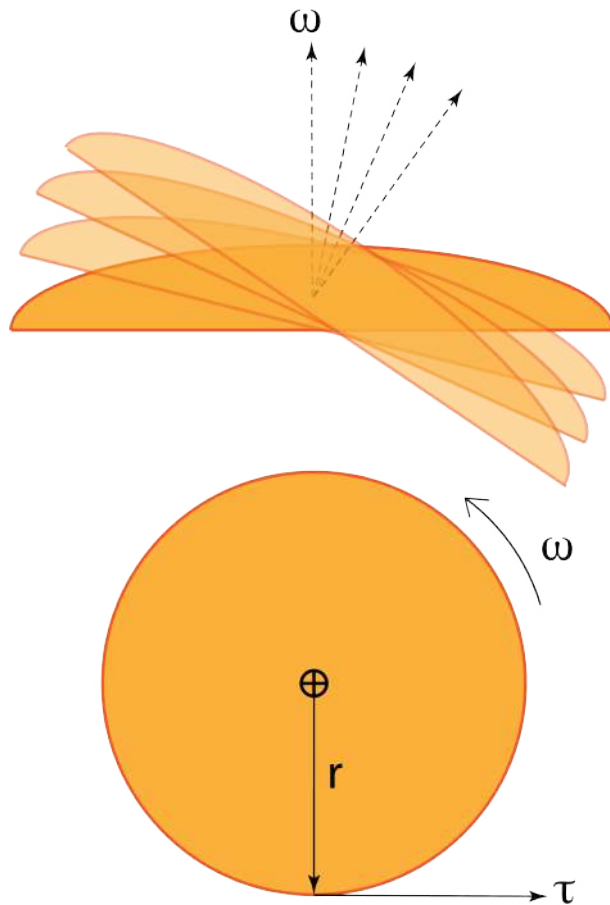


Figure 4.1: Explaining why Frisbees veer to the right/left due to Gyroscopic Precession

It is therefore of great interest to study the mechanics of rotation and spin in order to answer the aforementioned questions.

4.2 Kinematics of Rotation

Before carefully examining the dynamics of rigid bodies, such as a spinning Frisbee, we must first analyze the kinematics of rotating systems. The tools we shall develop will be of considerable convenience when building a mathematical model for rotating disks.

To specify the orientation of a body, it suffices to consider two systems of axes, one fixed in space relative to an external observer, and one fixed relative to the body. The angles that the two systems of axes make with each other define the orientation of the object.

Let us denote the fixed system of axes by \mathbf{e}'_i and the rotating system of axes by \mathbf{e}_i . Hence, the position vector to a point P can be written as $\mathbf{r} = x_i \mathbf{e}_i = x'_i \mathbf{e}'_i$. It follows that we may rewrite $\mathbf{e}_i = m_i \mathbf{e}'_i$. Hence, there must be an isometric transformation described by the orthogonal matrix

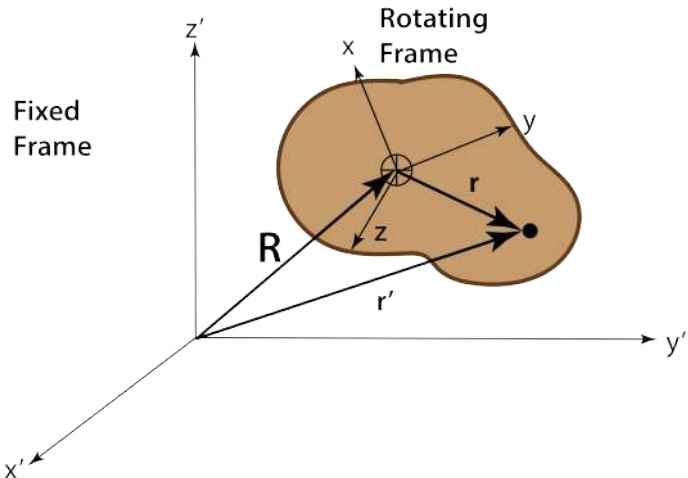


Figure 4.2: Kinematics of a Body in a Rotating Frame vs. Inertial Frame

M_{ij} satisfying:

$$\mathbf{e}_i = M_{ij} \mathbf{e}'_j \quad (4.1)$$

Differentiating (we follow some parts of S. Siklos Lecture notes on Classical Mechanics):⁴²

$$\dot{\mathbf{e}}_i = \dot{M}_{ij} \mathbf{e}'_j + \cancel{M_{ij}} \mathbf{e}'_j^0 \quad (4.2)$$

$$= \dot{M}_{ij} M_{jk}^{-1} \mathbf{e}_k \quad (4.3)$$

$$= \dot{M}_{ij} M_{kj} \mathbf{e}_k. \quad (4.4)$$

Let us define $\dot{M}_{ij}M_{kj} = \epsilon_{ikm}\omega_m$. We can then write:

$$\dot{\mathbf{e}}_i = \epsilon_{ikm}\omega_m \mathbf{e}_k \quad (4.5)$$

$$= \epsilon_{ikm}(\boldsymbol{\omega} \cdot \mathbf{e}_m) \mathbf{e}_k \quad (4.6)$$

$$= -\epsilon_{imk}(\boldsymbol{\omega} \cdot \mathbf{e}_m) \mathbf{e}_k \quad (4.7)$$

$$= -(\boldsymbol{\omega} \cdot \mathbf{e}_k)\epsilon_{ikm} \mathbf{e}_m \quad (4.8)$$

$$= -(\boldsymbol{\omega} \cdot \mathbf{e}_k) \mathbf{e}_i \times \mathbf{e}_k \quad (4.9)$$

$$= \omega_k \mathbf{e}_k \times \mathbf{e}_i \quad (4.10)$$

$$= \boldsymbol{\omega} \times \mathbf{e}_i \quad (4.11)$$

Alternatively, one could write:

$$R = \begin{pmatrix} \cos \theta & \sin \theta & 0 \\ -\sin \theta & \cos \theta & 0 \\ 0 & 0 & 1 \end{pmatrix} \quad (4.12)$$

$$\therefore \dot{R} = \dot{\theta} \begin{pmatrix} -\sin \theta & \cos \theta & 0 \\ -\cos \theta & -\sin \theta & 0 \\ 0 & 0 & 0 \end{pmatrix}, \quad RR^T = \begin{pmatrix} 0 & \dot{\theta} & 0 \\ -\dot{\theta} & 0 & 0 \\ 0 & 0 & 0 \end{pmatrix} \quad (4.13)$$

$$(4.14)$$

Comparing with $\epsilon_{ij}\omega_k$, we get that $\omega = \dot{\theta}$ as required. We may see the angular frequency ω as the "spin" of a rotating rigid body. Geometrically, this coincides with our understanding of rotation.

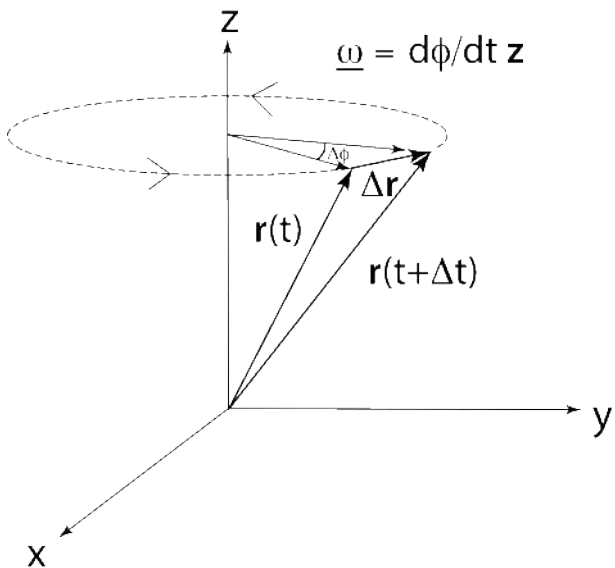


Figure 4.3: Angular Frequency of a rotating rigid body

Using this result to express the velocity of a body relative to the fixed frame:

$$\dot{\mathbf{r}} = \dot{x}_i \mathbf{e}_i + x_i (\boldsymbol{\omega} \times \mathbf{e}_i) \quad (4.15)$$

$$= \dot{x}_i \mathbf{e}_i + \boldsymbol{\omega} \times \mathbf{r} \quad (4.16)$$

This result is very intuitive. Indeed, the first term is the velocity of the body in the moving frame, whereas the second term is the velocity due to the rotation of the moving frame. Their addition will give the overall velocity of the body in an external fixed frame.

Differentiating $\dot{\mathbf{r}}$, we get:

$$\ddot{\mathbf{r}} = \ddot{x}_i \mathbf{e}_i + \dot{x}_i \boldsymbol{\omega} \times \mathbf{e}_i + \dot{\boldsymbol{\omega}} \times \mathbf{e}_i + \boldsymbol{\omega} \times (\dot{x}_i \mathbf{e}_i + \boldsymbol{\omega} \times \mathbf{r}) \quad (4.17)$$

$$= \ddot{x}_i \mathbf{e}_i + 2\dot{x}_i \boldsymbol{\omega} \times \mathbf{e}_i + \dot{\boldsymbol{\omega}} \times \mathbf{r} + \boldsymbol{\omega} \times (\boldsymbol{\omega} \times \mathbf{r}) \quad (4.18)$$

$$m\mathbf{a} = \mathbf{F}^{in} - \underbrace{2m\boldsymbol{\omega} \times \mathbf{v} - m\dot{\boldsymbol{\omega}} \times \mathbf{r} - m\boldsymbol{\omega} \times \mathbf{r}}_{\text{Fictitious Forces}} \quad (4.19)$$

We see from (4.19) that the forces acting on a rigid body in an inertial frame include fictitious forces. These are "fake forces" that account for a deviation in the observed behaviour between an inertial frame and a non-inertial frame. $2m\boldsymbol{\omega} \times \mathbf{v}$ is the Coriolis Force, $m\dot{\boldsymbol{\omega}} \times \mathbf{r}$ is the Euler force, and $m\boldsymbol{\omega} \times \mathbf{r}$ is the centrifugal force (not to be confused with the centripetal force, which unlike the centrifugal force, keeps an object in a circular trajectory).

Fictitious forces, as the name suggests, aren't real forces. They are fictional forces that account for deviations in observations taken in the inertial frame. Consider a car moving in a straight line, and another car moving around a curve. Let them depart from the same point at the same time at the same speed. From the perspective of the second car, the car moving in the straight line will seem to be acted upon by an external force, curving its trajectory. This force is the Coriolis effect. Indeed, if we consider a body moving in a circular trajectory, then the moment it is "released" at point P , it will move into a straight line from an external observer tangent to the circular trajectory at P . In frame P, the body will have a curved trajectory, instead of straight. To account for this difference, we must add a fictitious force acting horizontally to make sure Newton's Second Law still holds in frame P. We strongly recommend visiting [udiproad's video](#) for good visualisation of these forces.

4.2.1 The Coriolis Effect

Perhaps the most abstract fictitious force is the Coriolis force, despite being leading to the formation of countless natural phenomena: cyclones, jet streams, ocean and wind currents, turbidity currents, and even the vortices formed when flushing the toilet.

Consider once again a fixed set of axes \mathbf{e}'_i and a set of axes \mathbf{e}_i with coincident origins rotating

with angular frequency ω about one of \mathbf{e}'_i (\mathbf{e}'_2 in Figure), as shown below. Then, in a time interval dt the axis \mathbf{e}_3 has moved by $d\mathbf{e}_3 = \omega dt(\mathbf{e}_3 \times \hat{\omega})$. Hence, $\frac{d\mathbf{e}_3}{dt} = \omega(\mathbf{e}_3 \times \hat{\omega}) \implies \frac{d\mathbf{e}_3}{dt} = \boldsymbol{\omega} \times \mathbf{e}_3$

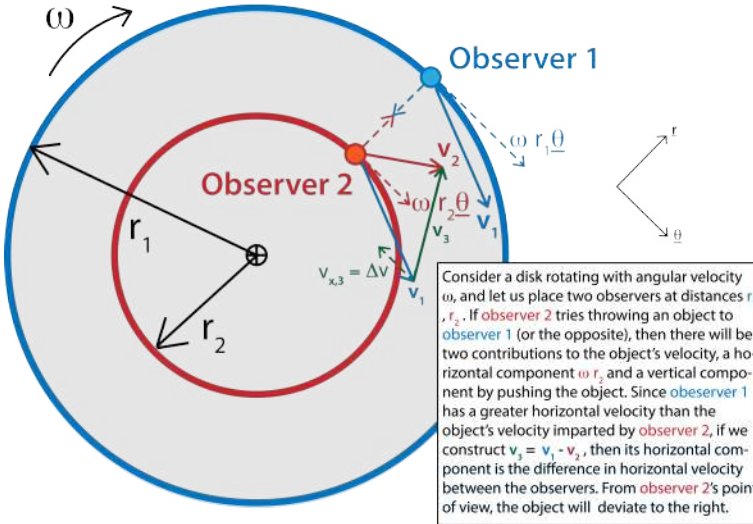


Figure 4.4: Coriolis Effect on a Rotating Disk

If we now consider a rotating disk. Then, an observer placed on the disk will move faster as they get farther and farther away from the axis of rotation. Let us now replace the disk by the Earth oriented such that the axis of rotation points out of the paper, as shown below. We place two observers, one at a distance r_1 and the other at a distance r_2 with $r_2 < r_1$. Now, imagine throwing an object from observer 1 to observer 2. Since observer 1 has a greater horizontal velocity, once it arrives at a distance r_1 from the axis of rotation, it will have "deviated" to the right compared to observer 2. Similarly, if observer 2 throws an object to observer 1, then it will be "deflected" to the left.

The same applies if we consider throwing an object from a tall building. From our previous analysis, ignoring any affects from wind, we expect there to be some horizontal deflection, since the ball is moving faster on top of the building than at the bottom. In fact, the velocity at the top of the building (height h) is $(R_\oplus + h)\omega$, where R_\oplus is the radius of the Earth and ω its angular frequency, whereas the velocity at the bottom is $R_\oplus\omega$. When the object is thrown, a velocity $(R_\oplus + h)\omega$ must be imparted. Hence, relative to "ground zero", the object is moving at $h\omega$ at $t = 0$. The net force acting on this body is:⁴²

$$\mathbf{F} = m\mathbf{g} - 2m\boldsymbol{\omega} \times \mathbf{v} - m\dot{\boldsymbol{\omega}} \times \mathbf{r} - m\boldsymbol{\omega} \times \mathbf{r} \quad (4.20)$$

Compared to the Coriolis effect, the Euler terms can be omitted. Furthermore, since we are not interested in forces acting radially, we will also omit the centrifugal term (which, unlike the centripetal term, doesn't act tangentially). We therefore get:

$$\mathbf{F} = m\mathbf{g} - 2m\boldsymbol{\omega} \times \mathbf{v} \quad (4.21)$$

Integrating once, and assuming $\dot{\mathbf{r}}_0 = 0$ since the object is released from rest, we get:

$$\ddot{\mathbf{r}} = \mathbf{g} - 2\boldsymbol{\omega} \times (\mathbf{r} - \mathbf{r}_0) \quad (4.22)$$

Substituting 4.22 into 4.21, we get:

$$\ddot{\mathbf{r}} = \mathbf{g} - 2\boldsymbol{\omega} \times (\mathbf{g}t - \underbrace{2\boldsymbol{\omega} \times (\mathbf{r} - \mathbf{r}_0)}_0) \quad (4.23)$$

$$= -\mathbf{g} - 2\boldsymbol{\omega} \times \mathbf{g}t \quad (4.24)$$

Integrating twice:

$$\mathbf{r} - \mathbf{r}_0 = \frac{1}{2}\mathbf{g}t^2 - \frac{1}{3}\boldsymbol{\omega} \times \mathbf{g}t^3 \quad (4.25)$$

Substituting $t = \sqrt{2h/g}$, and assuming we are on the equator (such that $|\boldsymbol{\omega} \times \mathbf{g}| = \omega g$):

$$\Delta x = \frac{2\sqrt{2}}{3} \left(\frac{h^{3/2}\omega}{\sqrt{g}} \right) \quad (4.26)$$

Therefore, if we were to drop an object from the Burj Khalifa (828 m) under ideal conditions, the deviation would be around 52 cm. Looking back at our initial discussion on the problem, we can now see that if the velocity of the ball relative to the ground is $h\omega$, then after time t , the deflection will be $h\omega t$, which coincides with our formula.

Furthermore, this result makes physically sense. Indeed, we expect that for a faster spinning planet, this deviation would be greater, since the discrepancy between the ground zero velocity and the velocity on top of the building would be greater. Moreover, for greater gravitational acceleration, the object has less time to deflect, which explains the inverse proportionality $\Delta x \propto \frac{1}{\sqrt{g}}$.

If we now look at masses of air moving in the atmosphere, we expect the Coriolis effect to be crucial in our understanding of meteorology, as explained in *D. Kleppner and R. Kolenkow (2014)*.⁴¹ Hence, masses from the northern hemisphere will be deflected to the left, and the southern hemisphere will be deflected to the right, forming a vortex. Note that the Coriolis effect is clearly null at the equator, which is why cyclones don't form there.

Let us look at an air packet rotating about a low pressure point, with a pressure difference ΔP , as shown below.

Analyzing the forces acting radially:

$$\frac{mv^2}{r} = S\Delta P - 2m\omega v \sin \theta \quad (4.27)$$

$$\frac{v^2}{r} = \frac{1}{\rho} \Delta P - 2\omega v \sin \theta \quad (4.28)$$

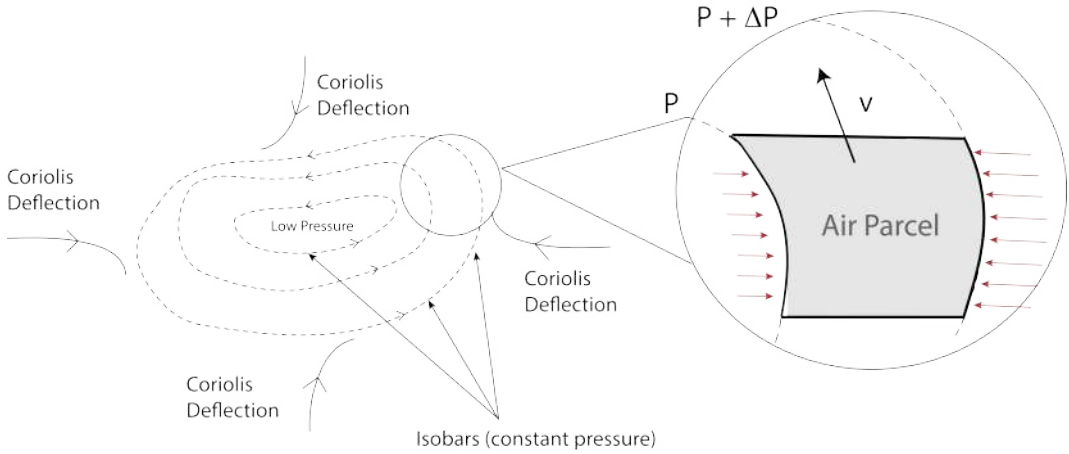


Figure 4.5: The formation of cyclones in the Northern Hemisphere

Taking $\Delta r \rightarrow 0$, and neglecting the $\frac{v^2}{r}$ ¹ (according to Navier Stoke's equation, for higher pressure regions as we get farther away from the cyclone eye, the wind current velocity is low):

$$v = \frac{1}{2\omega\rho \sin \theta} \frac{dP}{dr} \quad (4.30)$$

As the pressure gradient increases, we expect the forces acting radially on the air parcel to increase, increasing the cyclone's tangential velocity. This agrees with (4.30) Moreover, as the angular velocity of the Earth increases, then our formula tells us that the cyclone's tangential velocity will decrease

4.2.2 Euler Angles

Up until now, we have referred to "rotations" and rotating frames quite vaguely. We will now try to rigorously define what is meant by a rotating frame of reference. Consider a set of axes \mathbf{e}_a . Then, any fixed origin rotation of these axes can be parametrised using Euler Angles, as shown in.⁴⁰ This parametrisation consists in three separate rotations:

$$\mathbf{e}_a \xrightarrow{R(\phi)} \mathbf{e}'_a \xrightarrow{R(\theta)} \mathbf{e}''_a \xrightarrow{R(\psi)} \tilde{\mathbf{e}}_a \quad (4.31)$$

Firstly, we rotate the axes by ϕ about \mathbf{e}_3 , so that $\mathbf{e}_a = R(\phi)_{ab}\mathbf{e}_b$, where:

$$R(\phi) = \begin{pmatrix} \cos \phi & \sin \phi & 0 \\ -\sin \phi & \cos \phi & 0 \\ 0 & 0 & 1 \end{pmatrix} \quad (4.32)$$

¹For very strong wind currents, this term can't be neglected. The differential equation then turns into:

$$v = \sqrt{(r\omega \sin \theta)^2 + \frac{r}{\rho} \frac{dP}{dr}} - r\omega \sin \theta \quad (4.29)$$

Secondly, we rotate the new axes by θ about \mathbf{e}'_1 so that $\mathbf{e}''_a = R(\theta)_{ab}\mathbf{e}'_b$, where:

$$R(\theta) = \begin{pmatrix} 1 & 0 & 0 \\ 0 & \cos \theta & \sin \theta \\ 0 & -\sin \theta & \cos \theta \end{pmatrix} \quad (4.33)$$

Finally, we rotate the newest axes by ψ about \mathbf{e}''_3 so that $\tilde{\mathbf{e}}_a = R(\psi)_{ab}\mathbf{e}''_b$, where:

$$R(\psi) = \begin{pmatrix} \cos \psi & \sin \psi & 0 \\ -\sin \psi & \cos \psi & 0 \\ 0 & 0 & 1 \end{pmatrix} \quad (4.34)$$

We can represent these transformations geometrically: We can now use these angles to re-define

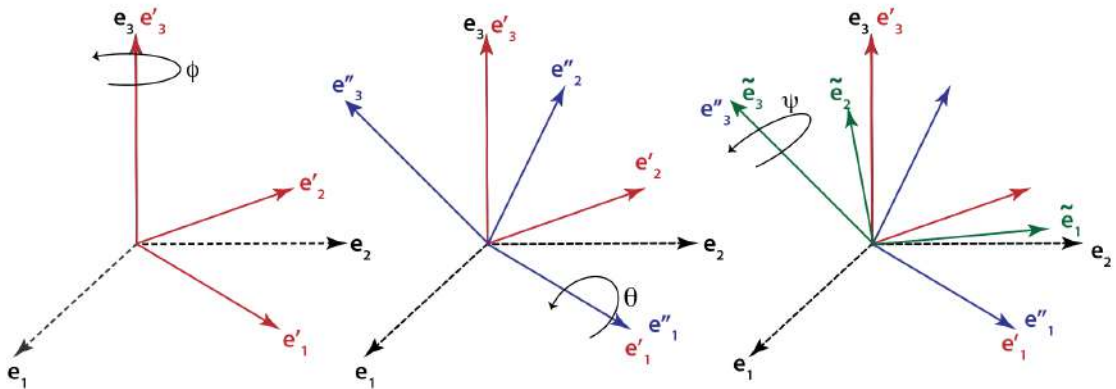


Figure 4.6: Specifying a body's orientation using Euler Angles

the angular frequency:

$$\boldsymbol{\omega} = \dot{\phi}\mathbf{e}_3 + \dot{\theta}\mathbf{e}'_1 + \dot{\psi}\tilde{\mathbf{e}}_3 \quad (4.35)$$

$$\mathbf{e}_3 = \sin \theta \sin \psi \tilde{\mathbf{e}}_1 + \sin \theta \cos \psi \tilde{\mathbf{e}}_2 + \cos \theta \tilde{\mathbf{e}}_3 \quad (4.36)$$

$$\mathbf{e}'_1 = \cos \psi \tilde{\mathbf{e}}_1 - \sin \psi \tilde{\mathbf{e}}_2 \quad (4.37)$$

$$\boldsymbol{\omega} = (\dot{\phi} \sin \theta + \dot{\theta} \cos \psi) \tilde{\mathbf{e}}_1 + (\dot{\phi} \sin \theta \cos \psi - \dot{\theta} \sin \psi) \tilde{\mathbf{e}}_2 + (\dot{\psi} + \dot{\phi} \cos \theta) \tilde{\mathbf{e}}_3 \quad (4.38)$$

4.3 Dynamics of Rigid Bodies

4.3.1 What are Rigid Bodies?

We will now begin examining the dynamics of rigid bodies,³⁹ systems of particles with zero internal degrees of freedom constraining individual particles to be a constant distant apart. If

we consider a system of N particles, then this is a rigid body as long as:

$$\frac{d}{dt}(|\mathbf{r}_i - \mathbf{r}_j|) = 0, \forall i, j = 0, 1, 2 \dots N \quad (4.39)$$

In general, a rigid body has six degrees of freedom, three for translational motion and three for the orientation of the body with respect to a system of axes.

Throughout the section, we will consider one inertial frame and one rotating frame whose origin coincides with the body's center of mass. Let us denote the position vector of any point particle in the body as \mathbf{r} in the rotating frame, and \mathbf{r}' in the fixed frame. Previous analysis has shown that:

$$\mathbf{v}' = \mathbf{v} + \boldsymbol{\omega} \times \mathbf{r} \quad (4.40)$$

This velocity can be decomposed into one term amounting for translation motion, the translational velocity, and one term amounting for rotational motion, the angular velocity.

4.3.2 The Inertia Tensor

How do we specify a rigid body's energy? Consider the kinetic energy for a system of particles: $T = \sum \frac{1}{2}m\mathbf{v}'^2$. Using (4.40):

$$T = \sum \frac{1}{2}m(\mathbf{v} + \boldsymbol{\omega} \times \mathbf{r})^2 \quad (4.41)$$

$$= \sum \frac{1}{2}mv^2 + \frac{1}{2} \sum m(\boldsymbol{\omega} \times \mathbf{r})^2 + \sum m\mathbf{v} \cdot (\boldsymbol{\omega} \times \mathbf{r}) \quad (4.42)$$

$$= \sum \frac{1}{2}mv^2 + \sum \frac{1}{2}m(\boldsymbol{\omega} \times \mathbf{r})^2 + \sum m\mathbf{r}^0 \cdot (\boldsymbol{\omega} \times \mathbf{v}) \quad (4.43)$$

$$= \frac{1}{2}Mv^2 + \frac{1}{2} \sum m(\boldsymbol{\omega} \times \mathbf{r}) \times (\boldsymbol{\omega} \times \mathbf{r}) \quad (4.44)$$

$$= \underbrace{\frac{1}{2}Mv^2}_{T_{tran}} + \underbrace{\frac{1}{2} \sum m[\boldsymbol{\omega}^2 r^2 - (\boldsymbol{\omega} \cdot \mathbf{r})^2]}_{T_{rot}} \quad (4.45)$$

Rewriting the last equation in tensor form:

$$T_{rot} = \frac{1}{2}m_i(\omega_i^2 r_i^2 - \omega_i \omega_k r_k r_i) \quad (4.46)$$

$$= \frac{1}{2}m_i(\omega_i \omega_k \delta_{ik} r_j^2 - \omega_i \omega_k r_i r_k) \quad (4.47)$$

$$= \frac{1}{2}\omega_i \omega_k \underbrace{m_i(r_i^2 \delta_{ij} - r_i r_k)}_{\text{Inertia Tensor } I_{ik}} \quad (4.48)$$

If we now define the Inertia Tensor to be $I_{ik} = m_i(r_i^2 \delta_{ij} - r_i r_k)$, then we can rewrite:

$$T_{rot} = \frac{1}{2}\omega_i \omega_k I_{ik} = \frac{1}{2}\boldsymbol{\omega} \cdot \mathbf{I} \cdot \boldsymbol{\omega} \quad (4.49)$$

Let us expand the inertia tensor:

$$I = \begin{bmatrix} m(y^2 + z^2) & -mxy & -mxz \\ -myx & m(x^2 + z^2) & -myz \\ -mzx & -mzy & m(x^2 + y^2) \end{bmatrix} \quad (4.50)$$

The diagonal entries I_{ii} are called the *Moments of Inertia* about their respective principal axes of rotation, whereas the other entries are called *Products of Inertia*. If we make the rotating frame coincide with the principal axes of rotation so that their origins coincide with the center of mass, then our expression for kinetic energy is greatly simplified:

$$T_{rot} = \frac{1}{2}(I_1\omega_1^2 + I_2\omega_2^2 + I_3\omega_3^2) \quad (4.51)$$

Note that the products of inertia terms vanished. This is because when our set of axes coincides with the symmetry axes of the body, then for every mass located at (x_i, y_i) , there will be an equal mass at $(x_i, -y_i)$. Hence the inertia term I_{xy} cancel out, and so do all other products of inertia. Physically, the moment of inertia defines the amount of torque needed to obtain a desired amount of angular acceleration. It is the equivalent of mass in translational mechanics. Indeed, they both depend on the shape and geometry of the object. If we now multiply the moment of inertia by angular velocity, then we get Angular momentum, analogous to traditional momentum.

4.3.3 Angular Momentum

We will now closely follow D. Tong Lectures on Classical Dynamics.⁴³ Let us define the angular momentum of a rigid body to be:

$$\mathbf{L} = \sum_i m_i(\mathbf{r}'_i \times \mathbf{v}'_i) \quad (4.52)$$

Differentiating:

$$\frac{d\mathbf{L}}{dt} = \sum_i (\mathbf{v}_i \times \mathbf{p}_i + \mathbf{r}_I \times \frac{d\mathbf{p}_i}{dt}) \quad (4.53)$$

$$= \sum_i \left[\mathbf{v}'_i \times m_i \mathbf{v}' + \mathbf{r}'_i \times (\mathbf{F}^{\text{ext}} + \sum_{i \neq j} \mathbf{F}_{ij}) \right] \quad (4.54)$$

$$= \underbrace{\sum_i \mathbf{r}'_i \times \mathbf{F}^{\text{ext}}}_{\text{Net ext. torque}} + \sum_i \sum_{i \neq j} \mathbf{r}'_i \times \mathbf{F}_{ij} \quad (4.55)$$

If we define the tet external torque as $\boldsymbol{\tau} = \sum_i \mathbf{r}_i \times \mathbf{F}^{\text{ext}}$, then:

$$\frac{d\mathbf{L}}{dt} = \boldsymbol{\tau} + \sum_i \sum_j \mathbf{r}'_i \times \mathbf{F}_{ij} \quad (4.56)$$

$$= \boldsymbol{\tau} + \sum_j \sum_i \mathbf{r}'_j \times \mathbf{F}_{ji} \quad (4.57)$$

$$= \boldsymbol{\tau} - \sum_i \sum_j \mathbf{r}'_j \times \mathbf{F}_{ij} \quad (4.58)$$

Summing 4.56 and 4.58, we get:

$$\frac{d\mathbf{L}}{dt} = \boldsymbol{\tau} - \frac{1}{2} \sum_i \sum_j (\mathbf{r}_i - \mathbf{r}_j) \times \overrightarrow{\mathbf{F}_{ij}}^0 \quad (4.59)$$

$$= \boldsymbol{\tau} \quad (4.60)$$

This relationship we have derived is the Principle of Conservation of Angular momentum (analogous to the Principle of Conservation of momentum).

Conservation of Angular Momentum

$$\frac{d\mathbf{L}}{dt} = \boldsymbol{\tau} \quad (4.61)$$

We can derive a similar relation in the rotating frame such that the origin coincides with the center of mass of the body. Let us define the position vector of the center of mass in the fixed frame to be $\mathbf{R} = \frac{1}{M} \sum_i m_i \mathbf{r}_i$:

$$\mathbf{L}' = \sum_i m_i \mathbf{r}'_i \times \mathbf{v}_i \quad (4.62)$$

$$= \sum_i m_i (\mathbf{r}_i - \mathbf{R}) \times (\dot{\mathbf{r}}_i - \dot{\mathbf{R}}) \quad (4.63)$$

$$= \sum_i m \mathbf{r}_i \times \dot{\mathbf{r}}_i - \sum_i m \mathbf{R}_i \times \dot{\mathbf{r}}_i - \sum_i m_i \mathbf{r}_i \times \dot{\mathbf{R}} + \sum_i m_i \mathbf{R} \times \dot{\mathbf{R}} \quad (4.64)$$

$$= \mathbf{L} - \mathbf{R} \times M \dot{\mathbf{R}} - M \mathbf{R} \times \dot{\mathbf{R}} + M \mathbf{R} \times \dot{\mathbf{R}} \quad (4.65)$$

$$= \mathbf{L} - \mathbf{R} \times M \dot{\mathbf{R}} \quad (4.66)$$

Differentiating:

$$\frac{d\mathbf{L}'}{dt} = \frac{d\mathbf{L}}{dt} - \mathbf{R} \times M\ddot{\mathbf{R}} \quad (4.67)$$

$$= \boldsymbol{\tau} - M\mathbf{R} \times \ddot{\mathbf{R}} \quad (4.68)$$

$$= \sum_i \mathbf{r}_i \times \mathbf{F}_i^{ext} - \sum m_i \mathbf{R} \times \mathbf{F}_i^{ext} \quad (4.69)$$

$$= \sum_i (\mathbf{r}_i - \mathbf{R}) \times \mathbf{F}_i^{ext} \quad (4.70)$$

$$= \sum_i \mathbf{r}'_i \times \mathbf{F}_i^{ext} \quad (4.71)$$

$$= \boldsymbol{\tau}' \quad (4.72)$$

We therefore have that in the rotating frame, where the origin coincides with the center of mass, the conservation of angular momentum takes the same form as in the inertial frame:

$$\frac{d\mathbf{L}'}{dt} = \boldsymbol{\tau}' \quad (4.73)$$

In general, the conservation of angular momentum tells us that if there is any net torque acting on a rigid body, then its angular momentum will "chase it". This is because the torque acts in the direction of change in angular momentum. For example, if the angular momentum acts on the axis of rotation of a spinning disk, and the net torque points into of the paper, then the angular momentum will start moving out of the paper, and the disk will nosedive from the reader's.

This is quite an interesting phenomenon. If we apply a force pointing downwards at the eastern edge of a disk spinning anticlockwise, then the disk will not depress to the right, it will depress backwards, as shown below. As we will see in the following sections, this phenomenon explains precession, the "wobble" in flying discs, and even the mechanics of orbits!

4.3.4 Euler's Equations

The principle of conservation of Angular Momentum tells us that:

$$\boldsymbol{\tau} = \frac{d\mathbf{L}}{dt} \quad (4.74)$$

$$= \frac{dL_a}{dt} \mathbf{e}_a + L_a \frac{d\mathbf{e}_a}{dt} \quad (4.75)$$

$$= \frac{dL_a}{dt} \mathbf{e}_a + L_a (\boldsymbol{\omega} \times \mathbf{e}_a) \quad (4.76)$$

$$= \frac{dL_a}{dt} \mathbf{e}_a + (\boldsymbol{\omega} \times \mathbf{L}_a) \quad (4.77)$$

Expanding:

$$\boldsymbol{\omega} \times \mathbf{L} = \begin{vmatrix} \mathbf{e}_1 & \mathbf{e}_2 & \mathbf{e}_3 \\ \omega_1 & \omega_2 & \omega_3 \\ L_1 & L_2 & L_3 \end{vmatrix} \quad (4.78)$$

hence

$$\boldsymbol{\omega} \times \mathbf{L}_a = \begin{cases} (\omega_2 L_3 - \omega_3 L_2) \mathbf{e}_1 & \text{for } a = 1 \\ (\omega_1 L_3 - \omega_3 L_1) \mathbf{e}_2 & \text{for } a = 2 \\ (\omega_1 L_2 - \omega_2 L_1) \mathbf{e}_3 & \text{for } a = 3 \end{cases} \quad (4.79)$$

We finally get the Euler equations:

Euler Equations for Rigid Bodies

$$\begin{cases} I_1 \dot{\omega}_1 + \omega_2 \omega_3 (I_3 - I_2) = \tau_1 \\ I_2 \dot{\omega}_2 + \omega_3 \omega_1 (I_1 - I_3) = \tau_2 \\ I_3 \dot{\omega}_3 + \omega_1 \omega_2 (I_2 - I_1) = \tau_3 \end{cases} \quad (4.80)$$

4.4 Gyroscopic Precession

We will now tackle the problem of determining a gyroscope's equations of motion, following *Kleppner and Kolenkow* (2014)⁴¹ and *Lemos* (2015)⁴⁰.

4.4.1 Uniform Precession

Let us consider a gyroscope with mass M and axle length l , spinning at rate ω_s with spin angular momentum L_s . Then, by the parallel axis theorem, the moment of inertia through the z axis is $I_p = I_{zz} + Ml^2$ so that $L_z = I_p \omega_z$. Similarly, the moment of inertia through the x axis is $I_p = I_{xx} + Ml^2$ so that $L_x = I_p \omega_x$. Consider a gyroscope rotating about the z axis for $\theta_z \ll 1$ with angular velocity ω_z . Then, we can decompose the angular momentum into its components:

$$L_x = -L_s \sin \theta_z \approx -L_s \theta_z \quad (4.81)$$

$$L_y = L_s \cos \theta_z \approx L_s \quad (4.82)$$

$$L_z = I_p \omega_z \quad (4.83)$$

Similarly, for rotation about the x-axis:

$$L_x = I_p \omega_x \quad (4.84)$$

$$L_y = L_s \cos \theta_x \approx L_s \quad (4.85)$$

$$L_z = L_s \sin \theta_x \approx L_s \theta_x \quad (4.86)$$

Summing these contributions, we find:

$$L_x = I_p \omega_x - L_s \theta_z \quad (4.87)$$

$$L_y = L_s \quad (4.88)$$

$$L_z = I_p \omega_z + L_s \theta_x \quad (4.89)$$

We can now differentiate, and equate $\dot{\mathbf{L}} = \tau_x \mathbf{e}_1 = -lW \mathbf{e}_1$:

$$I_p \dot{\omega}_x - L_s \omega_z = -lW \quad (4.90)$$

$$\dot{L}_s = 0 \quad (4.91)$$

$$I_p \dot{\omega}_z + L_s \omega_x = 0 \quad (4.92)$$

Differentiating 4.90, and substituting 4.92:

$$I_p \frac{d^2 \omega_x}{dt^2} - \frac{L_s^2}{I_p} \omega_x = 0 \quad (4.93)$$

from which we get the ODE:

$$\frac{d^2 \omega_x}{dt^2} - \left(\frac{L_s}{I_p} \right)^2 \omega_x = 0 \quad (4.94)$$

Setting $\gamma = \frac{L_s}{I_p}$, then the equations of motion for the gyroscope are:

$$\omega_x = A \cos(\gamma t + \psi) \quad (4.95)$$

$$\omega_z = \frac{lW}{L_s} - A \sin(\gamma t + \psi) \quad (4.96)$$

Integrating directly, and setting $\theta_x(0) = \theta_0$:

$$\theta_x = \theta_0 \sin(\gamma t) \quad (4.97)$$

$$\theta_z = \frac{lW}{L_s} t + \theta_0 \cos(\gamma t) \quad (4.98)$$

For uniform precession, we set $\theta_0 = 0$, so that the rate of precession Ω_{pre} is

$$\Omega_{pre} = \frac{lMg}{L_s} \quad (4.99)$$

Let us analyse this result physically. If we increase the torque acting on the flywheel, then we expect the rate of precession to increase, because the rate at which the angular momentum rotates around (hence the rate at which the axis of rotation of the flywheel precesses at) is equal to the torque. The greater the torque, the faster the angular momentum rotates, which agrees with our formula. If the angular momentum is greater however, then the flywheel will have a smaller tendency of changing its axis of rotation. Hence, the precession frequency will decrease, agreeing with our equation.

This is a fundamental point. The spin angular momentum dictates the tendency of an object's axis of rotation to change. This gives insight as to how a Frisbee is stabilised. By spinning the Frisbee, the angular momentum vector is large, and hence the Frisbee's axis of rotation is less likely to be affected by external torque. Not only, this also explains why faster spinning frisbees have a less noticeable precession.

4.4.2 Torque-Free Precession

Consider a spinning flywheel with spin angular momentum \mathbf{L}_ω about its symmetry axis, such that in the frame fixed to the body's center of mass: $\theta_x \ll 1$ and $\theta_y \ll 1$. We assume that the body isn't acted upon by external torque. Splitting up the body's angular momentum into components, we find:

$$L_x = I_{xx} \frac{d\theta_x}{dt} + L_\omega \sin \theta_y \quad (4.100)$$

$$L_y = I_{yy} \frac{d\theta_y}{dt} - L_\omega \sin \theta_x \quad (4.101)$$

$$L_z = I_s \omega_s \cos \theta_y \quad (4.102)$$

We now use small angle approximations and the principle of conservation of angular momentum:

$$I_{xx} \frac{d^2 \theta_x}{dt^2} + L_\omega \frac{d\theta_y}{dt} = 0 \quad (4.103)$$

$$I_{yy} \frac{d^2 \theta_y}{dt^2} - L_\omega \frac{d\theta_x}{dt} = 0 \quad (4.104)$$

$$I_s \frac{d\omega_s}{dt} = 0 \quad (4.105)$$

Consider the first two equations. Differentiating (4.104), we get

$$I_{yy} \frac{d^2 \omega_y}{dt^2} - L_\omega \frac{d\omega_x}{dt} = 0 \quad (4.106)$$

Substituting (4.103) into (4.106):

$$I_{yy} \frac{d^2 \omega_y}{dt^2} + \frac{L_\omega^2}{I_{yy}} \omega_y = 0 \quad (4.107)$$

$$I_{xx} I_{yy} \frac{d^2 \omega_y}{dt^2} + L_\omega^2 \omega_y = 0 \quad (4.108)$$

$$\frac{I_{xx}^2}{L_\omega^2} \frac{d^2 \omega_y}{dt^2} + \omega_y = 0 \quad (4.109)$$

We finally get the equation:

$$\frac{d^2 \omega_y}{dt^2} + \gamma^2 \omega_y = 0, \quad \gamma = \frac{L_\omega}{I_{xx}} \quad (4.110)$$

This is a standard differential equation. Letting the $\theta_{0x} = \theta_0$, then our solution is:

$$\begin{cases} \theta_x = \theta_0 \cos \gamma t \\ \theta_y = \theta_0 \sin \gamma t \end{cases} \quad (4.111)$$

These equations clearly trace out a circle. Thus, the gyroscope will start precessing, and the angular momentum vector will rotate following a circular path. It follows that we need not to exert external torque on a spinning rigid body to observe precession.

In a gyroscope (uniform precession), this torque is gravity. No matter how perfectly we try to balance the gyroscope, there will never be a non-zero angle between the axis of rotation of the flywheel and the z-axis in the center of mass frame. Hence, a slight deviation will offset the center of mass of the flywheel to a side, such that gravity will exert some torque. In our "idealized" world, we assume that gravity is the only force acting on the gyroscope. Then, the net torque at an instant t will perpendicular to the radius vector and the force vector. If gravity is acting to the east of the flywheel, then torque will act out of the paper towards the reader.

Since angular momentum "chases" torque by the principle of conservation of angular momentum, the axis of rotation of the wheel will follow the torque, changing its orientation. In our diagram, the gyroscope will depress towards the reader. The torque however is now acting to the left, and hence the disk will depress to the left etc... As this process repeats itself, it is easy to see that the gyroscope will precess.

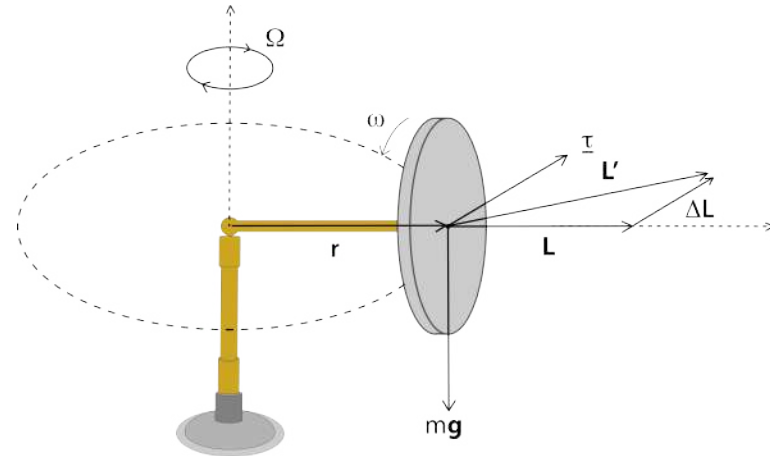


Figure 4.7: Geometrical Interpretation of Gyroscopic Precession

4.5 Spin Stabilised Disk and Precession

We will now extend our study of precession to the Frisbee. For sake of simplicity, we will ignore external torque. Consider the Euler equations:

$$\begin{cases} I_1\dot{\omega}_1 + \omega_2\omega_3(I_3 - I_2) = 0 \\ I_1\dot{\omega}_2 + \omega_3\omega_1(I_1 - I_3) = 0 \\ I_1\dot{\omega}_3 = 0 \end{cases} \quad (4.112)$$

Let us define the variable $\Omega\omega_3 = \frac{I_3 - I_1}{I_1}\omega_3$, so that:

$$\begin{cases} \dot{\omega}_1 + \Omega\omega_3\omega_2 = 0 \implies \dot{\omega}_2\omega_3 + \dot{\omega}_3\omega_2 + \frac{\dot{\omega}_1}{\Omega} = 0 \\ \dot{\omega}_2 = \Omega\omega_3\omega_1 \end{cases} \quad (4.113)$$

from which we finally get:

$$\ddot{\omega}_1 + \Omega^2\omega_3^2\omega_1 + \frac{\Omega\tau_3}{I_1}\omega_2 = 0 \quad (4.114)$$

For the sake of simplicity, we will assume that $\tau_3 = 0$, so that ω_3 is constant (since τ_3 acts to reduce spin velocity). We get:

$$\ddot{\omega}_1 + \Omega^2\omega_3^2\omega_1 = 0 \quad (4.115)$$

whose solutions are:

$$\boldsymbol{\omega} = \omega_0(\sin \Omega\omega_3 t \tilde{\mathbf{e}}_1 + \cos \Omega\omega_3 t \tilde{\mathbf{e}}_2) + \omega_3 \tilde{\mathbf{e}}_3 \quad (4.116)$$

Since angular momentum is conserved, the angle θ must be conserved as well. Comparing it with our expression of angular frequency in Euler angles, we get:

$$\dot{\psi} = \Omega\omega_3, \omega_3 = \dot{\phi} \cos \theta + \dot{\psi}, \dot{\theta} = 0 \quad (4.117)$$

We model the frisbee as a disk with half of its mass concentrated in a disk, and the rest of the mass concentrated on the rim. Simplifying, we get the equations of motion for the disk:

$$\dot{\psi} = \omega_3, \quad \dot{\phi} = \frac{2\omega_3}{\cos \theta}, \quad \dot{\theta} = 0 \quad (4.118)$$

In conclusion, this latter equation summarizes all our results about precession and the behaviour of flying disks. A Frisbee maintains its trajectory without falling over thanks to its spin. The greater the spin, the greater the spin angular momentum, which reduces the body's tendency to change orientation. Furthermore, the faster the Frisbee is spinning, the faster it will wobble, and for small bank angles ($\theta \ll 1$), the spin velocity is exactly half the precession frequency. All these phenomena coincide with real life observations, suggesting that our mathematical model is suitable.

4.6 Conclusion

We have examined the kinematics of rotation, and digressed to study the effect of the Coriolis force in the formation of hurricanes. We then derived the inertia tensor and the principle of conservation of angular momentum. Both results were applied to construct Euler's Equations for Rigid Bodies, and analyzed uniform and free precession. Finally, the equations of rotational motion for a Frisbee were derived, concluding our study of Frisbee physics.

Appendix A

Python Codes

A.1 Code 1: Minimal Surface Plots

```
import matplotlib.pyplot as plt
import scipy
import numpy as np
from mpl_toolkits.mplot3d import Axes3D

tht = scipy.linspace(-3,3,300)
r = scipy.linspace(-3,3,300)
[r,tht] = np.meshgrid(r,tht)

x = r * np.cos(tht)
y = r * np.sin(tht)
z = tht

fig = plt.figure()

ax = Axes3D(fig)

ax.plot_surface(x,y,z, rstride=1, cstride=1,
                cmap='viridis', edgecolor='none')

ax.set_xlabel(r"\mathrm{x-axis}", fontsize = 15)
ax.set_ylabel(r"\mathrm{y-axis}", fontsize = 15)
ax.set_zlabel(r"\mathrm{z-axis}", fontsize = 15)
ax.set_title(r"Helicoid for $k = 1$", fontsize=20)

plt.show()

v = scipy.linspace(-5,5,300)
u = scipy.linspace(-np.pi,np.pi,300)
```

```

[v,u] = np.meshgrid(v,u)

x = 3 * np.cosh(v/3) * np.cos(u)
y = 3 * np.cosh(v/3) * np.sin(u)
z = v

fig = plt.figure()

ax = Axes3D(fig)

ax.plot_surface(x,y,z, rstride=1, cstride=1,
                cmap='viridis', edgecolor='none')

ax.set_xlabel(r"\mathrm{x-axis}", fontsize = 15)
ax.set_ylabel(r"\mathrm{y-axis}", fontsize = 15)
ax.set_zlabel(r"\mathrm{z-axis}", fontsize = 15)
ax.set_title(r"Catenoid for $c = 3$", fontsize=20)

plt.show()

v = scipy.linspace(-5,5,300)
u = scipy.linspace(-np.pi,np.pi,300)
[v,u] = np.meshgrid(v,u)

x = 2 * np.cos(v) * np.sinh(u) + 2/3 * np.cos(3*v) * np.sinh(3*u)
y = 2 * np.sin(v) * np.sinh(u) + 2/3 * np.sin(3*v) * np.sinh(3*u)
z = 2 * np.cos(2*v) * np.cosh(2*u)

fig = plt.figure()

ax = Axes3D(fig)

ax.plot_surface(x,y,z, rstride=1, cstride=1,
                cmap='viridis', edgecolor='none')

ax.set_xlabel(r"\mathrm{x-axis}", fontsize = 15)
ax.set_ylabel(r"\mathrm{y-axis}", fontsize = 15)
ax.set_zlabel(r"\mathrm{z-axis}", fontsize = 15)
ax.set_title(r"Schwarz Minimal Surface", fontsize=20)

plt.show()

```

A.2 Code 2: Streamlines for Vector Field

```

import numpy as np
import matplotlib.pyplot as plt
# if using a Jupyter notebook, include:

x = np.arange(0, 2*np.pi+2*np.pi/20, np.pi/10)
y = np.arange(0, 2*np.pi+2*np.pi/20, np.pi/10)

X,Y = np.meshgrid(x,y)

u = np.sin(X)*np.sin(Y)
v = np.cos(X)*np.cos(Y)

fig, ax = plt.subplots(figsize=(15,15))

seeds = np.array([[3,3], [4,5]])

ax.quiver(X,Y,u,v)

plt.streamplot(X,Y,u,v, start_points = seeds, arrowsize=1, )

ax.xaxis.set_ticks([])
ax.yaxis.set_ticks([])
ax.axis([0,2*np.pi,0,2*np.pi])
ax.set_aspect('equal')

plt.show()

```

A.3 Code 3: Frisbee Flight Simulations

```

from pylab import *
import matplotlib.pyplot as plt
import numpy as np
from sympy import Symbol

def rk4(y, time, dt, derivs):
    k1 = dt * derivs(y,time)
    k2 = dt * derivs(y + 0.5*k1, time + 0.5*dt)
    k3 = dt * derivs(y + 0.5*k2, time + 0.5*dt)
    k4 = dt * derivs(y + k3, time + dt)
    y_next = y + 1/6*(k1 + 2*k2 + 2*k3 + k4)

    return y_next

```

```

N = 500

tau = 30

dt = tau/float(N-1)

g = 9.81
m = 0.18
rho = 1.23
d = 0.28
A = math.pi*(d/2)**2
alpha = np.radians(10)
alpha_0 = np.radians(-4)

C_La = 1.4
C_L0 = 0.15
C_Da = 2.72
C_D0 = 0.08

k_L = 0.5*A/m*(C_L0 + alpha * C_La)*rho

k_D = 0.5*A/m*(C_D0 + C_Da*(alpha - alpha_0)**2)*rho

v0 = 15

v_0x = v0*np.cos(alpha)
x0 = 0

v_0y = v0*np.sin(alpha)
y0 = 1

y = zeros([N,4])

y[0,0] = x0
y[0,1] = v_0x
y[0,2] = y0
y[0,3] = v_0y

def frisbee(state, time):
    g0 = state[1]
    g1 = -k_D * state[1] * state[1]/(np.cos(alpha)**2)
    g2 = state[3]
    g3 = k_L * state[1] * state[1]/(np.cos(alpha)**2) - g

```

```

    return array([g0, g1, g2, g3])

for j in range(N-1):
    y[j+1] = rk4(y[j], 0, dt, frisbee)

time = linspace(0, tau, N)
plt.plot(y[:,0], y[:,2])
plt.title("$v_0=15, \alpha = 10\\degree$")
plt.axis('scaled')
plt.xlim(0,30)
plt.ylim(0,20)
plt.grid(True)
xlabel("Distance (m)")
ylabel("Height (m)")

show()

print("The frisbee's maximum height reached is:",
round(max(y[:,2]), 2), "m")

```

Bibliography

- ¹ Gowlett J. A. J. "The discovery of fire by humans: a long and convoluted process," *Phil. Trans. R. Soc. B* **371**, no. 1696 (2016): 1, 3.
DOI : <https://doi.org/10.1098/rstb.2015.0164>
- ² Faraday, Michael, and W. Crookes. "A Course of Six Lectures on the Chemical History of a Candle," London: Griffin, Bohn & Co, 1861.
Retrieved from <https://www.bartleby.com/30/7.html>
- ³ Cambridge Dictionary, "flame." *Cambridge Dictionary*
Retrieved from <https://dictionary.cambridge.org/dictionary/english/flame>.
- ⁴ Cengel, Yanus A., Afshin Ghajar, "Heat and Mass Transfer," New York City: McGraw-Hill Education, 2014. p.562
ISBN 13: [9780073398181](#)
- ⁵ Planck, Max. "On the Law of Distribution of Energy in the Normal Spectrum." *Ann. Phys. (Berlin)* **4** no. (1901). p. 5-7
Retrieved from: <http://bourabai.kz/articles/planck/planck1901.pdf>
- ⁶ Wein, Wilhelm. "Ueber die Energievertheilung im Emissionsspectrum eines schwarzen Körpers," *Ann. d. Phys.* **294**, no. 4 (1896). pp.656.
Retrieved from http://myweb.rz.uni-augsburg.de/~eckern/adp/history/historic-papers/1896_294_662-669.pdf
- ⁷ Tenn, J. S. "Planck's Derivation of the Energy Density of Blackbody Radiation," University of Sononoma, 2013.
Retrieved from http://web.phys.ntnu.no/~stovneng/TFY4165_2013/BlackbodyRadiation.pdf
- ⁸ Griffiths, J. David. "Introduction to Electrodynamics," Cambridge: Cambridge University Press, 2017. p.383-384.
- ⁹ NRAO, "Essential Radio Astronomy, Chapter 2: Radiation Fundamental & Chapter 7: Spectral Lines", Lecture notes, 2018.
Retrieved from <https://www.cv.nrao.edu/~sransom/web/>
- ¹⁰ Tipler, A. Paul, and Llewellyn A. Ralph, "Modern Physics", New York: W. H. Freeman and Company, 2012. p. 40-41.
- ¹¹ For further reading into the UV catastrophe, please refer to: Boyer, H. Timothy. "Blackbody Radiation in Classical Physics: A Historical Perspective," *American Journal of Physics* **86** no. 495 (2018).
Retrieved from the arXiv database: <https://arxiv.org/abs/1711.04179>.
- ¹² Einstein, Albert. "Concerning an Heuristic Point of View Toward the Emission and Transformation of Light," *Ann. d. Phys.*, **17** no. 132 (1905). p. 132-148.
Retrieved from https://alternativeenergy.procon.org/sourcefiles/einstein_photoelectric_paper1.pdf
- ¹³ Dermot O'Reilly, "Planck's Radiation Law Derived 1." Filmed May 2018, Youtube video.
Retrieved from <https://www.youtube.com/watch?v=VgJeJHiUa24>.
- ¹⁴ See for better discussion of energy bounds: S. Braun, J. P. Ronzheimer, M. Schreiber, S. S. Hodgman, T. Rom, I. Bloch, and U. Schneider. "Negative Absolute Temperature for Motional Degrees of Freedom." *Science*, **339** no. 6115 (2013). p.53-54.
Retrieved from the arXiv database: <https://arxiv.org/pdf/1211.0545v1.pdf>

- ¹⁵ Chu, Steven, Graybeal D. Jack, Stoner O. John, Hurst S. George et al. *Encyclopaedia Britannica*, s.v. "Spectroscopy." Chicago: Encyclopaedia Britannica.
- ¹⁶ Science History Institute, "Robert Bunsen and Gustav Kirchhoff," updated December, 2017.
Retrieved from <https://www.sciencehistory.org/historical-profile/robert-bunsen-and-gustav-kirchhoff>
- ¹⁷ Where we followed the derivation : Kara M. Yedinak, Jack D. Cohen, Jason M. Forthofer and Mark A. Finney. "An examination of flame shape related to convection heat transfer in deep-fuel beds" *Int. J. Wildland Fire*, **19** no. 19 (2010). pp. 173
Retrieved from https://www.fs.fed.us/rm/pubs_other/rmrs_2010_yedinack_k001.pdf
- ¹⁸ A. Alsairafi, J.S. T'ien, S.T. Lee, D.L. Dietrich and H.D. Ross. "Modelling Candle Flame Behaviour in Variable Gravity," presented at the *Seventh International Workshop on Microgravity Combustion and Chemically Reacting Systems*, 2003. p. 261-264.
Retrieved from <https://ntrs.nasa.gov/archive/nasa/casi.ntrs.nasa.gov/20040053576.pdf>
- ¹⁹ National Candle Association, "CANDLE SCIENCE", Washington DC.
Retrieved from <https://candles.org/candle-science/>
- ²⁰ Lexico Dictionary, "surface tension," *Lexico Dictionary*.
Retrieved from https://www.lexico.com/en/definition/surface_tension
- ²¹ Cabre, Xavier, "Elliptic PDE's in probabilities in geometry and symmetry and regularity of solutions," *Disc. Cont. Dynamical Systems*, **20** no.3 (2007).
- ²² Brussup, "Amazing Water & Sound Experiment 2." Filmed March 2013, Youtube video.
Retrieved from https://www.youtube.com/watch?v=uENITui5_jU
- ²³ Skjæveland, Svein. "Derivations of the Young-Laplace equation.", 2015. p.10-19.
Retrieved from https://www.researchgate.net/publication/284338655_Derivations_of_the_Young-Laplace_equation.
- ²⁴ Presley, Andrew. "Gaussian, Mean and Principal Curvatures." Chapter 8 in *Elementary Differential Geometry*, 2nd ed. London: Springer, 2012. p.188
- ²⁵ Vella, J. R. Dominic. "The Fluid Mechanics of Floating and Sinking," Ph.D. diss. *University of Cambridge*, 2007. p. 9-10
Retrieved from <https://core.ac.uk/download/pdf/1319141.pdf>
- ²⁶ Chin-Lin Chen, "Foundations for Guided-Wave Optics", New Jersey: John Wiley and Sons Inc. 2007 p.413-415. Retrieved from <https://onlinelibrary.wiley.com/doi/pdf/10.1002/9780470042229.app2>
- ²⁷ Pellicer, Julio, J. A. Manzanares, Salvador Mafé. "The Physical Description of Elementary Surface Phenomena - Thermodynamics Versus Mechanics," *Amer. J. Phys.* **63** no. 542 (1995). p. 544-546
Retrieved from https://www.academia.edu/16906420/The_physical_description_of_elementary_surface_phenomena_Thermodynamics_versus_mechanics
- ²⁸ Barozzi, Giovanni S., D. Angeli. "A Note on Capillary Rise in Tubes," *Energy Procedia* **45** (2014). p.548-552
DOI: <https://doi.org/10.1016/j.egypro.2014.01.059>
- ²⁹ We loosely follow some methods and strategies introduced in: Berg, John. "Fluid Interfaces and Capillarity" Chapter 2 in *An Introduction to Interfaces and Colloids*, World Scientific, 2009. p. 49-66
DOI: https://doi.org/10.1142/9789814293082_0002
- ³⁰ Lasse, Makkonen. "Young's equation revisited." *Condens. Matter Phys.* **28** no.13 (2016). p.2-5
Retrieved from <https://iopscience.iop.org/article/10.1088/0953-8984/28/13/135001>
- ³¹ Ray, Saroj. "Surface Tension: Capillary Length," filmed February 2018, Youtube video.
Retrieved from <https://www.youtube.com/watch?v=sJY50YTm2-U>
- ³² First presented in de Gennes, Pierre-Gilles, F. Brochard-Wyart, D. Quere. "Capillarity and Wetting Phenomena: Drops, Bubbles, Pearls, Waves" *Physics Today*, **57** no. 12, 16.

- ³³ Presley, Andrea. "Minimal Surfaces." Chapter 12 in *Elementary Differential Geometry*, 2nd ed. London: Springer, 2012. p.306
- ³⁴ D. Callegari, "Minimal Surfaces," Lecture notes at the University of Chicago, 2014. p. 1-4.
Retrieved from https://math.uchicago.edu/~dannyc/courses/minimal_surfaces_2014/minimal_surfaces_notes.pdf
- ³⁵ Victor Ugaz, "Lecture 2: Introduction to Fluid Viscosity" at Texas A&M University, 2015.
Retrieved from <https://cosmolearning.org/video-lectures/introduction-fluid-viscosity/>.
- ³⁶ G.K. Batchelor, "An Introduction to Fluid Dynamics," New York: Cambridge University Press.
- ³⁷ Coleman, Neal. "A Derivation of the Navier Stokes Equations," *B.S. Undergraduate Mathematics Exchange*, 7 no. 1 (2010).
Retrieved from <https://lib.bsu.edu/beneficencepress/mathexchange/07-01/ADerivationoftheNavier-StokesEquations.pdf>
- ³⁸ Faculty of Khan, "Introduction to Tensors," filmed June 2018, Youtube video.
Retrieved from https://www.youtube.com/watch?v=uaQeXi4E7gA&list=PLdgVB0aXkb9D6zw47gsrtE5XqLeRPh27_
- ³⁹ Following: Landau, Lev D., and Evgenij M. Lifshitz, "Motion of a Rigid Body." Chapter 7 in *Course of Theoretical Physics Volume 1: Mechanics*, Oxford: Elsevier Butterworth-Heinemann, 1976.
- ⁴⁰ N. A. Lemos, "Dynamics of Rigid Bodies" Chapter 4 in *Analytical Mechanics*, Cambridge: Cambridge University Press, 2018.
- ⁴¹ Kleppner, David, and R. Kolenkow. "Non-Inertial Systems and Fictitious Forces" Chapter 9 in *An Introduction to Mechanics*, Cambridge: Cambridge University Press, 2014.
- ⁴² Siklos, Stephen, "Rotating Frames," lecture notes at the University of Cambridge, p. 3-6, 2011.
- ⁴³ Tong, David. "Lectures on Classical Dynamics", lectures notes at the University of Cambridge, 2013.
Retrieved from <https://www.dpmms.cam.ac.uk/~stcs/courses/dynamics/lecturenotes/section4.pdf>
- ⁴⁴ Schuurmans, Mace M. "Flight of the Frisbee", *New Scientist* 127 no.1727 (1990). p.37-40
Retrieved from https://www.researchgate.net/publication/271264015_Flight_of_the_Frisbee
- ⁴⁵ Hubbard, Mont, S.A. Hummel, "Simulation of Frisbee Flight", presented at the 5th Conference on Mathematics and Computers in Sport (2000).
Retrieved from https://www.researchgate.net/publication/253842372_Simulation_of_Frisbee_Flight
- ⁴⁶ V.R. Morrison. "The Physics of Frisbees", *Journal of Classical Mechanics and Relativity* (2005).
Retrieved from http://scripts.mit.edu/~womens-ult/frisbee_physics.pdf
- ⁴⁷ Brian Storey. "The Stress Tensor", Youtube video published in October 2014.
Retrieved from https://www.youtube.com/watch?v=u0_bW2zzrNU.
- ⁴⁸ Motoyama, Eugene. "The Physics of Flying Disks", 2002.
Retrieved from <http://people.csail.mit.edu/jrennie/discgolf/physics.pdf>
- ⁴⁹ K. F. Riley, M. P. Hobson, S. J . Bence. "Mathematical Methods for Physics and Engineering," Cambridge: Cambridge University Press, 2006.
- ⁵⁰ Whitrow, Gerald J. "Einstein: The Man and His Achievement," New York: Dover Publications 1973. p.42.
- ⁵¹ Feynman, Richard. "Fun to Imagine." BBC TV, 1983.
Retriece from <https://www.youtube.com/watch?v=P1ww1IXRfTA&t=63s>